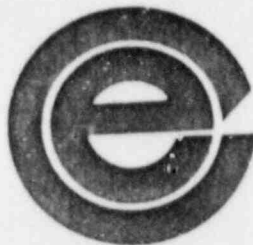


LICENSING REPORT  
ON  
HIGH DENSITY SPENT FUEL RACKS  
FOR  
BYRON UNITS 1 AND 2  
NRC DOCKET NO. 50 - 454  
50 - 455



COMMONWEALTH EDISON COMPANY  
CHICAGO, ILLINOIS 60603

MAY 1988  
(Revision 2)

## TABLE OF CONTENTS

<u>Section</u>	<u>Page</u>
1.0 INTRODUCTION	1-1
2.0 GENERAL ARRANGEMENT	2-1
3.0 RACK CONSTRUCTION	3-1
3.1 Fabrication Details	3-1
3.1.1 Region 1	3-1
3.1.2 Region 2	3-3
3.2 Codes, Standards, and Practices for the Spent Fuel Pool Modification	
4.0 CRITICALITY SAFETY ANALYSES	4-1
4.1 Design Bases	4-1
4.2 Summary of Criticality Analyses	4-2
4.2.1 Normal Operating Conditions	4-2
4.2.2 Abnormal and Accident Conditions	4-3
4.2.3 New Fuel Storage	4-4
4.3 Reference Fuel Storage Cell	
4.3.1 Reference Fuel Assembly	4-5
4.3.2 Region 1 Storage Cells	4-5
4.3.3 Region 2 Storage Cells	4-6
4.4 Analytical Methodology	4-6
4.4.1.1 Reference Analytical Methods and Bias	4-6
4.4.1.2 Analytical Methods and Bias for Modified Cases	4-8
4.4.2 Fuel Burnup Calculations	4-9
4.4.3 Effect of Axial Burnup Distribution	4-11
4.4.4 Long-Term Decay	4-12
4.5 Region 1 Criticality Analysis and Tolerance Variations	4-12
4.5.1 Nominal Design Case	4-12
4.5.2 Boron Loading Variation	4-13
4.5.3 Storage Cell Lattice Pitch Variation	4-13
4.5.4 Stainless Steel Thickness Tolerances	4-14
4.5.5 Fuel Enrichment and Density Variation	4-14



TABLE OF CONTENTS  
(continued)

<u>Section</u>		<u>Page</u>
4.5.6	Boraflex Width Tolerance Variation	4-14
4.5.7	Axial Cutback of Boraflex	4-15
4.6	Region 2 Criticality Analysis and Tolerance Variations	4-15
4.6.1	Nominal Design Case	4-15
4.6.2	Boron Loading Variation	4-16
4.6.3	Storage Cell Lattice Pitch Variations	4-17
4.6.4	Stainless Steel Thickness Tolerance	4-17
4.6.5	Fuel Enrichment and Density Variation	4-17
4.6.6	Boraflex Width Tolerance	4-17
4.7	Abnormal and Accident Conditions	4-17
4.7.1	Eccentric Positioning of Fuel Assembly in Storage Rack	4-17
4.7.2	Temperature and Water Density Effects	4-18
4.7.3	Dropped Fuel Assembly Accident	4-18
4.7.4	Abnormal Location of a Fuel Assembly	4-19
4.7.5	Lateral Rack Movement	4-19
4.8	New Fuel Storage	4-20
4.8.1	Storage in Region 1, Dry	4-20
4.8.2	Storage in Region 2, Flooded	4-20
4.8.3	Storage in Region 2, Dry	4-21
REFERENCES		4-22
5.0	THERMAL-HYDRAULIC ANALYSES	5-1
5.1	Decay Heat Calculations for the Spent Fuel	5-1
5.1.1	Basis	5-2
5.1.2	Model Description	5-5
5.1.3	Decay Heat Calculation Results	5-7
5.2	Thermal-Hydraulic Analyses for Spent Fuel Cooling	5-8
5.2.1	Basis	5-9
5.2.2	Model Description	5-9
5.2.3	Results	5-11
REFERENCES		5-13

TABLE OF CONTENTS  
(continued)

<u>Section</u>	<u>Page</u>
6.0 STRUCTURAL ANALYSIS	6-1
6.1 Analysis Outline	6-1
6.2 Fuel Rack - Fuel Assembly Model	6-3
6.2.1 Outline of Model	6-3
6.2.2 Model Description	6-5
6.2.3 Fluid Coupling	6-5
6.2.4 Damping	6-6
6.2.5 Impact	6-7
6.3 Assembly of the Dynamic Model	6-7
6.4 Time Integration of the Equations of Motion	6-9
6.4.1 Time-History Analysis Using Multi-Degree of Freedom Rack Model	6-9
6.4.2 Evaluation of Potential for Inter-Rack Impact	6-11
6.5 Structural Acceptance Criteria	6-11
6.6 Material Properties	6-13
6.7 Stress Limits for Various Conditions	6-13
6.7.1 Normal and Upset Conditions (Level A or Level B)	6-13
6.7.2 Level D Service Limits	6-15
6.8 Results	6-15
6.9 Impact Analyses	6-17
6.9.1 Impact Loading Between Fuel Assembly and Cell Wall	6-17
6.9.2 Impacts Between Adjacent Racks	6-17
6.10 Weld Stresses	6-17
6.10.1 Baseplate to Rack Welds and Cell-to-Cell Welds	6-18
6.10.2 Heating of an Isolated Cell	6-18
6.11 Summary of Mechanical Analyses	6-19
6.12 Definition of Terms Used in Section 6	6-20

TABLE OF CONTENTS  
(continued)

<u>Section</u>	<u>Page</u>
REFERENCES	6-21
7.0 ENVIRONMENTAL EVALUATION	7-1
7.1 Summary	7-1
7.2 Characteristics of Stored Fuel	7-1
7.3 Related Industry Experience	7-2
7.4 Byron Nuclear Power Station Experience	7-3
7.5 Spent Fuel Cooling and Cleanup System	7-3
7.6 Fuel Pool Radiation Shielding	7-4
7.6.1 Source Terms	7-4
7.6.2 Radiation Shielding	7-5
7.7 Radiological Consequences	7-6
7.8 Reracking Operation	7-6
7.9 Conclusions	7-7
REFERENCES	7-9
8.0 IN-SERVICE SURVEILLANCE PROGRAM FOR BORAFLEX NEUTRON ABSORBING MATERIAL	8-1
8.1 Program Intent	8-1
8.2 Description of Specimens	8-1
8.3 Specimen Evaluation	8-1
9.0 COST/BENEFIT ASSESSMENT	9-1
9.1 Specific Needs for Spent Fuel Storage	9-1
9.2 Cost of Spent Fuel Storage	9-1
9.3 Alternatives to Spent Fuel Storage	9-2
9.4 Resource Commitments	9-3

TABLE OF CONTENTS  
(continued)

<u>Section</u>	<u>Page</u>
REFERENCES	9-4
10.0 QUALITY ASSURANCE PROGRAM	10-1
10.1 Introduction	10-1
10.2 General	10-1
10.3 System Highlights	10-1
10.4 Summary	10-2
APPENDIX A     BENCHMARK CALCULATIONS	A-1
APPENDIX B     NRC QUESTIONS FROM DECEMBER 22, 1986 MEETING	B-1

## 1.0 INTRODUCTION

This report describes the design, fabrication, and safety analysis of high density spent fuel storage racks manufactured by Joseph Oat Corporation (Oat) for the Byron Station Unit 1 and Unit 2. The plant, which is located two miles east of the Rock River and approximately three miles southwest of Byron in Ogle County, is owned and operated by Commonwealth Edison Company (CECO).

Byron is a two-unit pressurized water reactor (PWR) with a net design capacity of 1120 megawatts electric for each unit. Each of the two reactor cores contains 193 fuel assemblies and is rated to produce 3411 thermal megawatts (Mwt). At present, there is one (normal core offload) batch spent fuel assemblies stored in the spent fuel pool. Unit 1 went into commercial operation in September of 1985. Unit 2 went into commercial operation in August, 1987.

The two units share one common spent fuel storage pool which is currently licensed for the storage of 1060 spent fuel assemblies. As shown in Table 1.1, the storage pool would lose full core discharge capability in 1994. The proposed reracking will increase the number of pool storage locations to 2870 (includes six failed fuel locations). Table 1.1 indicates that the new racks will provide adequate storage with full core discharge capability well into the next century (circa 2009). Table 1.1 is based on an estimated 18-month fuel cycle. Current trends toward longer cycles, extended burnup, and higher enrichment would further extend the time span of onsite storage.

The proposed racks are free-standing and self-supporting. The principal construction materials are ASTM A-240, Type 304L stainless steel for the structural members and shapes, with "Boraflex", a patented product of BISCO (a division of Brand, Inc.), and Boral, a patented product of AAR Brooks & Perkins for neutron attenuation. Whereas the fixed height support legs employ 304L series austenitic stainless plate and pipe material, the adjustable support legs are constructed from SA351-CF3 and SA217-CA15 casting stock, and for certain support legs 400 series stainless (SA479-410) steel material.

The specifications for design, construction, and quality assurance for the high density spent fuel storage racks were prepared by Sargent & Lundy Engineers (S&L) of Chicago, Illinois. The mechanical design and fabrication of the hardware was done by Oat. Seismic/structural analysis, thermal-hydraulic analysis, and other related calculations were performed by Holtec International of Mount Laurel, New Jersey and S&L. S&L provided the seismic response spectra and performed the spent fuel pool structure evaluation. S&L performed the radiation shielding analysis. Southern Science, a division of Black and Veatch, served as a consultant to Oat in the area of criticality analysis. Further criticality analysis was performed by Westinghouse Electric. The mathematical analysis responsibility for this contract was taken over by Holtec International of Mount Laurel, New Jersey, who prepared the December, 1986 amendment to this licensing report on behalf of Oat. The analyses performed by Holtec in conjunction with Black and Veatch and S&L demonstrate that acceptable margins of safety exist with respect to appropriate NRC and ASME acceptance criteria. A cost-benefit comparison of several potential spent fuel disposition alternatives indicates that reracking of the Byron pool is the lowest risk and most cost-effective alternative, and that neither the reracking operation nor the increased onsite storage of irradiated material pose an undue hazard to the plant staff or the public.

The following sections provide a synopsis of the design, fabrication, nuclear criticality analysis, thermal/hydraulic analysis, structural analysis, accident analysis, environmental analysis, and cost-benefit appraisal of the high density spent fuel racks. In particular, the integrity of the rack structure under the specified combinations of inertial, seismic, and mechanical loads and thermal gradient per NUREG-0800 is demonstrated.

Also included are descriptions of the rack In-Service Surveillance Program and the Oat Quality Assurance Program. This Quality Assurance Program has been reviewed and found acceptable for engineered fabrication of ASME Section III, Class 1, 2 and 3 and MC Components by both ASME and the NRC.

Table 1.1

BYRON UNIT 1 & UNIT 2 FUEL ASSEMBLY DISCHARGE  
(TENTATIVE SCHEDULE)

Unit	Date	Number of Assemblies Discharged	Total Discharged Batch Size	Remaining Capacity	
				Without Proposed Expansion	With*** Proposed Expansion
#1	Feb. 1987	88	88	972	2782
#1	Aug. 1988	88	176	884	2694
#2	Dec. 1988	88	264	796	2606
#1	Feb. 1990	88	352	708	2518
#2	June 1990	88	440	620	2430
#1	Aug. 1991	88	528	532	2342
#2	Dec. 1991	88	616	444	2254
#1	Feb. 1993	84	700	360	2170
#2	June 1993	88	788	272	2082
#1	Aug. 1994	84	872	188**	1998
#2	Dec. 1994	84	956	104	1914
#1	Feb. 1996	84	1040	20*	1830
#2	June 1996	84	1124		1746
#1	Aug. 1997	84	1208		1662
#2	Dec. 1997	84	1292		1578

- \* Partial core discharge capability lost - 84 assemblies  
 \*\* Full core discharge capability lost - 193 assemblies  
 \*\*\* Includes 6 failed fuel storage positions



Table 1.1 (Continued)  
 BYRON UNIT 1 & UNIT 2 FUEL ASSEMBLY DISCHARGE  
 (TENTATIVE SCHEDULE)

Unit	Date	Number of Assemblies Discharged	Total Discharged Batch Size	Remaining Capacity	
				Without Proposed Expansion	With*** Proposed Expansion
#1	Feb. 1999	84	1376		1494
#2	June 1999	84	1460		1410
#1	Aug. 2000	84	1544		1326
#2	Dec. 2000	84	1628		1242
#1	Feb. 2002	84	1712		1158
#2	June 2002	84	1796		1074
#1	Aug. 2003	84	1880		990
#2	Dec. 2003	84	1964		906
#1	Feb. 2005	84	2048		822
#2	June 2005	84	2132		738
#1	Aug. 2006	84	2216		654
#2	Dec. 2006	84	2300		570
#1	Feb. 2008	84	2384		486
#2	June 2008	84	2468		402
#1	Aug. 2009	84	2552		318
#2	Dec. 2009	84	2636		234
#1	Feb. 2011	84	2720		150**
#2	June 2011	84	2804		66*

\*\*\* Includes 6 failed fuel storage positions.



## 2.0 GENERAL ARRANGEMENT

The high density spent fuel racks consist of individual cells with 8.85-inch (nominal) square cross-section, each of which accommodates a single Westinghouse PWR fuel assembly or equivalent. A total of 2864 cells and six failed fuel storage cells are arranged in 23 distinct modules of varying sizes in two regions. Region 1 is designed for storage of new fuel assemblies with enrichments up to 4.2 weight percent U-235. Region 1 is also designed to store fuel assemblies with enrichments up to 4.2 weight percent U-235 that have not achieved adequate burnup for Region 2. The Region 2 cells are capable of accommodating fuel assemblies with various initial enrichments which have accumulated minimum burnups within an acceptable bound as depicted in Figure 4.1. Figure 2.1 shows the arrangement of the rack modules in the spent fuel pool.

The high density racks are engineered to achieve the dual objective of maximum protection against structural loadings (arising from ground motion, thermal stresses, etc.) and the maximization of available storage locations. In general, a greater width-to-height aspect ratio provides greater margin against rigid body tipping. Hence, the modules are made as large as possible within the constraints of transportation and site handling capabilities.

As shown in Figure 2.1, there are 23 discrete modules arranged in the fuel pool. Each rack module is equipped (see Figures 2.2a and 2.2b) with girdle bars, one-inch-thick by 3-1/2 inches high. The nominal gap between cell walls of adjacent modules is two inches. The modules make surface contact between their contiguous sides at the girdle bar locations and thus maintain a specified gap between them. Table 2.1 summarizes the typical physical data for each Region 1 and Region 2 rack. Table 2.2 summarizes other pertinent information on each rack module.

Table 2.1  
DESIGN DATA

Region	(Cell Pitch) Nominal in.	Min. Boral Loading	Min. B-10 Loading	Flux Trap Gap(nominal) in.
1 Nominal	10.32 N&S &10.42 E&W	N/A N/A	.020 gm/cm <sup>2</sup>	1.16* 1.26
Boral Insert	10.32 N&S &10.42 E&W	.020gm/cm <sup>2</sup>	.020gm/cm <sup>2</sup>	1.01 1.11
1 Boral Only	10.32 N&S &10.42 E&W	.025gm/cm <sup>2</sup>	N/A	1.18 1.28
2	9.03**	N/A	.010 gm/cm <sup>2</sup>	0.0

\* The minimum flux trap gap can be .040" less than the nominal gap.

\*\* The minimum pitch can be .040" less than the nominal pitch.

Table 2.2  
MODULE DATA

Region	Module Type	Number of Modules	Cells per Module	Module Size	Approximate Weight (lb/module)
I	A1	1	104	13x8	20,800
I	B1-3	3	96	12x8	19,200
II	C1-6	6	168	14x12	26,900
II	D1&3	2	126	14x9	20,150
II	D4	1	113	14x9 -(2x2+3x3)	18,360
II	D2	1	114	14x9-(4x3)	18,250
II	E1	1	112	14x8	17,900
II	F1	1	165	11x15	26,600
II	G1	1	90	10x9	14,700
II	H1	1	56	7x8	8,950
II	J1	1	35+6 failed fuel containers	7x5	10,150
II	K1	1	117	13x9	19,000
II	L1-L2	2	156	13x12	25,200
II	M1	1	98	14x7	16,000

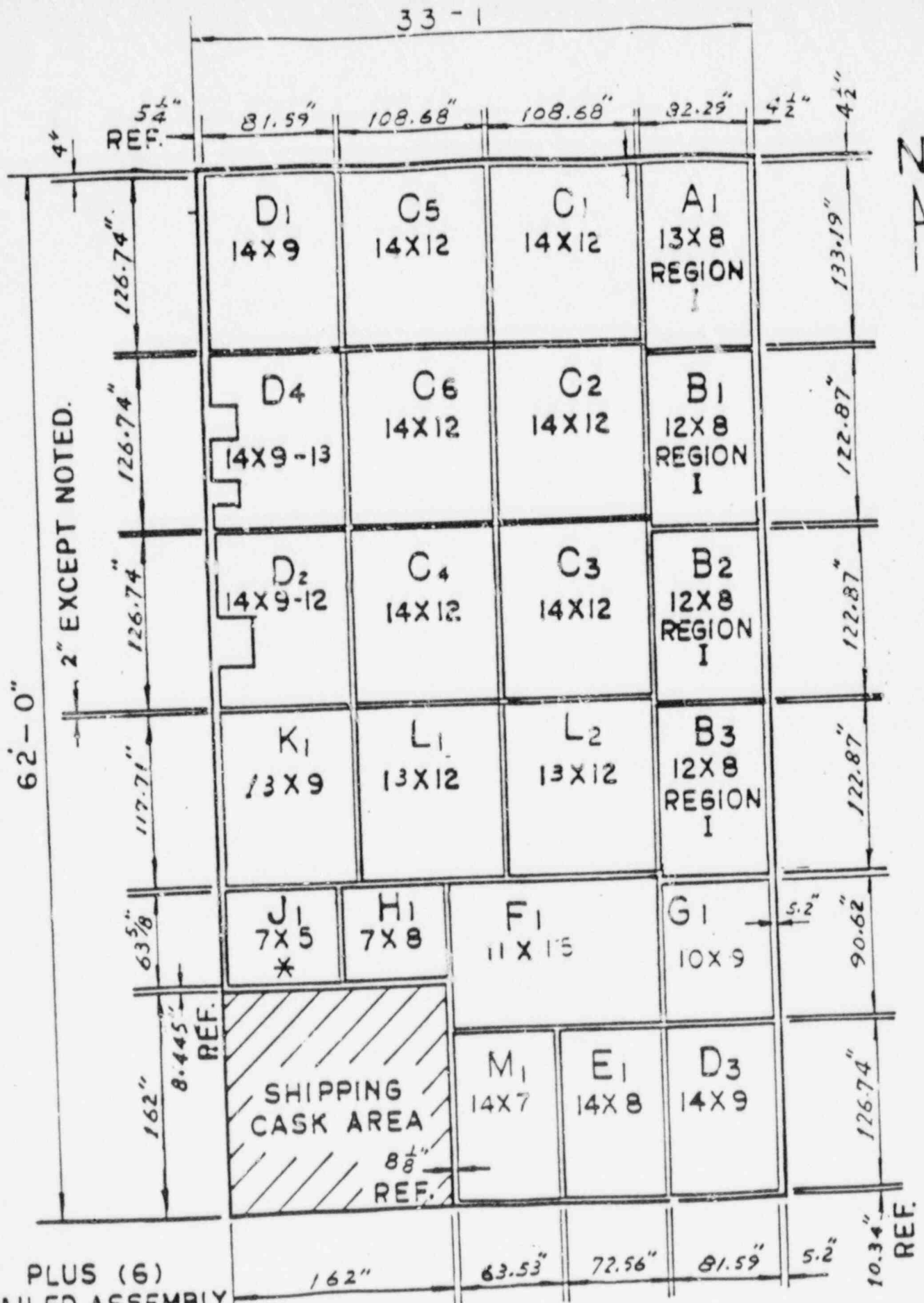


FIGURE 2.1 POOL LAYOUT

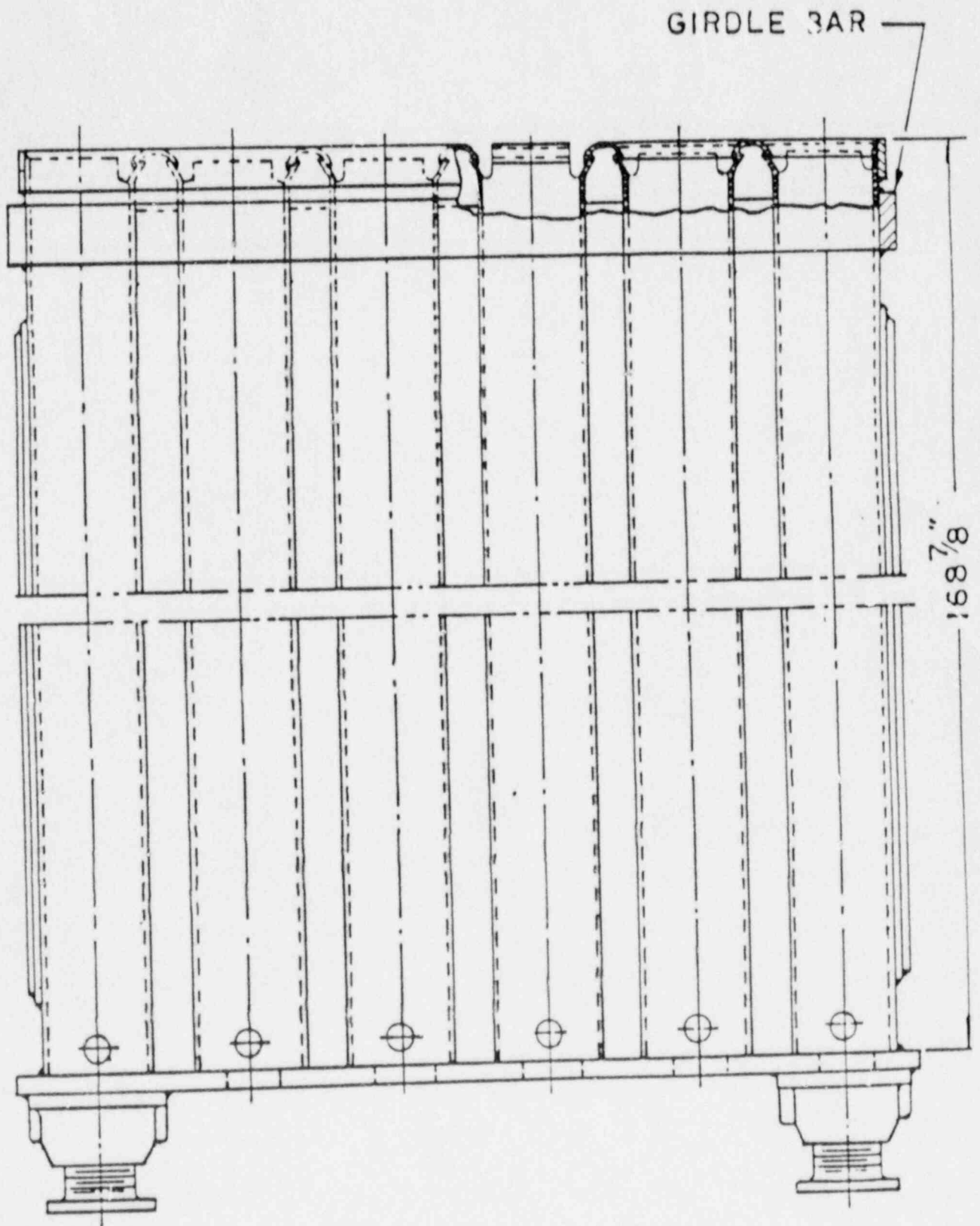


FIGURE 2.2a TYPICAL RACK ELEVATION-REGION 1

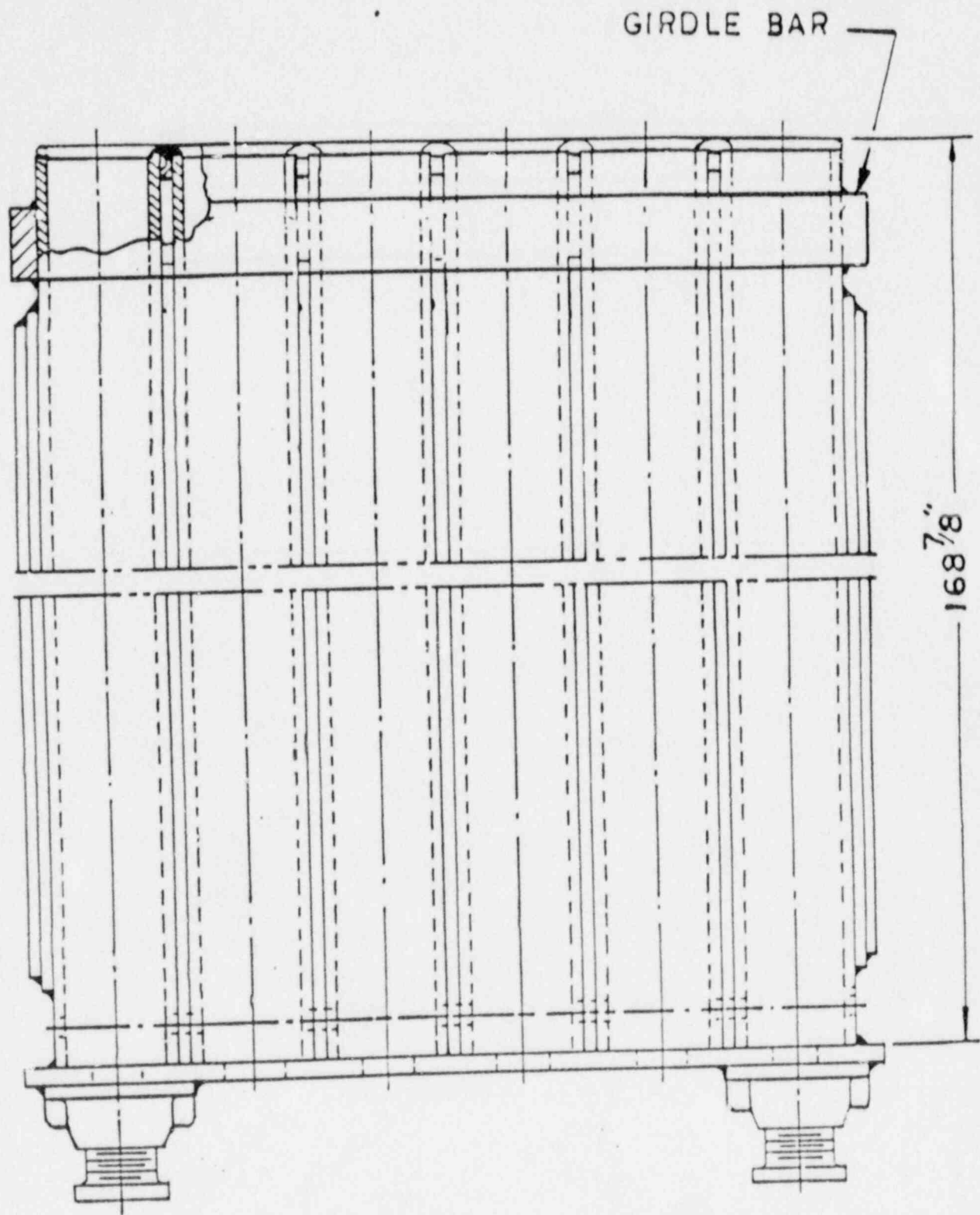


FIGURE 2.2b TYPICAL RACK ELEVATION-REGION 2



## 3.0 RACK CONSTRUCTION

### 3.1 FABRICATION DETAILS

#### 3.1.1 Region 1

The rack module is fabricated from ASTM A-240-304L austenitic stainless steel sheet and plate material, ASME SA351-CF3 and SA217-CA15 casting material and SA 479-410 material. The weld filler material utilized in body welds is ASME SFA-5.9, Type 308L and 308LSI. Boraflex and Boral serve as the neutron absorber material. The detailed neutronic properties of Boraflex may be found in Section 4. The Boraflex experience list is given in Table 3.1. The Boral experience is given to Table 3.1.a.

A typical module contains storage cells which have an 8.85-inch nominal square cross-sectional opening. This dimension ensures that fuel assemblies with maximum expected axial bow can be inserted and removed from the storage cells without any damage to the fuel assemblies or the rack modules.

Figure 3.1 shows a horizontal cross-section of a 3x3 array. The cells provide a smooth and continuous surface for lateral contact with the fuel assembly. The anatomy of the rack modules is best explained by describing the components of the design, namely:

- 0 Internal square box
- 0 Neutron absorber material (Boraflex,Boral)
- 0 Poison sheathing
- 0 Gap element
- 0 Baseplate
- 0 Support assembly
- 0 Top Lead-in

#### a. Internal Square Box

This element provides the lateral bearing surface to the fuel assembly. It is fabricated by joining two formed channels (Figure 3.2) using a controlled seam welding operation. This element is an 8.85-inch square (nominal) cross-section by 168-7/8 inches long.

b. Neutron Absorber Material (Boraflex, Boral)

Boraflex is placed on all four sides of a square tube over a length of 139-1/2 inches, which covers the active fuel length except the top and bottom 2.25 inches, for Region 1 Nominal Case. In addition to the Boraflex, Boral sheets are added to the flux traps of two Region 1 racks (B2 and B3) which have already been built. Boral sheets shall be used in place of Boraflex to cover the entire active fuel on Region 1 racks (A1 and B1) which are not yet built. For Region 2 the Boraflex length is 144 inches and it covers the entire length of the active fuel.

c. Poison Sheathing

The poison sheathing (cover plate) shown in Figure 3.4, serves to position and retain the poison material in its designated space. This is accomplished by spot welding the cover sheet to the square tube along the former's edges at numerous (at least 20) locations. This manner of attachment ensures that the poison material will not sag or laterally displace during fabrication processes and under any subsequent loading condition.

d. Gap Element

Gap elements, illustrated in Figure 3.3, position two inner boxes at a predetermined distance to maintain the minimum flux trap gap required between two boxes. The gap element is welded to the inner box by fillet welds. An array of composite box assemblies welded as indicated in Figure 3.1 form the honeycomb gridwork of cells which harnesses the structural strength of all sheet and plate type members in an efficient manner. The array of composite boxes has overall bending, torsional, and axial rigidities which are an order of magnitude greater than configurations utilizing grid bar type of construction.

e. Baseplate

The baseplate is a 5/8-inch thick plate type member which has 6-inch diameter holes concentrically located with respect to the internal square tube, except at support leg locations, where the hole size is 5 inches in diameter. These holes provide the primary path for coolant flow. Secondary flow paths are available between adjacent cells via the lateral flow holes (1 inch in diameter) near the root of the honeycomb (Figures 3.5a and 3.5b) which preclude flow blockages. The honeycomb is welded to the baseplate with 3/32-inch fillet welds.

f. Support Assembly

Each module has at least four support legs. Most supports are adjustable in length to enable levelling of the rack. The variable height support assembly consists of a flat-footed spindle which rides into an internally-threaded cylindrical member. The cylindrical member is attached to the underside of the baseplate



through fillet and partial penetration welds. The base of the flat-footed spindle sits on the pool floor. Levelling of the rack modules is accomplished by turning the square sprocket in the spindle using a long arm (approximately 46 feet long) square head wrench. Figure 3.6A shows a vertical cross-section of the adjustable support assembly.

The supports elevate the module baseplate approximately 7-1/2 inches above the pool floor, thus creating the water plenum for coolant flow. The lateral holes in the cylindrical member provide the coolant entry path leading into the bottom of the storage locations.

Short adjustable legs are used on racks E1, L2, C2 (for detail see Fig. 3.6B). In addition, one small fixed support leg is used on rack D<sub>2</sub> (for detail see Fig. 3.6C).

g. Top Lead-in

Lead-ins are provided on each cell to facilitate fuel assembly insertion. The lead-ins of contiguous walls of adjacent cells are structurally connected at the lead-in. These lead-in joints aid in reducing the lateral deflection of the inner square tube due to the impact of fuel assemblies during the ground motion (postulated seismic motion specified in the FSAR). This type of construction leads to natural venting locations for the inter-cell space where the neutron absorber material is located.

3.1.2 Region 2

The rack modules in Region 2 are fabricated from the same material as that used for Region 1 modules, i.e., ASTM A-240-304L austenitic stainless steel.

A typical Region 2 module storage cell also has an 8.85-inch nominal square cross-sectional opening. Figure 3.5b shows a partial vertical section of Region 2 module. Figure 3.7 shows a horizontal cross-section of a 3 x 3 array. The rack construction varies from that for Region 1 inasmuch as the stainless steel cover plates, gap elements, and top lead-ins are eliminated. Hence, the basic components of this design are as follows:

- 0 Internal square box
- 0 Neutron absorber material
- 0 Side strips
- 0 Baseplate
- 0 Support assembly

In this construction, two channel elements form a box with an 8.85-inch nominal square cross-sectional opening. The poison material is placed between two boxes as shown in Figure 3.7. Stainless steel side strips are inserted in both sides of the poison material to firmly locate it in the lateral direction. The bottom strip positions the poison material in the vertical direction to envelope the entire active fuel length of a fuel assembly (Figure 3.5b). Two adjacent boxes and the side strip between boxes are welded together as shown in Figure 3.7, to form the honeycomb rack module.

The baseplate and adjustable support assemblies are incorporated in exactly the same manner as described for Region 1 in the preceding section.

### 3.2 CODES, STANDARDS, AND PRACTICES FOR THE SPENT FUEL POOL MODIFICATION

The fabrication of the rack modules is performed under a strict quality assurance system suitable for ASME Section III, Class 1, 2 and 3 manufacturing which has been in place at Oat for over 10 years.

The following codes, standards and practices were used as applicable for the design, construction, and assembly of the spent fuel storage racks and analysis of the pool structure. Additional specific references related to detailed analyses are given in each section.

#### a. Design Codes

- (1) AISC Manual of Steel Construction, 8th Edition, 1980.
- (2) ANSI N210-1976, "Design Objectives for Light Water Reactor Spent Fuel Storage Facilities at Nuclear Power Stations."
- (3) American Society of Mechanical Engineers (ASME), Boiler and Pressure Vessel Code, Section III, 1983 Edition up to and including Summer 1983 Addenda (Subsection NF).
- (4) ASNT-TC-1A June, 1980 American Society for Nondestructive Testing (Recommended Practice for Personnel Qualifications).

#### b. Material Codes

- (1) American Society for Testing and Materials (ASTM) Standards - A-240.

- (2) American Society of Mechanical Engineers (ASME), Boiler and Pressure Vessel Code, Section II - Parts A and C, 1983 Edition, up to and including Summer 1983 Addenda.

c. Welding Codes

ASME Boiler and Pressure Vessel Code, Section IX - Welding and Brazing Qualifications, 1983 Edition up to and including Summer, 1983 Addenda.

d. Quality Assurance, Cleanliness, Packaging, Shipping, Receiving, Storage, and Handling Requirements

- (1) ANSI N45.2.2 - Packaging, Shipping, Receiving, Storage and Handling of Items for Nuclear Power Plants.
- (2) ANSI 45.2.1 - Cleaning of Fluid Systems and Associated Components during Construction Phase of Nuclear Power Plants.
- (3) ASME Boiler and Pressure Vessel, Section V, Nondestructive Examination, 1983 Edition, including Summer and Winter 1983 Addenda.
- (4) ANSI - N16.1-75 Nuclear Criticality Safety Operations with Fissionable Materials Outside Reactors.
- (5) ANSI - N16.9-75 Validation of Calculation Methods for Nuclear Criticality Safety.
- (6) ANSI - N45.2.11, 1974 Quality Assurance Requirements for the Design of Nuclear Power Plants.

e. Other References

- (1) NRC Regulatory Guides, Division 1, Regulatory Guides 1.13, Rev. 2 (proposed); 1.29, Rev. 3; 1.31, Rev. 3; 1.61, Rev. 0; 1.71, Rev. 0; 1.85, Rev. 22; 1.92, Rev. 1; 1.124, Rev. 1; and 3.41, Rev. 1.
- (2) General Design Criteria for Nuclear Power Plants, Code of Federal Regulations, Title 10, Part 50, Appendix A (GDC Nos. 1, 2, 61, 62, and 63).
- (3) NUREG-0800, Standard Review Plan (1981).
- (4) "OT Position for Review and Acceptance of Spent Fuel Storage and Handling Applications," dated April 14, 1978, and the modifications to this document of January 18, 1979.

Table 3.1

## BORAFLEX EXPERIENCE FOR HIGH DENSITY RACKS

Site	Unit No.	Plant Type	NRC Docket No.	Licensing Status
Point Beach	1 & 2	PWR	50-226 & 301	Licensed
Nine Mile Point	1	BWR	50-220	Licensed
Oconee	1 & 2	PWR	50-269 & 270	Licensed
Prairie Island	1 & 2	PWR	50-282 & 306	Licensed
Calvert Cliffs	2	PWR	50-318	Licensed
Quad Cities*	1 & 2	BWR	50-254 & 265	Licensed
Watts Bar	1 & 2	PWR	50-390 & 391	Pending
Waterford	3	PWR	50-382	Pending
Fermi*	2	BWR	50-341	Licensed
H.B. Robinson	2	PWR	50-261	Licensed
River Bend	1	BWR	50-458	Licensed
Rancho Seco*	1	PWR	50-312	Licensed
Nine Mile Point	2	BWR	50-410	To Be applied for
Shearon Harris	1	PWR	50-400	To be applied for
Millstone	3	PWR	50-423	To be applied for
Grand Gulf*	1	BWR	50-416	Pending
Oyster Creek*		BWR	50-219	Licensed
V.C. Summer*		PWR	50-395	Licensed
Diablo Canyon*	1 & 2	PWR	50-275 & 323	Licensed

\* Joseph Oat Corporation fabricated racks

Table 3.1.a

## BORAL EXPERIENCE FOR HIGH DENSITY RACKS

Site	Unit No.	Plant Type	NRC Docket No.	Licensing Status
Bellefonte	1&2	PWR	50-438	
D. C. Cook	1&2	PWR	50-316	
Indian Point	3	PWR	50-286	
Maire Yankee			50-309	
Salem	1&2	PWR	50-272	
Seabrook		PWR	50-443	
Sequoyah	1&2	PWR	50-327	
Yankee Rowe		PWR	50-029	
Zion	1&2	PWR	50-295	
Browns Ferry	1,2&3	BWR	50-259, 260, 296	
Brunswick	1&2	BWR	50-325	
Clinton		BWR	50-461	
Cooper		BWR	50-298	
Dresden	2&3	BWR	50-237, 249	
Duane Arnold		BWR	50-331	
J. A. Fitzpatrick		BWR	50-333	
E.I. Hatch	1&2	BWR	50-231, 366	
Hope Creek		BWR	50-354	
Humbolt Bay			50-133	
La Crosse		BWR	50-409	
Limerick	1&2	BWR	50-352	
Monticello		BWR	50-263	
Peachbottom	2&3	BWR	50-277	
Perry	1&2	BWR	50-440, 441	
Pilgrim		BWR	50-293	
Shoreham		BWR	50-322	
Susquehanna	1&2	BWR	50-387	
Vermont Yankee		BWR	50-271	

NEUTRON  
ABSORBER  
(BORAL SHEET)

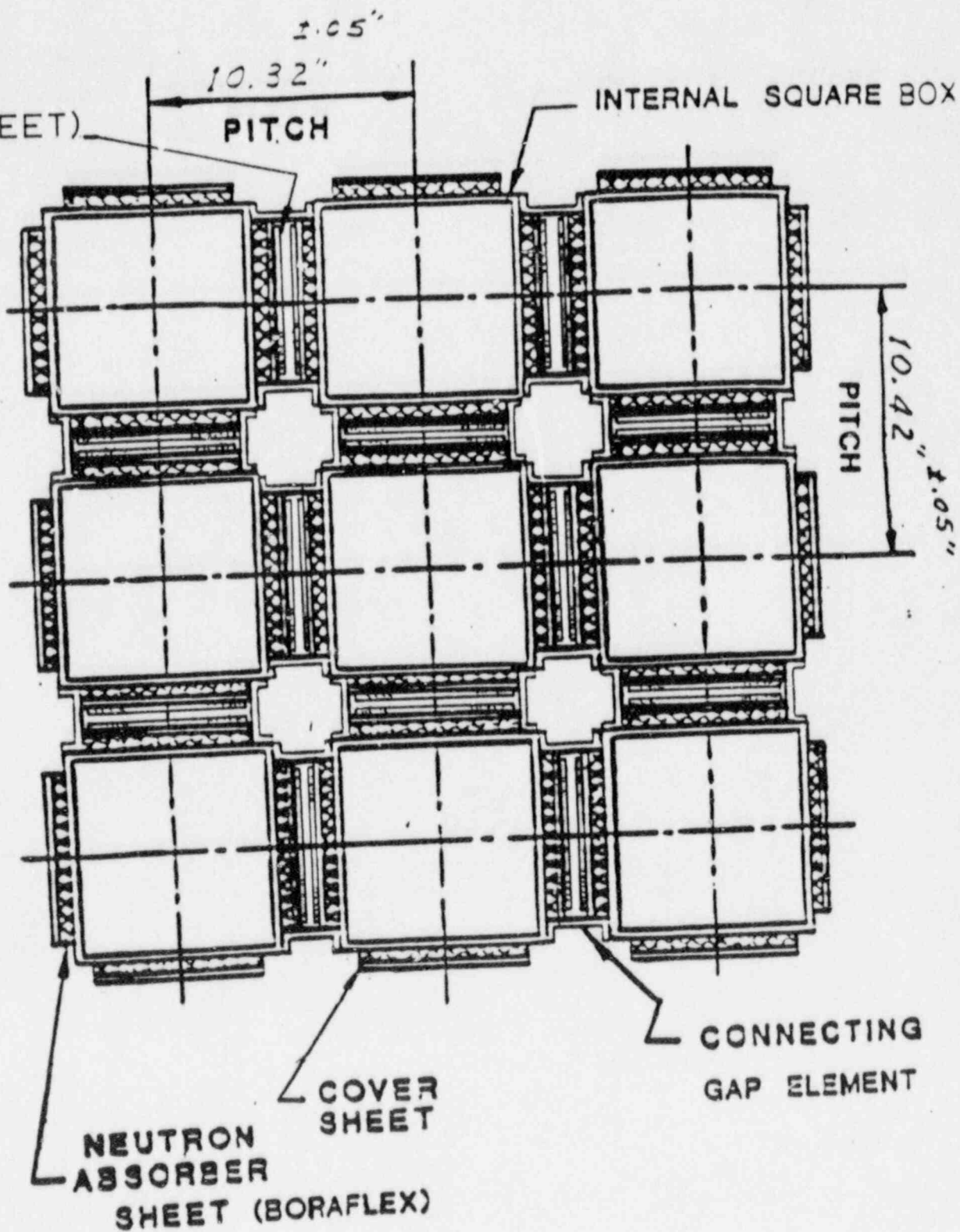


FIGURE 3.1 3 x 3 TYP. ARRAY REGION 1



NEUTRON  
ABSORBER  
(BORAFLEX)

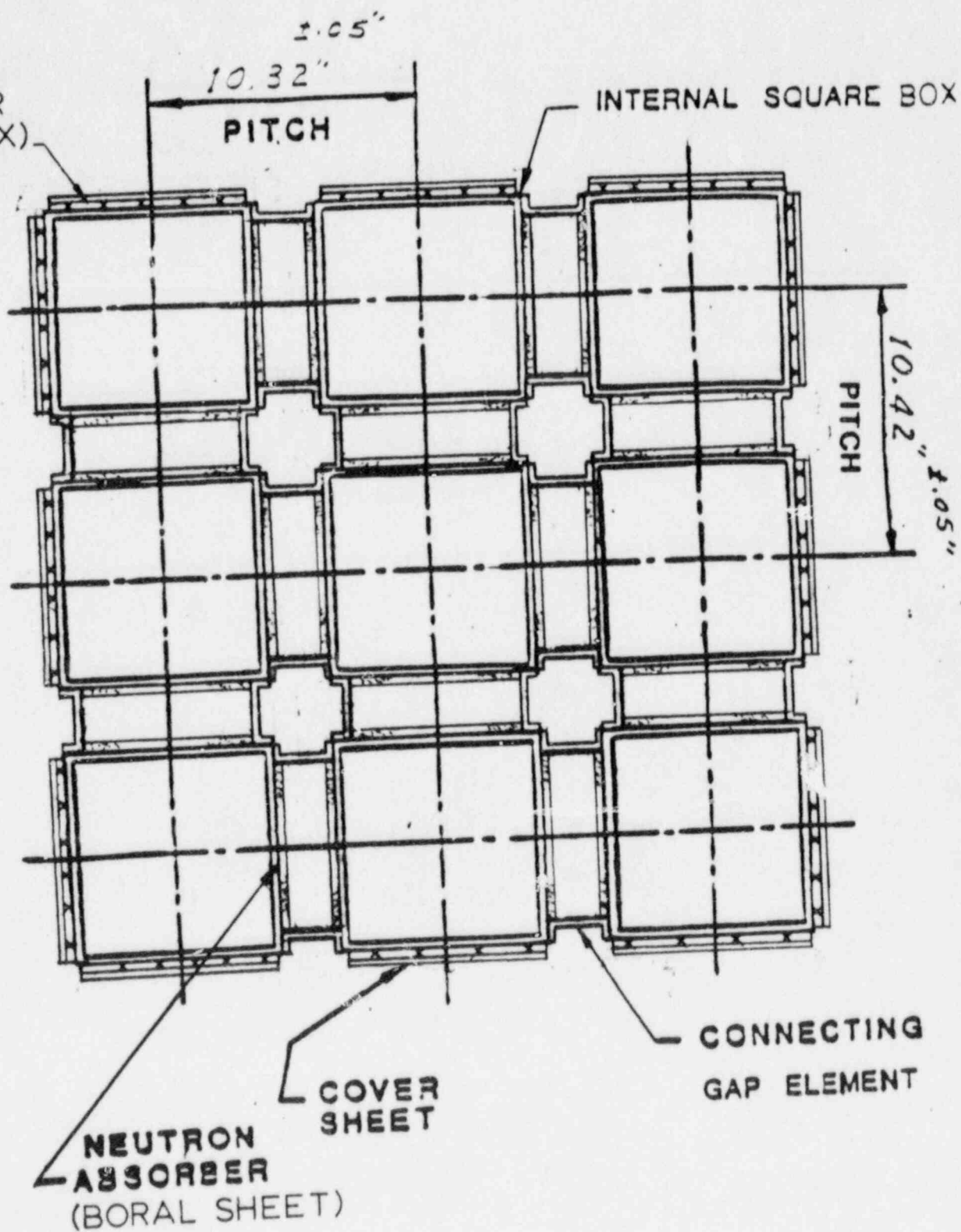


FIGURE 3.1a 3 x 3 TYP. ARRAY REGION 1

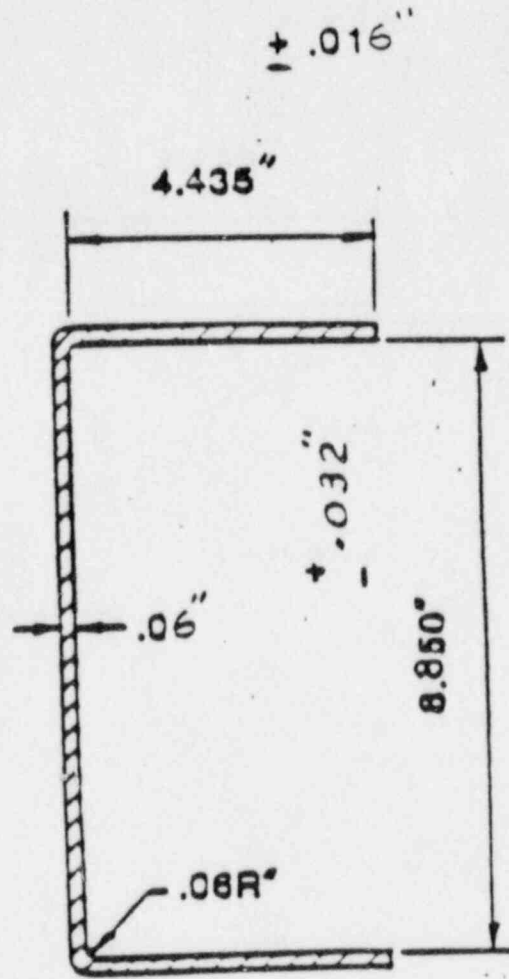


FIGURE 3.2 CHANNEL ELEMENT - REGION 1 & 2 (2 FOR SQUARE CELL)

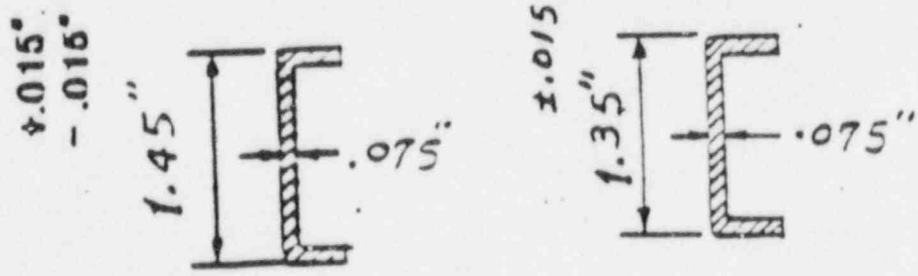


FIGURE 3.3 GAP ELEMENTS

REGION 1



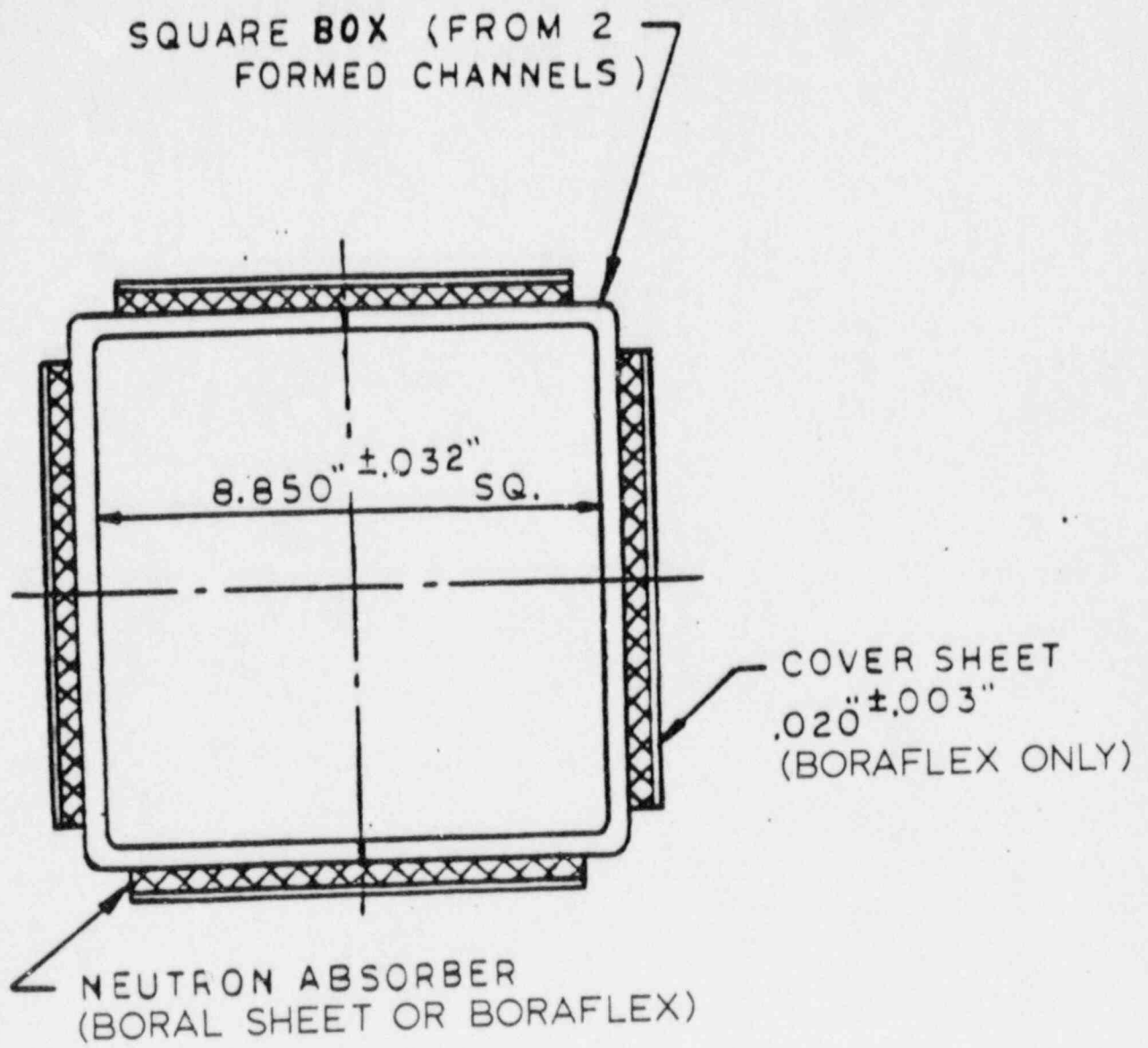


FIG. 3.4 COMPOSITE BOX ASSEMBLY - REGION I

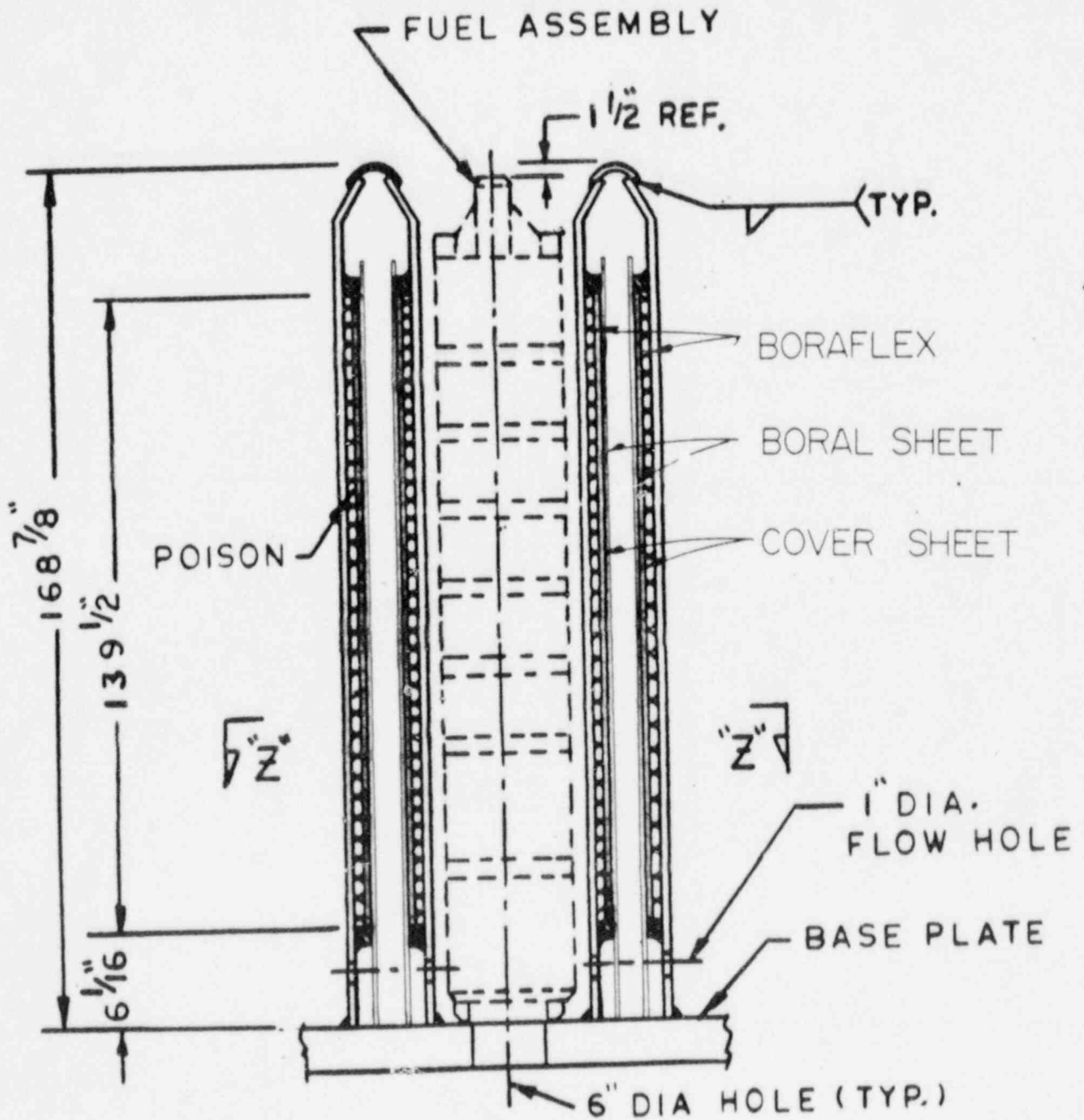
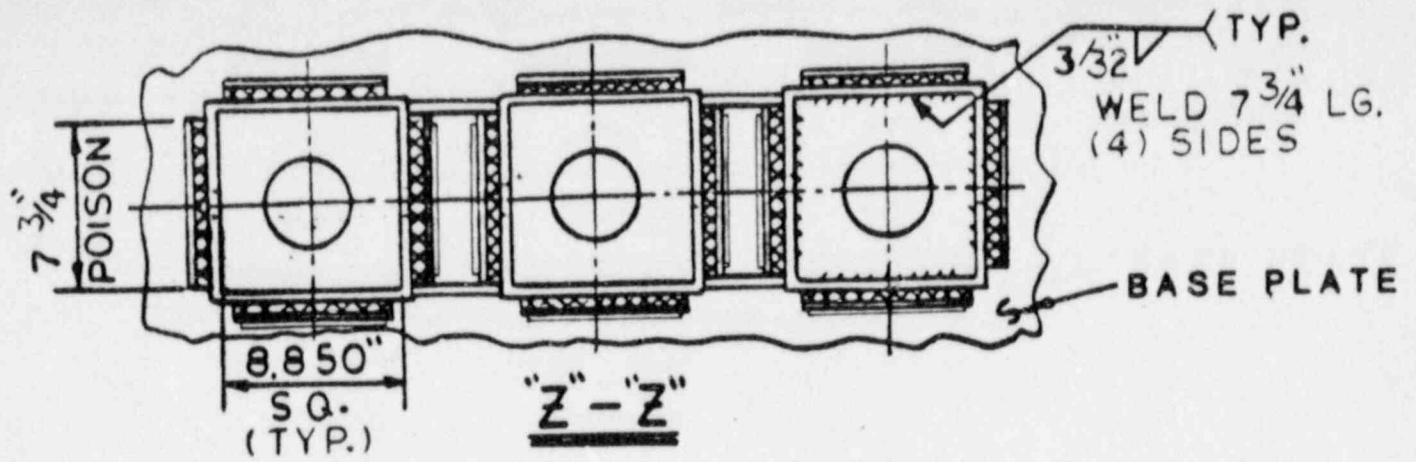


FIG. 3.5a TYPICAL CELL ELEVATION -REGION 1

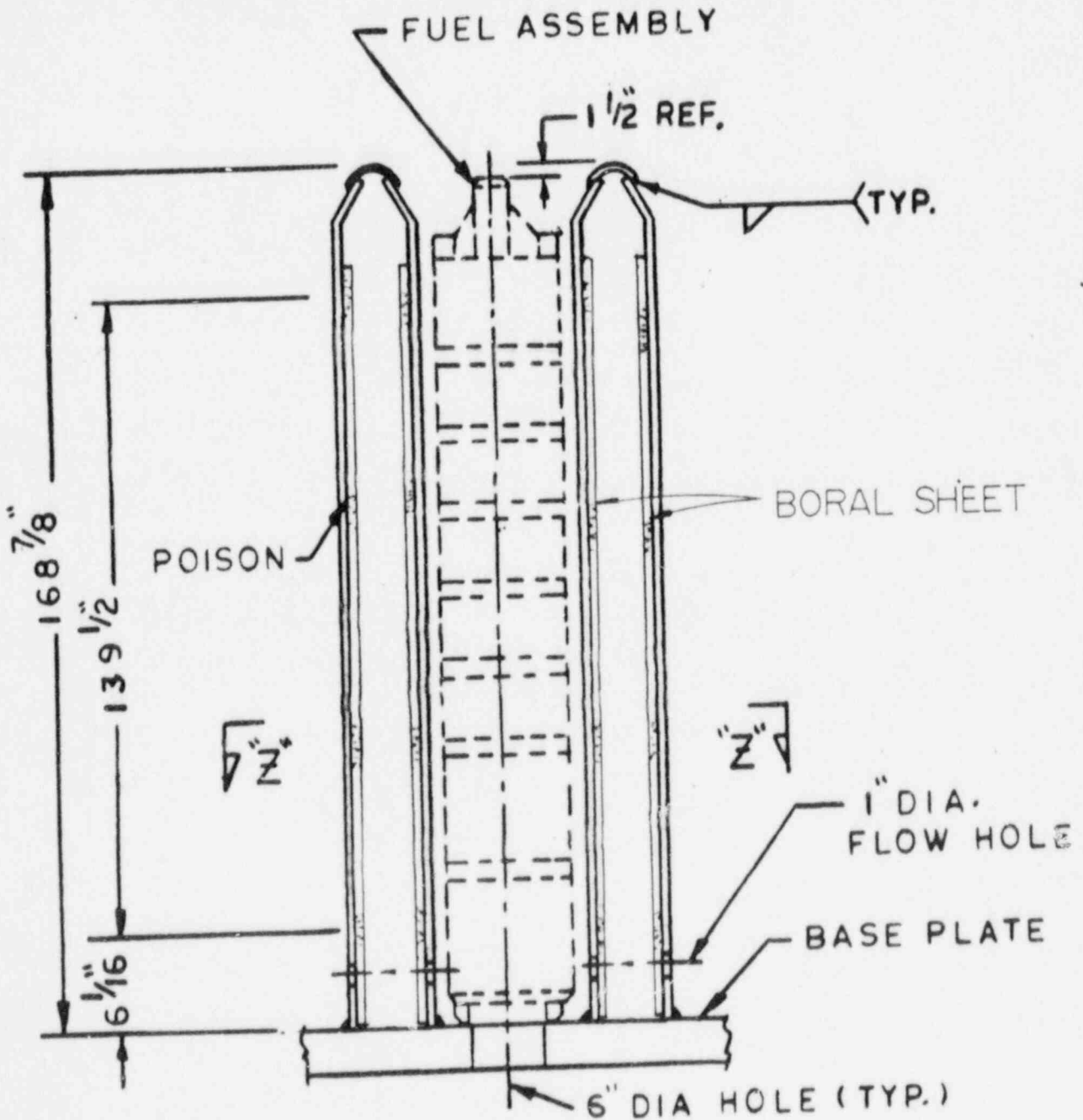
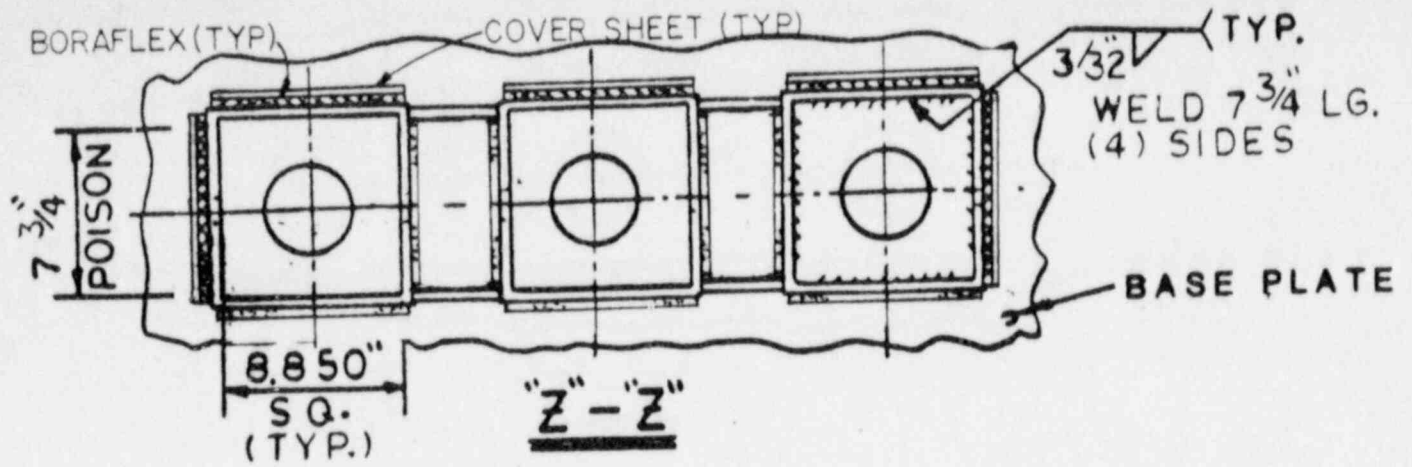


FIG. 3.5a.1 TYPICAL CELL ELEVATION - REGION 1

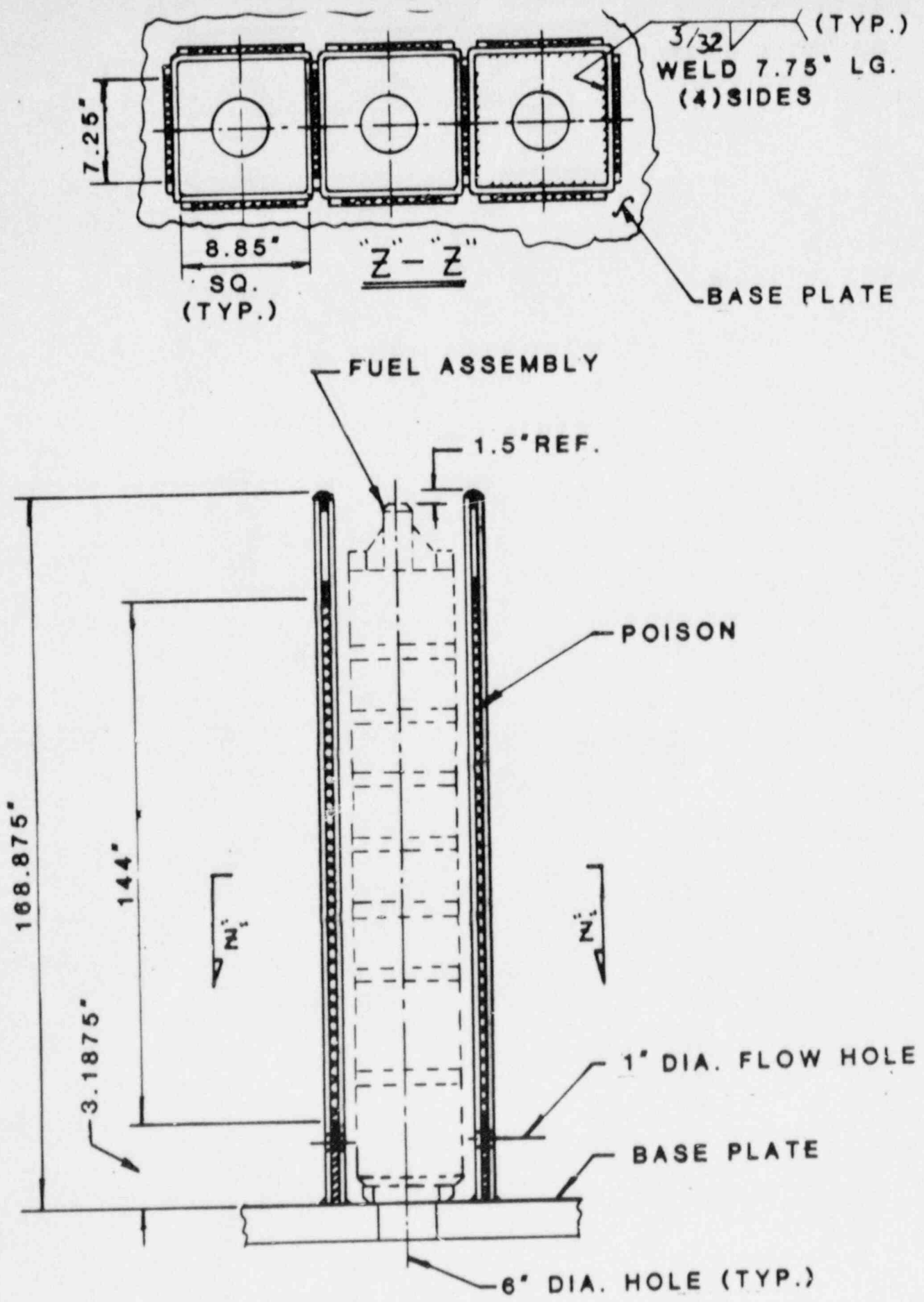


FIG. 3.5b TYPICAL CELL ELEVATION-REGION 2

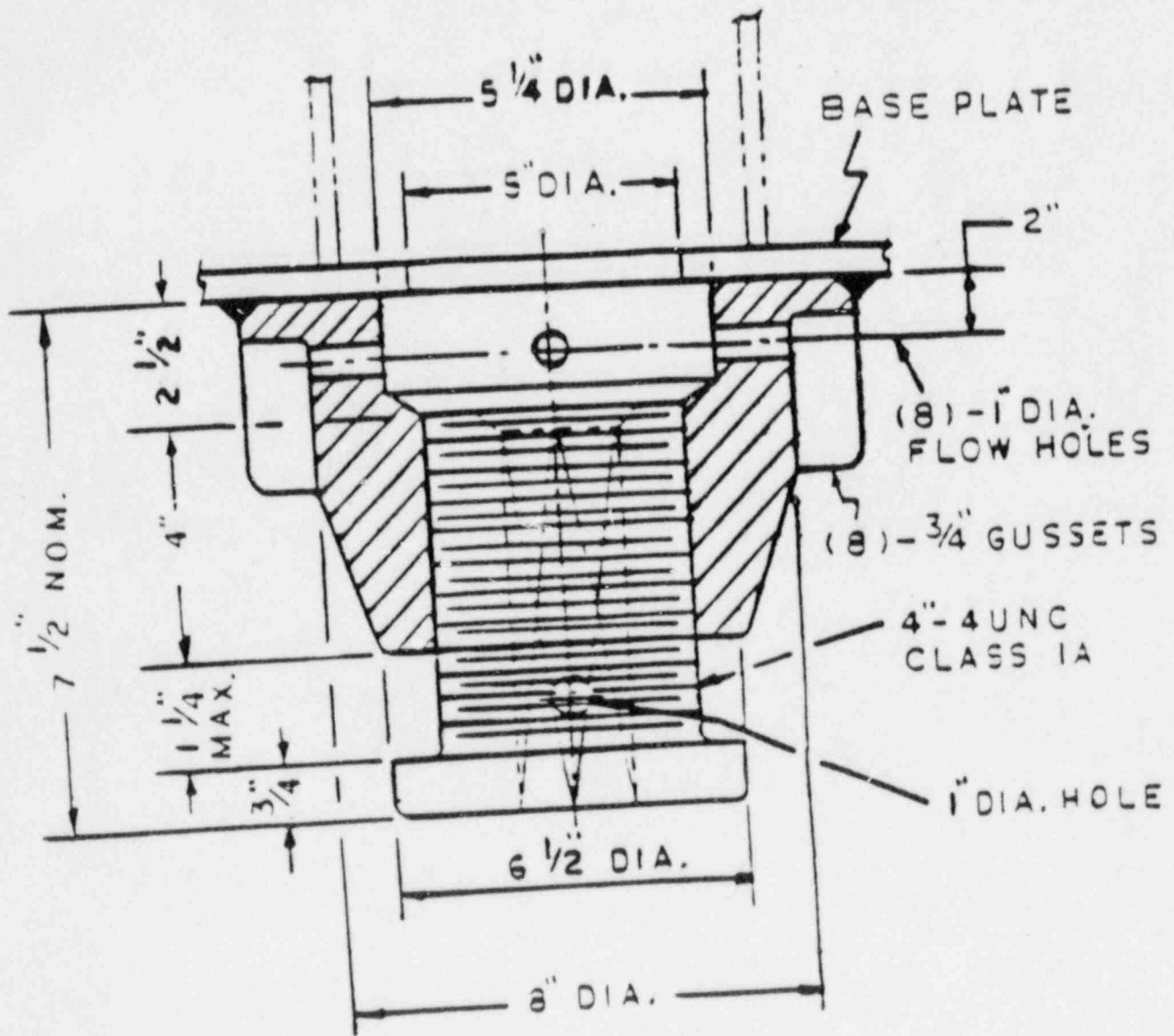


FIG. 3.6A ADJUSTABLE SUPPORT

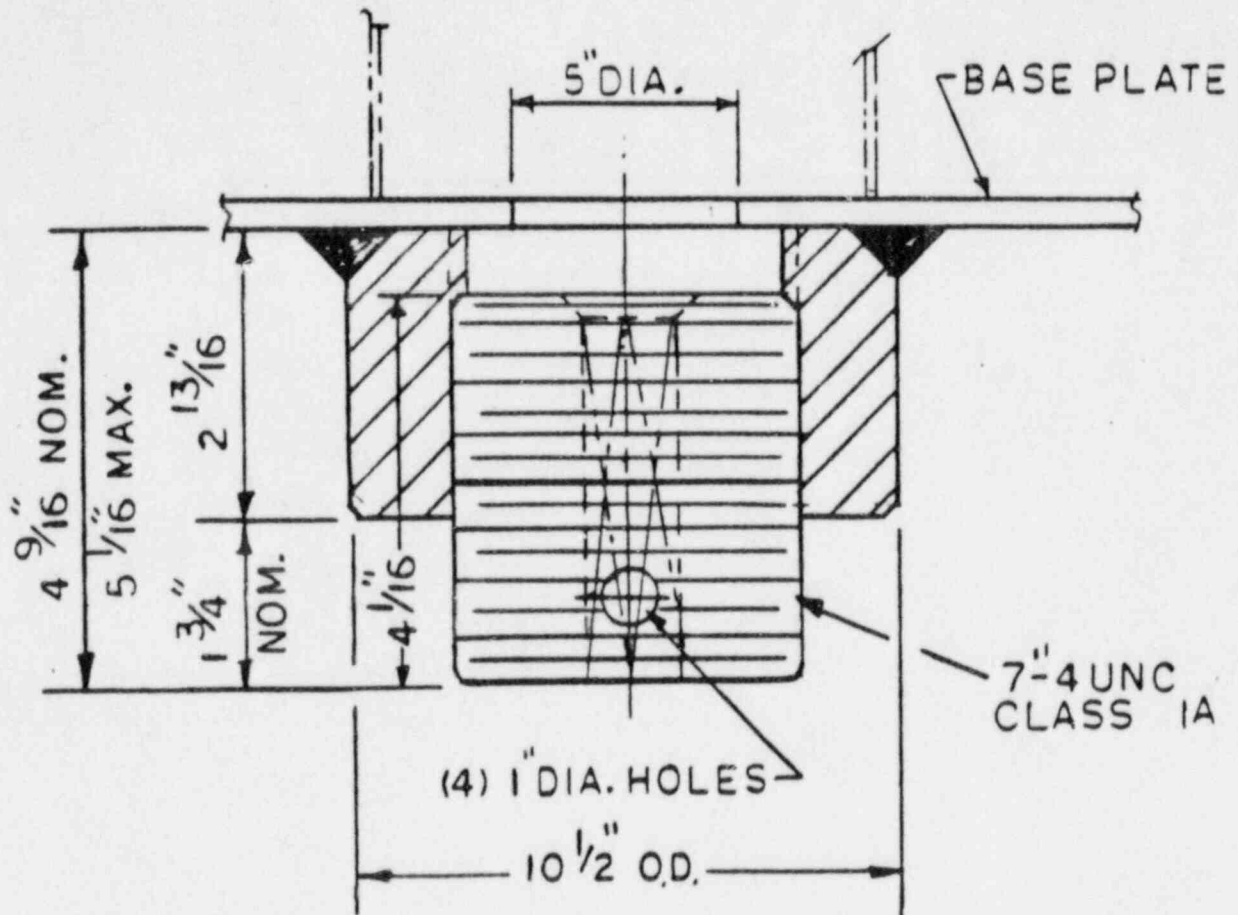
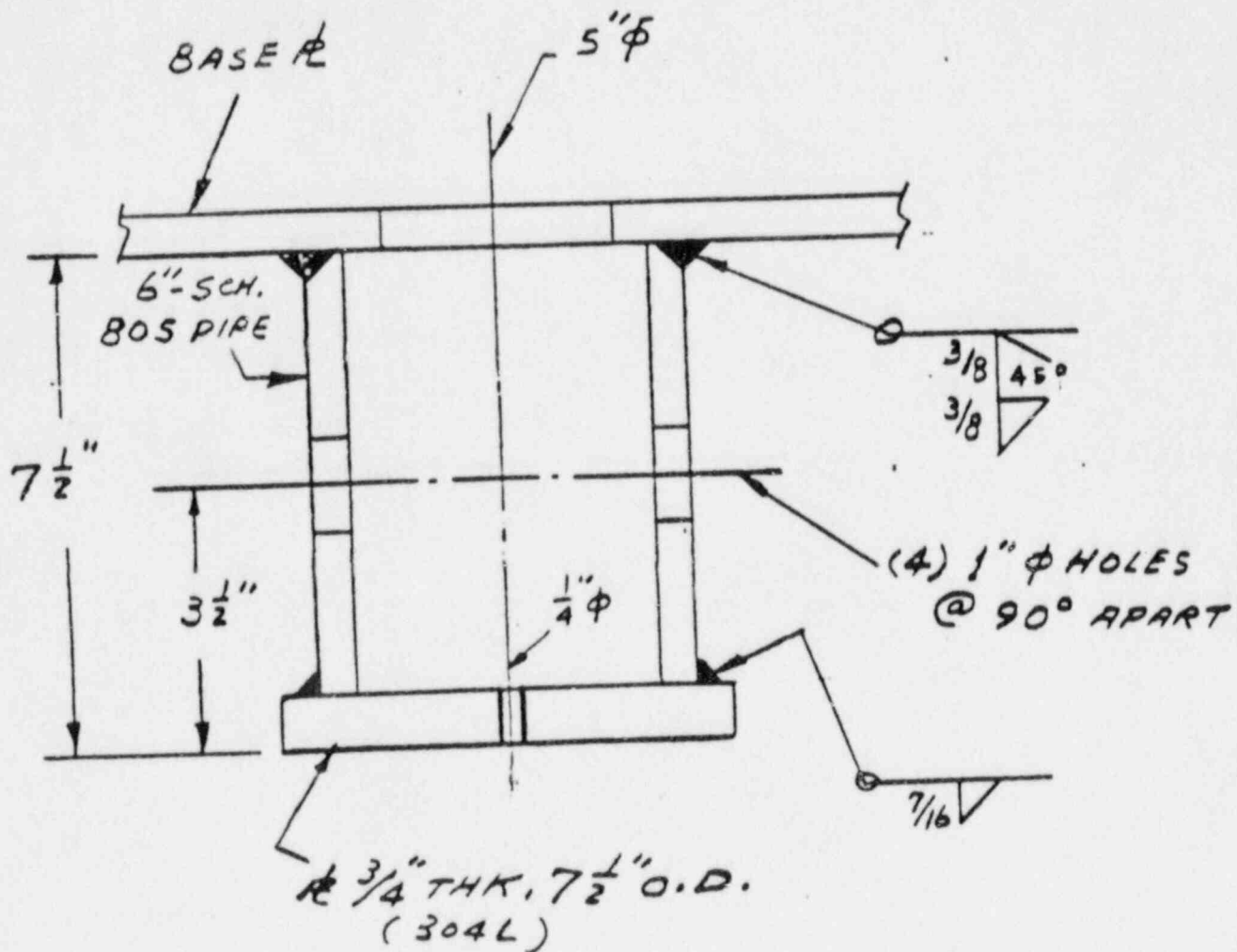


FIG. 3.6 B SHORT ADJUSTABLE SUPP'T.



SMALL FIXED SUPPT

FIGURE 3.6C



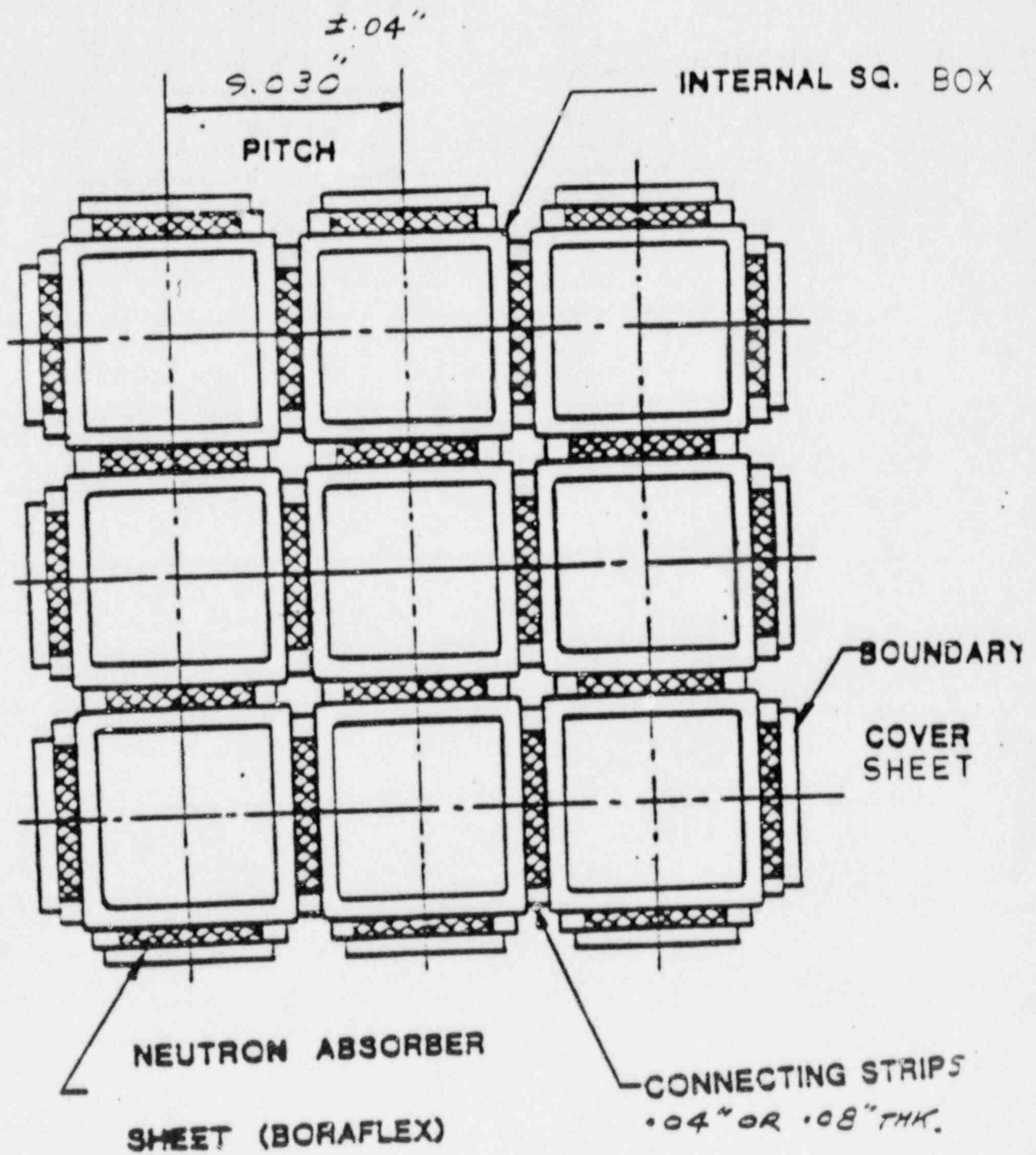


FIGURE 3.7

3 X 3 TYPICAL ARRAY REGION

NOTE: Connecting strips vary in thickness from .040" to .080", resulting in average wall to wall separation of .06" in as-welded condition.



## 4.0 NUCLEAR CRITICALITY ANALYSIS

### 4.1 DESIGN BASES

The high density spent fuel storage racks for the Byron Nuclear Power Station are designed to assure that the neutron multiplication factor ( $k_{eff}$ ) is equal to or less than 0.95 with the racks fully loaded with fuel of the highest anticipated reactivity in each of two regions, and flooded with unborated water at temperature corresponding to the highest reactivity. The maximum calculated reactivity includes a margin for uncertainty in reactivity calculations and in mechanical tolerances, statistically combined, such that the true  $k_{eff}$  will be equal to or less than 0.95 with a 95% probability at a 95% confidence level.

Applicable codes, standards, and regulations, or pertinent sections thereof, including the following:

- 0 General Design criterion 62, Prevention of Criticality in Fuel Storage and Handling.
- 0 USNRC Standard Review Plant, NUREG-0800, Section 9.1.1, New Fuel Storage, and Section 9.1.2, Spent Fuel Storage.
- 0 USNRC letter of April 14, 1978, to all Power Reactor Licensees - OT Position for Review and Acceptance of Spent Fuel Storage and Handling Applications, including modification letter dated January 18, 1979.
- 0 USNRC Regulatory Guide 1.13, Spent Fuel Storage Facility Design Basis, Rev. 2 (proposed), December 1981.
- 0 USNRC Regulatory Guide 3.41, Validation of Computational Methods for Nuclear Criticality Safety (and related ANSI N16.9-1975).
- 0 ANSI/ANS-57.2-1983, Design Requirements for Light Water Reactor Spent Fuel Storage Facilities at Nuclear Power Plants.
- 0 ANSI N210-1976, Design Objectives for Light Water Reactor Spent Fuel Storage Facilities at Nuclear Power Plants.
- 0 ANSI N18.2-1973, Nuclear Safety Criteria for the Design of Stationary Pressurized Water Reactor Plants.

To assure the true reactivity will always be less than the calculated reactivity, the following conservative assumptions were made:

- 0 Moderator is pure, unborated water at a temperature corresponding to the highest reactivity.
- 0 Lattice of storage racks is assumed infinite in all directions, i.e., no credit is taken for axial or radial neutron leakage (except in the assessment of certain abnormal/accident conditions).
- 0 Neutron absorption in minor structural members is neglected, i.e., spacer girds are replaced by water.

The design basis fuel assembly is a 17x17 Westinghouse optimized fuel assembly containing UO<sub>2</sub> at a maximum initial enrichment of 4.2% U-235 by weight, corresponding to 48.6 grams U-235 per axial centimeter of fuel assembly. Two separate storage regions are provided in the spent fuel storage pool, with separate criteria defining the highest anticipated reactivity in each of the two regions as follows:

- 0 Region 1 is designed to accommodate new fuel with a maximum enrichment of 4.2 wt% U-235, or spent fuel regardless of the discharge fuel burnup.
- 0 Region 2 is designed to accommodate fuel of various initial enrichments which have accumulated minimum burnups within an acceptable bound as depicted in Figure 4.1.

## 4.2 SUMMARY OF CRITICALITY ANALYSES

### 4.2.1 Normal Operating Conditions

The criticality analyses of each of the two separate regions of the spent fuel storage pool previously described are summarized in Table 4.1 for the anticipated normal storage conditions. The calculated maximum reactivity in Region 2 includes a burnup-dependent allowable for uncertainty in depletion calculations and, furthermore, provides an additional margin of more than 2%  $k$  below the limiting effective multiplication factor ( $k_{eff}$ ) of 0.95. As cooling time increases in long-term storage, decay of Pu-241 results in a significant decrease in reactivity, which will provide an increasing subcriticality margin and tends to further compensate for any uncertainty in depletion calculations. Spacing between the two different rack modulus is sufficient to preclude adverse nuclear interaction between modules.

Region 2 can accommodate fuel of various initial enrichments and discharge fuel burnups, provided the combination falls within the acceptable domain illustrated in Figure 4.1. For convenient reference, the minimum burnup values in Figure 4.1 have been fitted by linear tangents at various values and the results are tabulated below.

<u>Initial Enrichment, %</u>	<u>Minimum Burnup, MWD/MTU</u>	<u>Initial Enrichment, %</u>	<u>Minimum Burnup, MWD/MTU</u>
1.52	0	3.00	22,490
1.80	5,230	3.20	25,000
2.00	8,750	3.40	27,510
2.20	11,340	3.60	30,020
2.40	14,390	3.80	32,540
2.60	17,050	4.00	34,960
2.80	19,700	4.20	37,370

Linear interpolation between the tabulated values will always yield values on or conservatively above the curve of limiting burnups.

These data will be implemented in appropriate administrative procedures to assure verified burnup as specified in draft Regulatory Guide 1.13, Revision 2. Administrative procedures will also be employed to confirm and assure the presence of soluble poison in the pool water during fuel handling operations, as a further margin of safety and as a precaution in the event of fuel misplacement during fuel handling operations as discuss in Section 4.2.2.

#### 4.2.2 Abnormal and Accident Conditions

Although credit for the soluble poison normally present in the spent fuel pool water is permitted under abnormal or accident conditions,\* most abnormal or accident conditions will not result in exceeding the Limiting reactivity ( $k_{eff}$  of 0.95) even in the absence of soluble poison. The effects on reactivity of credible abnormal and accident conditions are summarized in Table 4.2. Of these abnormal/accident conditions, only one has the potential for a more than negligible positive reactivity effect.

\*Double contingency principle of ANSI N16.1-1975, as specified in the April 14, 1978, NRC letter (Section 1.2) and implied in the proposed revision (draft) to Regulatory Guide 1.13 (Section 1.4, Appendix A).

The inadvertent misplacement of a new fuel assembly (either into a Region 2 storage cell or outside and adjacent to a rack module) has the potential for exceeding the limiting reactivity should there be a concurrent and independent accident condition resulting in the loss of all soluble poison.

Administrative procedures to assure the presence of soluble poison during fuel handling operations will preclude the possibility of the simultaneous occurrence of these two independent accident conditions. The largest reactivity increase occurs from accidentally placing a new fuel assembly into a Region 2 storage cell with all other cells fully loaded. Under this condition, the presence of only 300 ppm soluble boron assures that the infinite multiplication factor would not exceed the design basis reactivity for Region 2. With the nominal concentration of soluble poison present (2000 ppm boron), the maximum reactivity,  $k_B$ , is less than 0.95 even if Region 2 were to be fully loaded with fresh fuel of 4.2% enrichment.

#### 4.2.3 New Fuel Storage

Region 1 of the storage racks is designed to safely accommodate new unirradiated fuel of 4.2% enrichment, when fully flooded with clean unborated water. Under certain circumstances, it may be desirable to store new fuel in the dry condition in Region 1 or to utilize Region 2 for the temporary storage of new fuel, either dry or fully flooded. These conditions were analyzed to assure the acceptability of Region 1 in the dry condition and to determine an arrangement in Region 2 that would assure criticality safety in conformance with the requirements of SRP9.1.1, "New Fuel Storage."

Criticality analyses confirmed that Region 1 does not exhibit a peak in reactivity at low moderator densities (e.g., for or foam moderation) and that the optimum moderation (highest  $k_{eff}$ ) occurs for the fully flooded condition. This condition is the design basis for Region 1 where the maximum  $k_B$ , including all uncertainties, is less than 0.947.

In Region 2, it was determined that a checkerboard pattern (fuel assemblies aligned diagonally) provided an acceptable  $k_B$ , in either the fully flooded or the dry (low density moderation) condition for new fuel assemblies of 4.2%

enrichment. These calculations indicated a nominal  $k_B$  of  $0.813 \pm 0.014$  (1s) when fully flooded with clean unborated water--a value substantially less than the limiting  $k_{eff}$  of 0.95, even with an additional allowance for uncertainties (maximum  $k_B$  of 0.86 at 95%/95% tolerance limits).

Calculations, using Monte Carlo techniques, did not reveal a peak in reactivity at low moderator densities, and fully flooded condition corresponds to the highest reactivity (optimum moderation). Thus, the checkerboard pattern of new 4.2% enriched fuel in Region 2 represents a safe configuration in conformance with SRP 9.1.1. and 9.1.2.

#### 4.3 REFERENCE FUEL STORAGE CELL

##### 4.3.1 Reference Fuel Assembly

The design basis fuel assembly, illustrated in Figure 4.2, is a 17x17 array of fuel rods with 25 rods replaced by 24 control rod guide tubes and 1 instrument thimble. Table 4.3 summarizes the Westinghouse optimized fuel assembly (OFA) design specifications and the expected range of significant variations.

##### 4.3.2 Region 1 Storage Cells

The nominal spent fuel storage cells used for the original criticality analyses of Region 1 storage cells is shown in Figure 4.2.1. The rack is composed of Boraflex absorber material sandwiched between a 0.060-inch inner stainless steel box and a 0.020-inch outer stainless steel (SS) coverplate (0.125-inch coverplate for module periphery cell walls). The fuel assemblies are centrally located in each storage cell on a nominal lattice spacing of  $10.320 \pm 0.050$  inches in one direction and  $10.420 \pm 0.050$  inches in the other direction. Stainless steel gap channels connect one storage cell box to another in a rigid structure and define an outer water space between boxes. This outer water space constitutes a flux-trap between the two Boraflex absorber sheets that are essentially opaque (black) to thermal neutrons. The Boraflex absorber has a thickness of  $0.075 \pm 0.007$  inch and a nominal B-10 areal density of 0.0238 gram per  $cm^2$ .

Figure 4.2.2 shows the nominal cell modified with Boral inserts. The Boral has a minimum B-10 loading of  $.020\text{gm/cm}^2$  and thickness of  $.075 \pm .004$  inch. The minimum boron loading is combined with the maximum thickness as a "worst case" conservatism. The Boral plates are to be flush with the Boraflex cover plate. However a manufacturing tolerance allowing  $.125$  inch clearance is assumed for the analysis.

Figure 4.2.3 shows the cell with Boral replacing Boraflex. The cover plate has been eliminated as it serves no useful purpose. The Boral has a minimum B-10 loading of  $0.025\text{ gm/cm}^2$  and a thickness of  $.085 \pm .004$  inch. These are again used simultaneously for a "worst case" calculation.

#### 4.3.3 Region 2 Storage Cells

Region 2 storage cells were initially designed for fuel of 3.2 wt% U-235 initial enrichment burned to 25,000 MWD/MTU and extended to encompass fuel of 4.2% initial enrichment burned to 37,370 MWD/MTU. In this region, the storage cells are composed of a single Boraflex absorber sandwiched between the 0.060-inch stainless steel walls of adjacent storage cells. These cells shown in Figure 4.3, are located on a lattice spacing of  $9.03 \pm 0.04$  inches.

### 4.4 ANALYTICAL METHODOLOGY

#### 4.4.1.1 Reference Analytical Methods and Bias for Nominal Case

The CASMO-2E computer code (References 1, 2 and 3), a two-dimensional multigroup transport theory code for fuel assemblies, has been benchmarked (see Appendix A) and is used both as a primary method of analysis and as a means of evaluating small reactivity increments associated with manufacturing tolerances. CASMO-2E benchmarking resulted in a calculational bias of  $0.0013 \pm 0.0018$  (95%/95%).

In fuel rack analyses, for independent verification, criticality analyses of the high density spent fuel storage racks were also performed with the AMPX-KENO computer package (References 4 and 5), using the 27-group SCALE\* cross-



section library (Reference 6) with the NITAWL subroutine for U-238 resonance shielding effects (Nordheim integral treatment). Details of the benchmark calculations with the 27-group SCALE cross-section library are also presented in Appendix A. These benchmark calculations resulted in a bias of  $0.0106 \pm 0.0048$  (95%/95%).

In the geometric model used in KENO, each fuel rod and its cladding were described explicitly. For two-dimensional X-Y analysis, a zero current (white albedo) boundary condition was applied in the axial direction and, for Region 1, at the centerline through the outer water space (flux-trap) on all four sides of the cell, effectively creating an infinite array of storage cells. In Region 2, the zero current boundary condition was applied at the center of the Boraflex absorber sheets between storage cells. The AMPX-KENO Monte Carlo calculations inherently include a statistical uncertainty due to the random nature of neutron tracking. To minimize the statistical uncertainty of the KENO-calculated reactivity, a total of 50,000 neutron histories is normally accumulated for each calculation, in 100 generations of 500 neutrons each.

CASMO-2E is also used for burnup calculations, with independent verification by EPRI-CELL and NULIF calculations. In tracking long-term (30 year) reactivity effect of spent fuel stored in Region 2 of the fuel storage rack, EPRI-CELL calculations indicate a continuous reduction in reactivity with time (after Xe decay) due primarily to Pu-241 decay and Am-241 growth.

A third independent method of criticality analysis, utilizing diffusion/blackness theory, was also used for additional confidence in results of the primary calculational methods, although no reliance for criticality safety is placed on the reactivity value from the diffusion/blackness theory technique. This technique, however, is used for auxiliary calculations of small incremental reactivity effects (e.g., axial cutback or mechanical tolerances) that would otherwise be lost in normal KENO statistical variations, or would be inconsistent with CASMO-2E geometry limitations.

\*SCALE is an acronym for Standard Computer Analysis for Licensing Evaluation.



Cross sections for the diffusion/blackness theory calculations were derived from CASMO-2E or calculated by the NULIF computer code (Reference 7), supplemented by a blackness theory routine that effectively imposes a transport theory boundary condition at the surface of the Boraflex neutron absorber. Two different spatial diffusion theory codes, PDQ07 (Reference 8 in two dimensions and SNEID\* in one dimension, were used to calculate reactivities. The two-dimensional PDQ07 code was used to describe the actual storage cell geometry, with NULIF cell-homogenized constants representing each fuel rod and its associated water moderator. SNEID is one-dimensional model, in cylindrical or slab geometry, used for the calculation of axial cutback reactivity effects and in the assessment of abnormal occurrences.

#### 4.4.1.2 Analytical Methods and Bias for Modified Cases

The design method used to demonstrate the criticality safety of fuel in the modified fuel storage racks uses the AMPX system of computer codes [4] for cross-section generation (NITAWL-S and XSDRNPM-S), and the KENO-IV (CRC) code [5] for reactivity determination. Tolerance variations of the nominal case were then applied.

An ORNL 227 energy group ENDF/B-V cross-section library [15,16] was utilized for the criticality analysis. The NITAWL program computes resonance cross-sections and prepares a 227 neutron group  $P_3$  cross-section data file for use in the XSDRNPM one-dimensional  $S_n$  neutron transport code. The Nordheim Integral Treatment [17] used. Energy and spatial weighting of cross-sections to reduce the 227 group data to 27 group (SCALE) data is performed by the XSDRNPM program. Zone weighted cross-sections are used in the fuel regions that are modeled as discrete fuel rods in KENO. Discrete modeling of structural regions such as the storage cell structures also use zone weight cross-sections.

\*SNEID is one-dimensional diffusion theory routine developed by Black & Veatch and verified by comparison with PDQ07 one-dimensional calculations.

KENO-IV is used in the evaluation of criticality of the Byron storage racks. KENO-IV is a three-dimensional Monte Carlo theory program designed for reactivity calculations.

The calculational method and cross-section values which were used in the criticality analysis of the fuel storage racks have been verified by comparison with critical experiment data for assemblies similar to those for which the racks are designed. This benchmarking data is sufficiently diverse to establish that the method bias and uncertainty will apply to fuel storage rack conditions which include strong neutron absorbers and low moderator densities.

A set of 33 critical experiments has been analyzed to demonstrate its applicability to criticality analysis and to establish the method bias and variability. The experiments range from water moderated oxide fuel array separated by various materials (BORAL, steel and water) that simulate LWR fuel shipping and storage conditions [18], to dry, harder spectrum uranium metal cylinder arrays with various interspersed materials [19] (Plexiglas, paraffin and air) that demonstrate the wide range of applicability of the method.

The results and some descriptive factors about each of the 33 benchmark critical experiments are give in Table 4.9. The average  $K_{eff}$  of the benchmarks is 0.9917 which demonstrates that there is a 0.0083 bias associated with the method. The standard deviation of the  $K_{eff}$  values is 0.00082  $\Delta k$ . The 95/95 one-side tolerance limit factor for 33 values is 2.19. There is a 95 percent probability with 95 percent confidence level that the uncertainty in reactivity, due to the method, is not greater than 0.0018  $\Delta k$ .

#### 4.4.2 Fuel Burnup Calculations

Fuel burnup calculations in the hot operating condition were performed primarily with the CASMO-2E code. However, to enhance the credibility of the burnup calculations (in lieu of critical experiments), the CASMO-2E results were independently checked by calculations with the NULIF code (Reference 7) and with EPRI-CELL (Reference 9). Figure 4.4 compares results of these

independent methods of burnup analysis under hot reactor operating conditions. The results agree within 0.008 Wk in the hot operating condition.

In addition to depletion calculations under hot operating conditions, reactivity comparisons under conditions more representative of fuel to be stored in the racks (cold, xenon-free) are also significant in storage rack criticality analyses. Table 4.4 compares the cold, xenon-free reactivities calculated by CASMO-2E, NULIF/PDQ07, and EPRI-CELL. In the cold condition, the CASMO-2E calculations gave a slightly higher reactivity value for the Region 2 fuel storage cell and the good agreement generally observed lends credibility to the calculations, particularly in view of the known bias and uncertainty in CASMO-2E calculations (Appendix A).

No definitive method exists for determining the uncertainty in burnup-dependent reactivity calculations. All of the codes discussed above have been used to accurately follow reactivity loss rates in operating reactors. CASMO-2E has been extensively benchmarked (Appendix A; References 1, 2, 3 and 10) against cold, clean, critical experiments (including plutonium-bearing fuel), Monte Carlo calculations, reactor operations, and heavy-element concentrations in irradiated fuel. In particular, the analyses (Reference 10) of 11 critical experiments with plutonium-bearing fuel gave an average  $k_{eff}$  of  $1.002 \pm 0.011$  (95%/95%), showing adequate treatment of the plutonium nuclides. In addition, Johansson (Reference 11) has obtained very good agreement in calculations of close-packed, high-plutonium-content, experimental configurations.

Since critical-experiment data with spent fuel is not available, it is necessary to assign an uncertainty in reactivity based on other considerations, supported by the close agreement between different calculational methods and the general industry experience in predicting reactivity loss rates in operating plants. Over a considerable portion of the burnup, the reactivity loss rate in PWRs is approximately 0.01 Wk for each 1,000 MWD/MTU, becoming somewhat smaller at the higher burnups. By conservatively assuming an uncertainty in reactivity\* of  $0.5 \times 10^{-6}$  times the burnup in MWD/MTU, a burnup-dependent uncertainty is defined that increases

with increasing fuel burnup, as would be reasonably expected. This assumption provides an estimate of the burnup uncertainty that is more conservative and bounds estimates frequently employed in other fuel rack licensing applications (i.e., 5% of the total reactivity decrement). Table 4.5 summarizes results of the burnup analyses and estimated uncertainties. These uncertainties are appreciably larger, in general, than would be suggested by the industry experience in predicting reactivity loss rates and boron let-down curves over many cycles in operating plants. The increasing level of conservatism at the higher fuel burnups provides an adequate margin in the uncertainty estimate to accommodate the possible existence of a small positive reactivity increment from the axial distribution in burnup (see Section 4.4.3). In addition, although the burnup uncertainty may be either positive or negative, it is treated as an additive term rather than being combined statistically with other uncertainties. Thus, the allowance for uncertainty in burnup calculations is believed to be a conservative estimate, particularly in view of the substantial reactivity decrease with aged fuel as discussed in Section 4.4.4.

#### 4.4.3 Effect of Axial Burnup Distribution

Initially, fuel loaded into the reactor will burn with a slightly skewed cosine power distribution. As burnup progresses, the burnup distribution will tend to flatten, becoming more highly burned in the central regions than in the upper and lower ends. This effect may be clearly seen in the curves compiled in Reference 12. At high burnup, the more reactive fuel near the ends of the fuel assembly (less than average burned) occurs in regions of lower reactivity worth due to neutron leakage. Consequently, it is expected that distributed-burnup fuel assemblies would exhibit a slightly lower reactivity than that calculated for the average burnup. As burnup progresses, the distribution, to some extent, tends to be self-regulating as controlled by the axial power distribution, precluding the existence of large regions of significantly reduced burnup.

A number of one-dimensional diffusion theory analyses have been made based upon calculated and measured axial burnup distributions. These analyses confirm the minor and generally negative reactivity effect of axially

distributed burnup. The trends observed, however, suggest the possibility of a small positive reactivity effect at the high burnup values, and the uncertainty in  $k_B$  due to burnup, assigned at the higher burnups (Section 4.4.2), is adequately conservative to encompass the potential for a small positive reactivity effect of postulated axial burnup distributions. Furthermore, reactivity decreases with time in storage (Section 4.4.4), and, in addition, there is a large margin in reactivity ( $>0.02$  Wk) below the limiting  $k_{eff}$  value (0.95) which can accommodate any reasonable reactivity effects that might be larger than expected.

#### 4.4.4 Long-Term Decay

Since the fuel racks in Region 2 are intended to contain spent fuel for long periods of time, calculations were made using EPRI-CELL (which incorporates the CINDER code) to follow the long-term changes in reactivity of spent fuel over a 30-year period. CINDER tracks the decay and burnup dependence of some 179 fission products. Early in the decay period, xenon grows in (reducing reactivity) and subsequently decays, with the reactivity reaching a maximum at 100-200 hours. The decay of Pu-241 (13-year half-life) and growth of Am-241 substantially reduce reactivity during long term storage, as indicated in Table 4.6. The reference design criticality calculations do not take credit for this long-term reduction in reactivity, other than to indicate an increasing subcriticality margin in Region 2 of the spent fuel storage pool.

### 4.5 REGION 1 CRITICALITY ANALYSIS AND TOLERANCE VARIATIONS

#### 4.5.1 Nominal Design Case

Under normal conditions, with nominal dimensions, the  $k_B$  values calculated by the three methods of analysis are as follows:

<u>Analytical Method</u>	<u>Bias-corrected <math>k_B</math></u>	<u>Maximum <math>k_B</math> (95%/95%)</u>
CASMO-2E	$0.9387 \pm 0.0018$	0.9405
AMPX-KENO	$0.9301 \pm 0.0061$	0.9362
Diffusion blackness theory	0.9393	0.9393



The AMPFX-KENO calculations include a one-sided tolerance factor (Reference 13) of 1.799 corresponding to 95% probability at a 95% confidence limit. For the nominal design case, the CASMO-2E calculation yields the highest (most conservative) reactivity, and, therefore, the independent verification calculations substantiate CASMO-2E as the primary calculational method.

#### 4.5.2 Boron Loading Verification

The Boraflex absorber sheets used in Region 1 storage cells are nominally 0.075-inch thick, with a B-10 areal density of 0.0238 g/cm<sup>2</sup>. Independent manufacturing tolerance limits are  $\pm 0.007$  inch in thickness and  $\pm 0.0017$  g/cm<sup>2</sup> in B-10 content. This assures that at any point where the minimum boron concentration (0.0221 gram B-10/cm<sup>2</sup>) and minimum Boraflex thickness (0.068 inch) may coincide, the boron-10 areal density will not be less than 0.020 gram/cm<sup>2</sup>. Differential CASMO-2E calculations indicate that these tolerance limits result in an incremental reactivity uncertainty of  $\pm 0.0021$  Wk for boron content and  $\pm 0.0047$  for Boraflex thickness variations.

#### 4.5.3 Storage Cell Lattice Pitch Variation

The design storage cell lattice spacing between fuel assemblies in Region 1 is 10.32 inches in one direction and 10.42 inches in the other direction. A decrease in storage cell lattice spacing may or may not increase reactivity depending upon other dimensional changes that may be associated with the decrease in lattice spacing. Increasing the water thickness between the fuel and the inner stainless steel box results in a small increase in reactivity. The reactivity effect of the flux-trap water thickness, however, is more significant, and decreasing the flux-trap water thickness increases reactivity. Both of these effects have been evaluated for independent design tolerances.

The inner stainless steel box dimension,  $8.850 \pm 0.032$  inches, defines the inner water thickness between the fuel and the inside box. For the tolerance limit, the uncertainty in reactivity is  $\pm 0.0018$  Wk as determined by differential CASMO-2E calculations, with  $k_B$  increasing as the inner stainless steel box dimension (and derivative lattice spacing) increases.

The design flux-trap water thicknesses are  $1.160 \pm 0.040$  inches and  $1.260 \pm 0.040$  inches, which result in an uncertainty of  $\pm 0.0038$  Wk due to the tolerance in flux-trap water thickness, assuming the water thickness is simultaneously reduced on all four sides. Since the manufacturing tolerances on each of the four sides are statistically independent, the actual reactivity uncertainties would be less than  $\pm 0.0038$ , although the more conservative value has been used in the criticality evaluation.

#### 4.5.4 Stainless Steel Thickness Tolerances

The nominal stainless steel thickness in Region 1 is 0.60 inch for the inner stainless steel box and 0.020 inch for the Boraflex coverplate (0.125 inch on module boundary). The maximum positive reactivity effect of the expected stainless steel thickness tolerance variations, statistically combined, was calculated (CASMO-2E) to be  $\pm 0.0025$  Wk.

#### 4.5.5 Fuel Enrichment and Density Variation

The design maximum enrichment is  $4.20 \pm 0.05$  wt% U-235. Calculations of the sensitivity to small enrichment variations by CASMO-2E yielded a coefficient of 0.0047 Wk per 0.01 wt% U-235 at the design enrichment. For a tolerance on U-235 at the design enrichment. For a tolerance on U-235 enrichment of  $\pm 0.05$  in wt%, the uncertainty on  $\beta$  is  $\pm 0.0024$  Wk.

Calculations were made with the  $UO_2$  fuel density increased to maximum value of 97% theoretical density (TD). For the midrange value (95% TD) used for the reference design calculations, the uncertainty in reactivity is  $\pm 0.0026$  Wk over the range of  $UO_2$  densities expected.

#### 4.5.6 Boraflex Width Tolerance Variation

The reference storage cell design for Region 1 (Figure 4.2) uses a Boraflex blade width of  $7.75 \pm 0.0625$  inches. A positive increment in reactivity occurs for a decrease in Boraflex absorber width. For reduction in width of the maximum tolerance, 0.0625 inch, the calculated positive reactivity increment is  $+0.0007$  Wk.



#### 4.5.7 Axial Cutback of Boraflex

The axial length of the Boraflex poison material is less than the active fuel length by three inches at the top and at the bottom of the Revision 1 storage rack modules. To account for the reactivity effect of this axial cutback, one-dimensional (slab) diffusion theory calculations were made using flux-weighted homogenized diffusion theory constants edited from CASMO-2E calculations of the array of storage cells, with and without Boraflex present. In the one-dimensional calculations, an infinite (30-cm) water reflector was used above and below the fuel assembly, with the lengths of the unpoisoned "cutback" regions, top and bottom, varied in a series of parametric calculations. Results of these calculations showed that the  $k_{eff}$  remains less than the  $k_B$  of the reference central storage cell region, until the axial cutback exceeds four inches top and bottom. Thus, the actual axial neutron leakage more than compensates for the three-inch design cutback, and the reference infinite multiplication factor,  $k_B$ , remains a conservative overestimate of the true reactivity

### 4.6 REGION 2 CRITICALITY ANALYSIS AND TOLERANCE VARIATIONS

#### 4.6.1 Nominal Design Case

The principal method of analysis in Region 2 was CASMO-2E code, using the restart option in CASMO to transfer fuel of a specified burnup into the storage rack configuration at a reference temperature of 0°C. Calculations were made for fuel of several different initial enrichments and, for each enrichment, a limiting  $k_B$  value established which included an additional factor for uncertainty in the burnup analysis and for the axial burnup distribution. The restart CASMO-2E calculations (cold, clean, rack geometry) were then interpolated to define the burnup value yielding the limiting  $k_B$  value for each enrichment, as indicated in Table 4.7. These converged burnup values define the boundary of the acceptable domain shown in Figure 4.1.

At a burnup of 37,000 MWD/MTU, the sensitivity to burnup is calculated to be -0.0079 Wk per 1000 MWD/MTU. During long-term storage, the  $k_B$  values of the Region 2 fuel rack will decrease continuously from decay of Pu-241 as indicated in Section 4.4.4.

Two independent calculational methods were used to provide additional confidence in the reference Region 2 criticality analyses. Fuel of 1.5% initial enrichment (approximately equivalent to the reference rack design for burned fuel) was analyzed by AMPX-KENO (27-group SCALE cross-section library) and by the CASMO-2E model used for the Region 2 rack analysis. For this case CASMO-2E  $k_B$  (0.9014) was within the statistical uncertainty of the bias-corrected value ( $0.9043 \pm 0.0030$  (1s)) obtained in the AMPX-KENO calculations. This agreement confirms the validity of the primary CASMO-2E calculations.

The second independent method of analysis used the NULIF code for burnup analysis, and for generating diffusion theory constants (cold, clean) for the NULIF-calculated composition at 25,000 MWD/MTU with fuel of 3.2% initial enrichment. These constants, together with blackness theory constants for the Boraflex absorber, were then used in a two-dimensional PDQ07 calculation for the storage rack configuration. Results of this calculation ( $k_B$  of 0.9017) compared favorably with the CASMO-2E calculation for the same conditions ( $k_B$  of 0.9061) and thus tend to confirm the validity of the Primary calculational method.

#### 4.6.2 Boron Loading Variation

The Boraflex absorber sheets used in the Region 2 storage cells are nominally 0.041 inch thick with B-10 areal density of  $0.0130 \text{ g/cm}^2$ . Independent manufacturing limits are  $\pm 0.007$  inch in thickness and  $\pm 0.0009 \text{ g/cm}^2$  in B-10 content. This assures that at any point where the minimum boron concentration ( $0.01206 \text{ B-10 g/cm}^2$ ) and the minimum Boraflex thickness (0.034 inch) may coincide, the boron-10 areal density will not be less than  $0.010 \text{ g/cm}^2$ . Differential CASMO-2E calculations indicate that these tolerance limits result in an incremental reactivity uncertainty of  $\pm 0.0028$  Wk for boron content and  $\pm 0.0078$  Wk for Boraflex thickness.

#### 4.6.3 Storage Cell Lattice Pitch Variations

The value used for the storage cell lattice spacing between fuel assemblies in Region 2 is  $9.03 \pm 0.040$  inches, corresponding to an uncertainty in reactivity of 0.0011 Wk.

#### 4.6.4 Stainless Steel Thickness Tolerance

The nominal thickness of the stainless steel box wall is 0.060 inch with a tolerance limit of  $\pm 0.005$  inch, resulting in an uncertainty in reactivity of  $\pm 0.0001$  Wk.

#### 4.6.5 Fuel Enrichment and Density Variation

Uncertainties in reactivity due to tolerances on fuel enrichment and  $UO_2$  density in Region 2 are assumed to be the same as those determined for Region 1.

#### 4.6.6 Boraflex Width Tolerance

The reference storage cell design for Region 2 (Figure 4.3) uses a Boraflex absorber width of  $7.25 \pm 0.625$  inches. For a reduction in width of the maximum tolerance, the calculated positive reactivity increment is 0.0009 Wk.

### 4.7 ABNORMAL AND ACCIDENT CONDITIONS

#### 4.7.1 Eccentric Positioning of Fuel Assembly in Storage Rack

The fuel assembly is normally located in the center of the storage rack cell with bottom fittings and spacers that mechanically limit lateral movement of the fuel assemblies. Nevertheless, calculations were made with the fuel assemblies moved into the corner of the storage rack cell (four-assembly cluster at closest approach). These calculations indicated that the reactivity decreases very slightly in both regions, as determined by PDQ07 calculations with diffusion coefficients\* generated by NULIF and a blackness

theory routine. The highest reactivity therefore corresponds to the reference design with the fuel assemblies positioned in the center of the storage cells.

#### 4.7.2 Temperature and Water Density Effects

The moderator temperature coefficient of reactivity in both regions is negative; a moderator temperature of 0°C, with a water density of 1.0 g/cm<sup>3</sup>, was assumed for the reference designs, which assures that the true reactivity will always be lower, regardless of temperature.

Temperature effects on reactivity have been calculated and the results are shown in Table 4.8. Introducing voids in the water internal to the storage cell (to simulate boiling) decreased reactivity, as shown in the table. Voids due to boiling will not occur in the outer (flux-trap) water region of Region 1.

With soluble poison present, the temperature coefficients of reactivity would be expected to differ from those inferred from the data in Table 4.8. However, the reactivities would also be substantially lower at all temperatures with soluble boron present, and the data in Table 4.8 is pertinent to the higher-reactivity unborated case.

#### 4.7.3 Dropped Fuel Assembly Accident

To investigate the possible reactivity effect of a postulated fuel assembly drop accident, calculations were made for unpoisoned assemblies separated only by clean unborated water. Figure 4.5 shows the results of these calculations. From these data, the reactivity ( $k_B$ ) will be less than 0.95 for any water gap spacing greater than 6 to 7 inches in the absence of any absorber material, other than water, between assemblies. For a drop on top of the rack, the fuel assembly will come to rest horizontally on top of the rack with a minimum separation distance of more than 12 inches. Maximum expected

---

\*This calculational approach was necessary since the reactivity effects are too small to be calculated by KENO, and CASMO-2E geometry is not readily amendable to eccentric positioning of a fuel assembly.

deformation under seismic or accident conditions will not reduce the minimum spacing between fuel assemblies to less than 12 inches. Consequently, fuel assembly drop accident will not result in an increase in reactivity above that calculated for the infinite nominal design storage rack. Furthermore, soluble boron in the pool water would substantially reduce the reactivity and assure that the true reactivity is always less than the limiting value for any conceivable fuel handling accident.

#### 4.7.4 Abnormal Location of a Fuel Assembly

The abnormal location of a fresh unirradiated fuel assembly of 4.2% enrichment could, in the absence of soluble poison, result in exceeding the design reactivity limitation ( $k_B$  of 0.95). This could occur if the assembly were to be either positioned outside and adjacent to a storage rack module or loaded into a Region 2 storage cell, with the latter condition producing the larger positive reactivity increment. Soluble poison, however, is normally present in the spent fuel pool water (for which credit is permitted under these conditions) and would maintain the reactivity substantially less than the design limitation.

The largest reactivity increase occurs for accidentally placing a new fuel assembly into a Region 2 storage cell with all other cells fully loaded. Under this condition, the presence of 300 ppm soluble boron assures that the infinite multiplication factor would not exceed the design basis reactivity. With the nominal concentration of soluble poison present (2000 ppm boron), the maximum reactivity,  $k_B$ , is less than 0.95 even if Region 2 were to be fully loaded with fresh fuel of 4.2% enrichment. Administrative procedures will be used to confirm and assure the continued presence of soluble poison in the spent fuel pool water during fuel handling operations.

#### 4.7.5 Lateral Rack Movement

Lateral motion of the rack modules under seismic conditions could potentially alter the spacing between rack modules. However, girdle bars on the modules prevent closing the spacing to less than 2.0 inches, which is greater than the normal flux-trap water gap in the Region 1 reference design. Region 2 storage

cells do not use flux-trap and the reactivity is insensitive to the spacing between modules. Furthermore, soluble poison would assure that a reactivity less than the design limitation is maintained under all conditions.

#### 4.8 NEW FUEL STORAGE

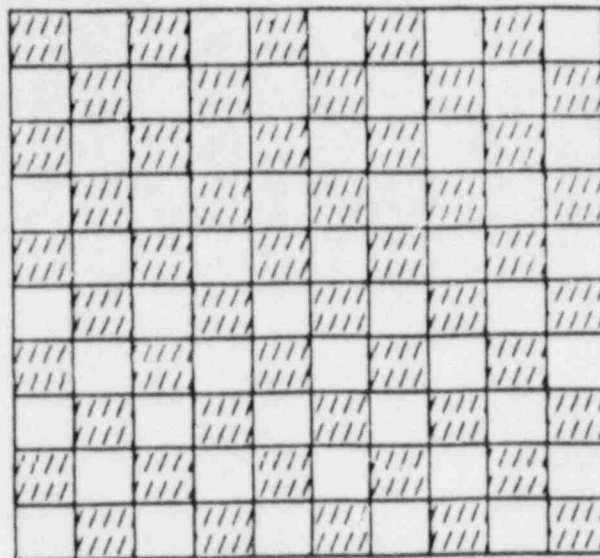
##### 4.8.1 Storage in Region 1, Dry



Region 1 is normally designed to accommodate new unirradiated fuel assemblies in the fully flooded condition. For storage in the dry condition, the racks must also conform to the requirements of SRP 9.1.1 which specify a limiting  $k_{eff}$  value of 0.98 under optimum low density moderation. Calculations were made, using AMPX-KENO, for several hypothetical low-moderator densities down to 0.05 g/cc simulating fog or foam moderation. These calculations showed a continuously decreasing  $k_B$  as the moderator density decreased, yielding a  $k_B$  of  $0.546 \pm 0.008$  (1s) at 10% moderator density. Axial leakage was neglected in these calculations, but would substantially reduce the already low  $k_B$  values. These results are consistent with the general observation that a low-density optimum-moderation peak in reactivity does not exist in poisoned racks (Reference 14).

##### 4.8.2 Storage in Region 2, Flooded

In a succession of trial-and-error calculations, it was found that a checkerboard storage pattern in Region 2 would allow new fuel assemblies of 4.2% enrichment to be safely accommodated without exceeding the limiting 0.95  $k_{eff}$  value. In this checkerboard loading pattern, the fuel assemblies are located on a diagonal array, as illustrated below, with alternate storage cells empty of any fuel.





 USABLE  
 NON-USABLE  
 (empty)

Monte Carlo calculations (AMPX-KENO) resulted in a  $k_B$  of  $0.8133 \pm 0.0138$ . With a one sided K-factor (Reference 13) for 95% probability at a 95% confidence level and a Wk of 0.009 for uncertainties (Table 4.1 for Region 2), the maximum  $k_B$  is 0.863, which is substantially less than the 0.95 limiting value. Thus, Region 2 may be safely used for the temporary storage of new fuel assemblies provided the storage configuration is restricted to the checkerboard pattern indicated above.

#### 4.8.3 Storage in Region 2, Dry

As indicated in Section 4.8.1 above, a peak in reactivity ( $k_{eff}$ ) at low moderator densities is not expected for poisoned rack designs. AMPX-KENO calculations confirmed the absence of a low-moderator-density peak in Region 2 with 4.2% enriched fuel arranged in the checkerboard pattern. At 10% moderator density, the calculated  $k_B$  was 0.552, which would be substantially reduced if axial leakage were to be included. Thus, Region 2 conforms to the requirements of SRP 9.1.1 ( $k_B < 0.98$  at optimum moderation) for the safe storage of 4.2% enriched fuel, dry, in the checkerboard loading pattern.



## REFERENCES

1. A. Ahlin, M. Edenius, H. Haggblom, "CASMO - Fuel Assembly Burnup Program," AE-RF-76-4158, Studsvik report (proprietary).
2. A. Ahlin and M. Edenius, "CASMO - A Fast Transport Theory Depletion Code for LWR Analysis," ANS Transactions, Vol. 26, p. 604, 1977.
3. M. Edenius et al., "CASMO Benchmark Report," Studsvik/RF-78-6293, Aktiebolaget Atomenergi, March 1978.
4. Green, Lucious, Petrie, Ford, White, Wright, "PSR-63/AMPX-1 (code package), AMPX Modular Code System for Generating Coupled Multigroup Neutron-Gamma Libraries from ENDF/B," ORNL-TM-36-706, Oak Ridge National Laboratory, March 1976.
5. L. M. Petrie and N. F. Cross, "KENO-IV, An Improved Monte Carlo Criticality Program," ORNL-4938, Oak Ridge National Laboratory, November 1975.
6. R. M. Westfall et al., "SCALE: A Modular Code System for Performing Standardized Computer Analyses for Licensing Evaluation," NUREG/CR-0200, 1979.
7. W. A. Wittkopf, "NULIF -Neutron Spectrum Generator, Few-Group Constant Generator and Fuel Depletion Code," BAW-426, The Babcock & Wilcox Company, August 1976.
8. W. R. Cadwell, PDQ07 Reference Manual, WAPD-TM-678, Bettis Atomic Power Laboratory, January 1967.
9. W. J. Eich, "Advanced Recycle Methodology Program, CEM-3," Electric Power Research Institute, 1976.
10. E. E. Pilat, "Methods for the Analysis of Boiling Water Reactors (Lattice Physics)," YAEC-1232, Yankee Atomic Electric Co., December 1980.
11. E. Johansson, "Reactor Physics Calculations on Close-Packed Pressurized Water Reactor Lattices," Nuclear Technology, Vol. 68, pp. 263-268, February 1985.
12. H. Richings, Some Notes on PWR (W) Power Distribution Probabilities for LOCA Probabilistic Analyses, NRC Memorandum to P. S. Check, dated July 5, 1977.
13. M. G. Natrella, Experimental Statistics National Bureau of Standards, Handbook 91, August 1963.
14. J. M. Cano et al., "Supercriticality Through Optimum Moderation in Nuclear Fuel Storage," Nuclear Technology, Vol. 48, pp. 251-260, May 1980.

15. W. E. Ford III, et al, "CRSL-V: Processed ENDF/B-V 227 Neutron Group and Pointwise Cross Section Libraries for Criticality Safety, Reactor and Shielding Studies," ORNL/CSD/TM-160, June, 1982.
16. R. Kinsey, Ed. "ENDF/B Summary Documentation," BNL-NCS-17541 (ENDF-201), 3rd Edition, Brookhaven National Laboratory, 1979.
17. T. W. Nordheim, "The Theory of Resonance Absorption," Proceeding of Symposia in Applied Mathematics, Vol. XI, p. 58, Garrett Birkhoff and Eugene Wigner, Eds., AM. Math. Soc., 1961.
18. M. N. Baldwin et al, "Critical Experiment Supporting Close Proximity Water Storage of Power Reactor Fuel," BAE-1484-7, July, 1979.
19. J. T. Thomas, "Critical Three-Dimensional Arrays of U(93.2) Metal Cylinders," Nuclear Science and Engineering, Volume 52, pages 350-359, 1973.

Table 4.1

## SUMMARY OF CRITICALITY SAFETY ANALYSES

	Region 1 Nominal	Region 1 Boral Inserts
Minimum acceptable burnup @ 4.2% initial enrichment	0	0 MWD/MTU
Temperature assumed for analysis	0°C	0°C
Reference $k_B$ (nominal)	0.9374	0.9215
Calculational bias	0.0013	0.0083
Uncertainties		
Bias	+0.0018	+0.0018
KENO	N/A	±0.0041
B-10 concentration (Boraflex)	+0.0021	+0.0021
Boraflex thickness	+0.0047	+0.0047
Boraflex width	+0.0007	+0.0007
Inner box dimension	+0.0018	+0.0018
Water gap thickness	+0.0038	+0.0038
SS thickness	+0.0025	+0.0025
Fuel enrichment	+0.0024	+0.0024
Fuel density	+0.0026	+0.0026
Eccentric assembly position	negative	negative
Statistical combination (1)	+0.0082	+0.0091
Allowance for burnup uncertainty	N/A	N/A
Total	0.9387 ± 0.0082	0.9298 ± 0.0091
Maximum reactivity	0.9469	0.9389

(1) Square root of sum of squares.

Table 4.1 Cont'd)

## SUMMARY OF CRITICALITY SAFETY ANALYSES

	Region 1 Boral	Region 2
Minimum acceptable burnup @ 4.2% initial enrichment	0	37,370 MWD/MTU
Temperature assumed for analysis	0°C	0°C
Reference $k_B$ (nominal)	0.9282	0.8999
Computational bias	0.0083	0.0013
Uncertainties		
Bias	+0.0018	+0.0018
KENO	$\pm$ 0.0041	N/A
B-10 concentration (Boraflex)	N/A	+0.0028
Boraflex thickness	N/A	+0.0078
Boraflex width	N/A	+0.0009
Inner box dimension	+0.0018	+0.0011
Water gap thickness	+0.0038	N/A
SS thickness	+0.0025	+0.0001
Fuel enrichment	+0.0024	+0.0024
Fuel density	+0.0026	+0.0026
Eccentric assembly position	<u>negative</u>	<u>negative</u>
Statistical combination (1)	+0.0073	+0.0093
Allowance for burnup uncertainty	N/A	N/A
Total	0.9365 $\pm$ 0.0073	0.9199 $\pm$ 0.0093
Maximum reactivity	0.9438	0.9292

(1) Square root of sum of squares.

Table 4.2

## REACTIVITY EFFECTS OF ABNORMAL AND ACCIDENT CONDITIONS

---

Accident/Abnormal Conditions	Reactivity Effect
Temperature increase	Negative in both regions
Void (boiling)	Negative in both regions
Assembly dropped on top of rack	Negligible
Lateral rack module movement	Negligible
Misplacement of a fuel assembly	Positive

---

Table 4.3

## FUEL ASSEMBLY DESIGN SPECIFICATIONS

## Fuel Rod Data

Outside diameter, in.	0.360
Cladding thickness, in.	0.0225
Cladding material	Zircaloy-4
Pellet diameter, in.	0.3088
UO <sub>2</sub> pellet density, % TD	95 ± 2
UO <sub>2</sub> stack density, g/cm <sup>3</sup>	10.288 ± 0.217
Enrichment, wt% U-235	4.2 ± 0.05

## Fuel Assembly Data

Number of fuel rods	264 (17 x 17 array)
Fuel rod pitch, in.	0.496
Control rod guide tube	
Number	24
Outside diameter, in.	0.474
Thickness, in.	0.016
Material	Zircaloy-4
Instrument thimble	
Number	1
Outside diameter, in.	0.474
Thickness, in.	0.016
Material	Zircaloy-4
U-235 loading	
g/axial cm of assembly	48.6 ± 1.0

Table 4.4

COMPARISON OF COLD, CLEAN REACTIVITIES CALCULATED  
AT 25,000 MWD/MTU BURNUP AND 3.2% ENRICHMENT

Calculational Method	$k_B$ Xe-free 0°C	
	Fuel Assembly	In Region 2 Cell
CASMO-2E	1.1206	0.9061
NULIF/PDQ07	1.1294	0.9017
EPRI-CELL	1.1201 <sup>(1)</sup>	-

(1) EPRI-CELL  $k_B$  at maximum value during long-term (30-year) storage.

Table 4.5

ESTIMATED UNCERTAINTIES IN REACTIVITY  
DUE TO FUEL DEPLETION EFFECTS

Initial Enrichment	Design Burnup MWD/MTU	$0.5 \times 10^{-6}$ Times Burnup, Wk	Reactivity Loss, Wk <sup>(1)</sup>
1.8	5,230	0.0026	0.0475
2.5	15,720	0.0079	0.1575
3.2	25,000	0.0125	0.2337
3.7	31,280	0.0156	0.2757
4.2	37,370	0.0187	0.3107

(1) Total reactivity decrease, calculated for the cold, Xe-free condition in the fuel storage rack, from the beginning-of-life to the design burnup.



Table 4.6  
LONG-TERM CHANGES IN REACTIVITY IN STORAGE RACK  
(XENON-FREE)

Wk from Shutdown (Xenon-free)		
Storage Time, years	3.2%E @25,000 MWD/MTU	4.2%E @37,000 MWD/MTU
0.5	-0.0046	-0.0057
1.0	-0.0080	-0.0103
10.0	-0.0406	-0.0529
20.0	-0.0588	-0.0756
30.0	-0.0692	-0.0886

Table 4.7  
FUEL BURNUP VALUES FOR REQUIRED REACTIVITIES ( $k_B$ )  
WITH FUEL OF VARIOUS INITIAL ENRICHMENTS

Initial Enrichment	Reference $k_B$	Uncertainty <sup>(1)</sup> In Burnup, W	Design Limit $k_B$	Fuel Burnup, MWD/MTU
1.58	0.9186	0	0.9186	0
1.8	0.9186	0.0026	0.9160	5,230
2.5	0.9186	0.0079	0.9107	15,720
3.2	0.9186	0.0125	0.9061	25,000
3.7	0.9186	0.0156	0.9030	31,280
4.2	0.9186	0.0187	0.8999	37,370

<sup>(1)</sup>See Section 4.4.2.

Table 4.8

EFFECT OF TEMPERATURE AND VOID ON  
CALCULATED REACTIVITY OF STORAGE RACK

Case	Incremental Reactivity Change, Wk	
	Region 1	Region 2
0°C	Reference	Reference
20°C	-0.0022	-0.0047
50°C	-0.0084	-0.0081
80°C	-0.0165	-0.0121
120°C	-0.0298	-0.0178
120°C + 20% void	-0.0953	-0.0520

TABLE 4.9

## BENCHHARK EXPERIMENTS

	<u>General</u> <u>Description</u>	<u>U-235</u> <u>W/O</u>	<u>Reflector</u>	<u>Separating</u> <u>Material</u>	<u>Soluble</u> <u>Boron</u> <u>ppm</u>	<u>Keff</u>
1.	UO2 rod lattice	2.46	Water	Water	0	0.9857 +/- .0028
2.	UO2 rod lattice	2.46	Water	Water	1037	0.9906 +/- .0018
3.	UO2 rod lattice	2.46	Water	Water	764	0.9895 +/- .0015
4.	UO2 rod lattice	2.46	Water	B4C pins	0	0.9914 +/- .0025
5.	UO2 rod lattice	2.46	Water	B4C pins	0	0.9891 +/- .0026
6.	UO2 rod lattice	2.46	Water	B4C pins	0	0.9955 +/- .0020
7.	UO2 rod lattice	2.46	Water	B4C pins	0	0.9889 +/- .0026
8.	UO2 rod lattice	2.46	Water	B4C pins	0	0.9983 +/- .0025
9.	UO2 rod lattice	2.46	Water	Water	0	0.9931 +/- .0028
10.	UO2 rod lattice	2.46	Water	Water	143	0.9928 +/- .0025
11.	UO2 rod lattice	2.46	Water	SS	514	0.9967 +/- .0020
12.	UO2 rod lattice	2.46	Water	SS	217	0.9943 +/- .0019
13.	UO2 rod lattice	2.46	Water	Borated Al	15	0.9892 +/- .0023
14.	UO2 rod lattice	2.46	Water	Borated Al	92	0.9884 +/- .0023
15.	UO2 rod lattice	2.46	Water	Borated Al	395	0.9832 +/- .0021
16.	UO2 rod lattice	2.46	Water	Borated Al	121	0.9848 +/- .0024
17.	UO2 rod lattice	2.46	Water	Borated Al	487	0.9895 +/- .0020
18.	UO2 rod lattice	2.46	Water	Borated Al	197	0.9885 +/- .0022
19.	UO2 rod lattice	2.46	Water	Borated Al	634	0.9921 +/- .0019
20.	UO2 rod lattice	2.46	Water	Borated Al	320	0.9920 +/- .0020
21.	UO2 rod lattice	2.46	Water	Borated Al	72	0.9939 +/- .0020
22.	U metal cylinders	93.2	Bare	Air	0	0.9905 +/- .0020
23.	U metal cylinders	93.2	Bare	Air	0	0.9976 +/- .0020
24.	U metal cylinders	93.2	Bare	Air	0	0.9947 +/- .0025
25.	U metal cylinders	93.2	Bare	Air	0	0.9928 +/- .0019
26.	U metal cylinders	93.2	Bare	Air	0	0.9922 +/- .0026
27.	U metal cylinders	93.2	Bare	Air	0	0.9950 +/- .0027
28.	U metal cylinders	93.2	Bare	Plexiglas	0	0.9941 +/- .0030
29.	U metal cylinders	93.2	Paraffin	Plexiglas	0	0.9928 +/- .0041
30.	U metal cylinders	93.2	Bare	Plexiglas	0	0.9968 +/- .0018
31.	U metal cylinders	93.2	Paraffin	Plexiglas	0	1.0042 +/- .0019
32.	U metal cylinders	93.2	Paraffin	Plexiglas	0	0.9963 +/- .0030
33.	U metal cylinders	93.2	Paraffin	Plexiglas	0	0.9919 +/- .0032

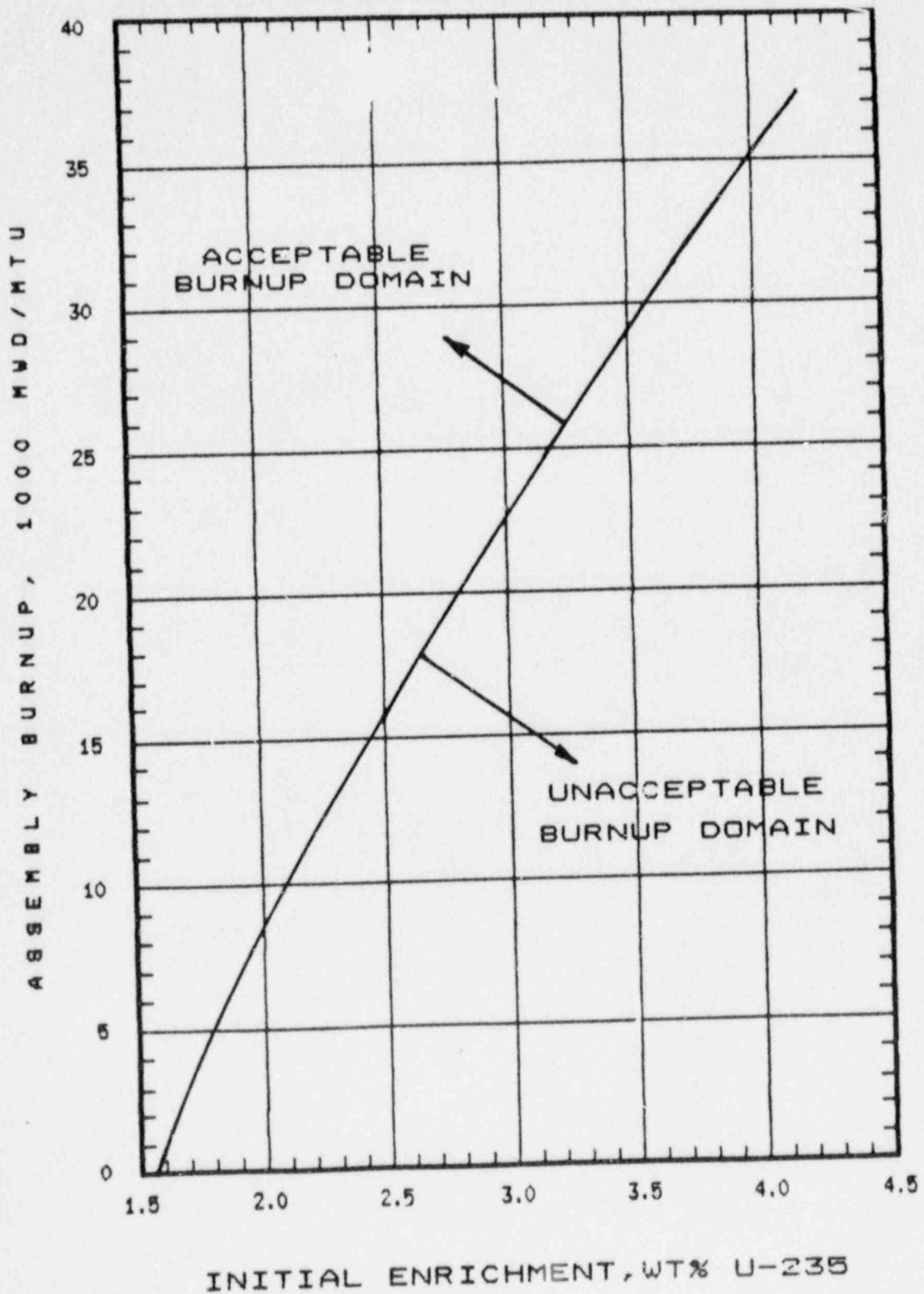


Fig. 4.1 ACCEPTABLE BURNUP DOMAIN IN REGION 2 OF THE BYRON STATION SPENT FUEL STORAGE RACKS.

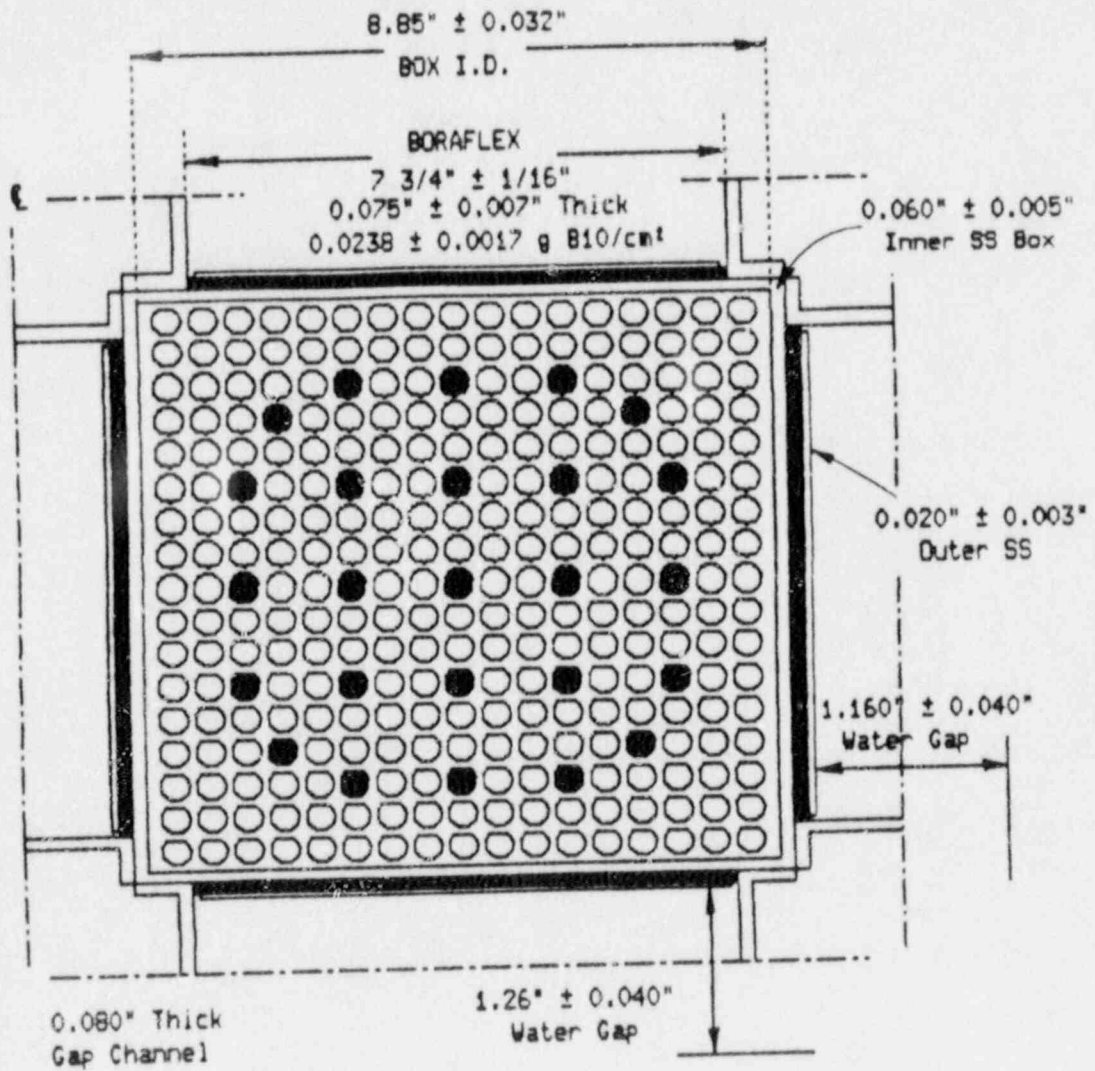


Fig. 4.2.1 REGION 1 STORAGE CELL GEOMETRY.

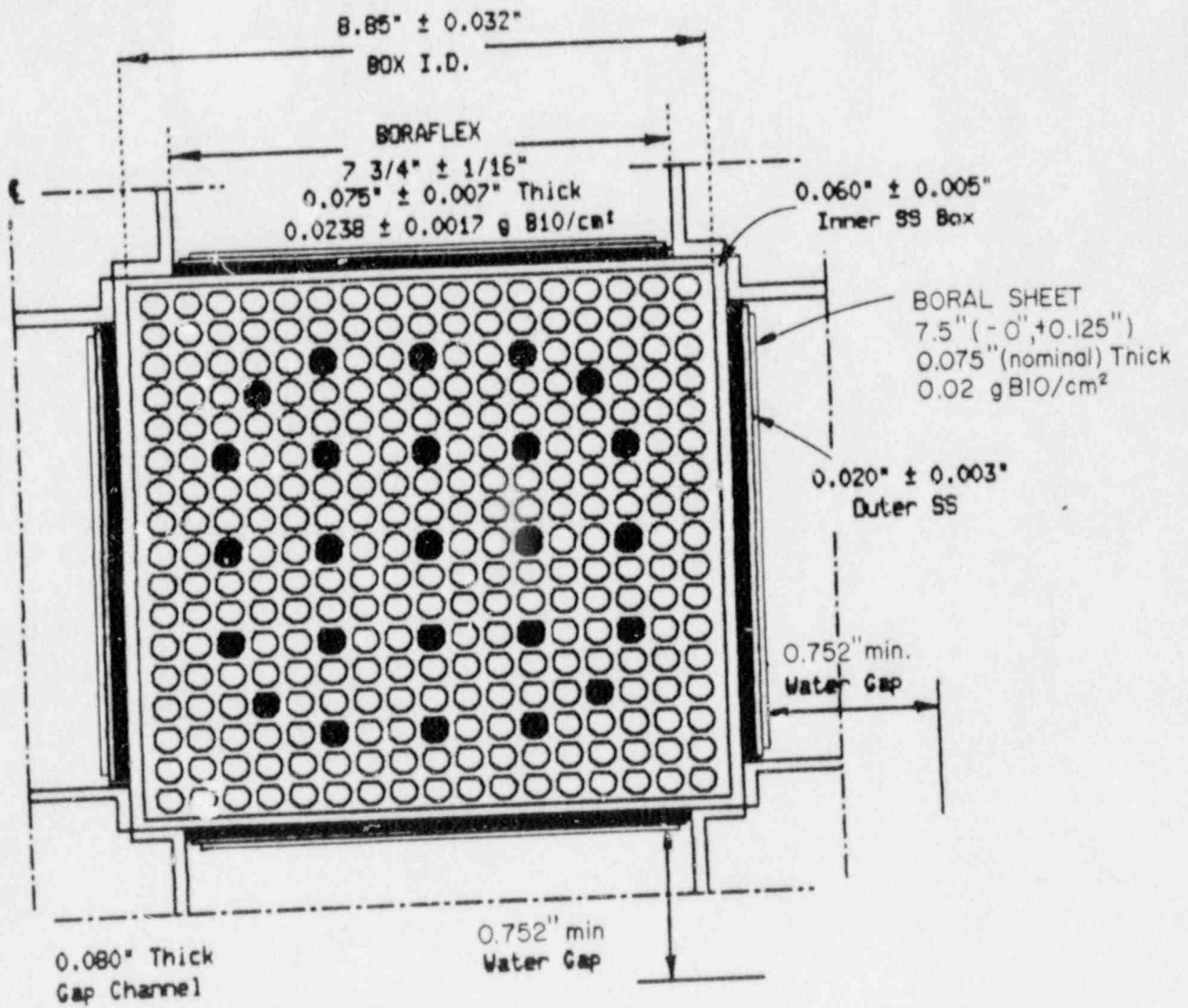


Fig. 4.2.2 REGION 1 STORAGE CELL GEOMETRY.



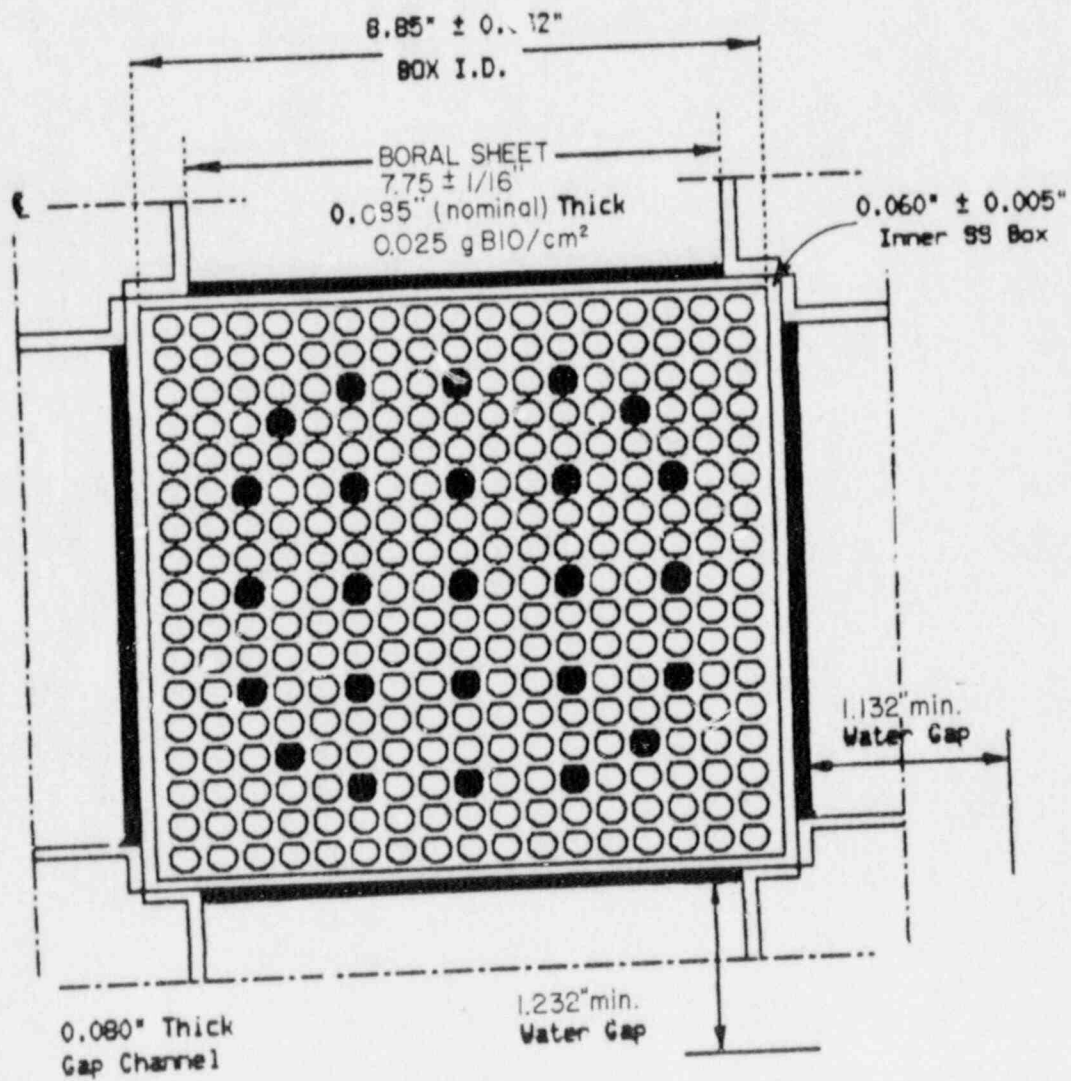


Fig. 4.2.3 REGION 1 STORAGE CELL GEOMETRY.

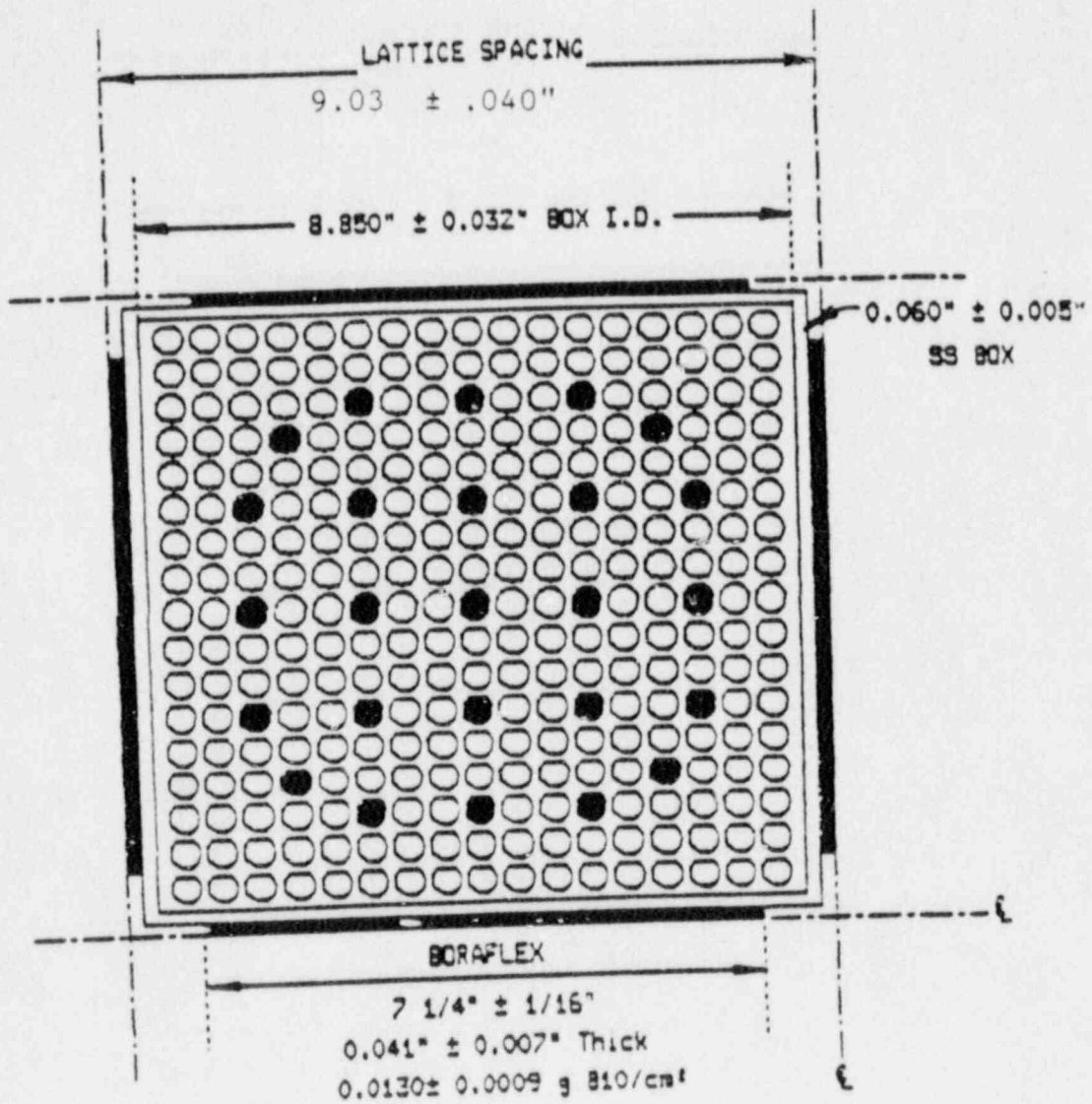
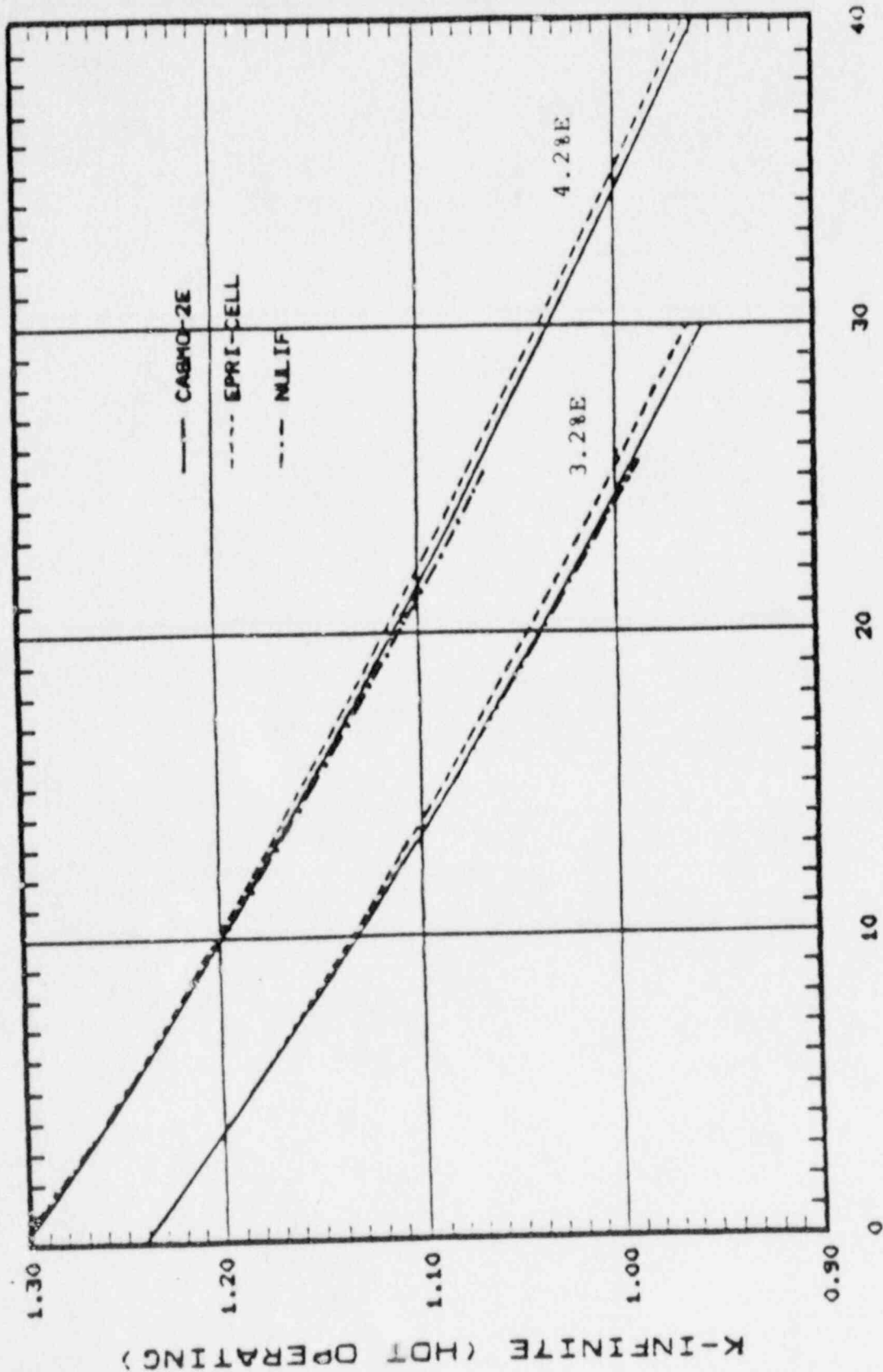


Fig. 4.3 Region 2 storage cell geometry.



FUEL BURNUP, 1000 MWD/MTU

Fig. 4.4 Comparison of depletion calculations for fuel of 3.28 and 4.28 initial enrichments.

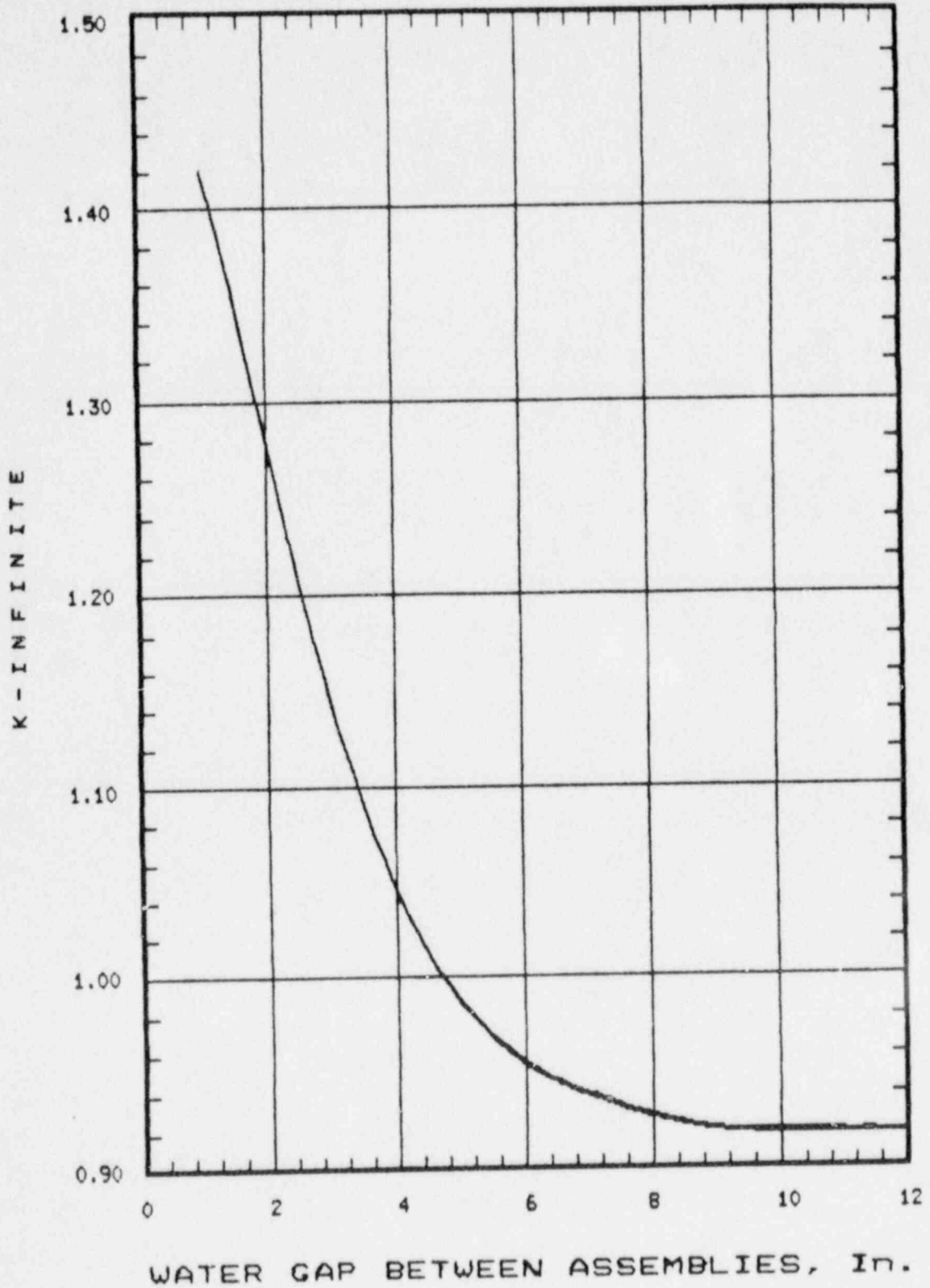


Fig. 4.5 REACTIVITY EFFECT OF WATER SPACING BETWEEN fuel assemblies.

## 5.0 THERMAL-HYDRAULIC CONSIDERATIONS

A primary objective in the design of the high density spent fuel storage racks is to ensure adequate cooling of the fuel assembly cladding. In the following, a brief synopsis of the design basis, the method of analysis, and computed results are given. Similar analysis has been used in previous licensing reports on high density spent fuel racks for Fermi 2 (Docket 50-341), Quad Cities 1 and 2 (Dockets 50-254 and 50-265), Rancho Seco (Docket 50-312), Grand Gulf Unit 1 (Docket 50-416), Oyster Creek (Docket 50-219), Virgil C. Summer (Docket 50-395), and Diablo Canyon 1 and 2 (Dockets 50-275 and 50-323).

### 5.1 DECAY HEAT CALCULATIONS FOR THE SPENT FUEL

This report section covers requirement III.1.5(2) of the NRC's "OT Position for Review and Acceptance of Spent Fuel Storage and Handling Applications" issued on April 14, 1978. This requirement states that calculations for the amount of thermal energy removed by the spent fuel cooling system shall be made in accordance with Branch Technical Position APCS 9-2, "Residual Decay Energy for Light Water Reactors for Long Term Cooling" (Ref. 1). The calculations contained herein have been made in accordance with this requirement.

### 5.1.1 Basis

The Byron Nuclear Power Station Units 1 and 2 reactors are both rated at 3411 megawatts thermal (Mwt). Each core contains 193 fuel assemblies. Thus, the average operating power per fuel assembly,  $P_o$ , is 17.6736 MW. The fuel discharge can be made in one of the following two modes:

- o Normal refueling discharge
  
- o Full core discharge

Another mode exists where a normal discharge from one unit could be followed 17 days later by a full core discharge from the other unit.

An equilibrium reload consists of 84 assemblies (with 18-month cycles). The four transitional reloads for each unit consist of 88 assemblies. The fuel transfer begins after 100 hours of decay time in the reactor (time after shutdown). It is assumed that the time period of discharge of this batch is 28 hours (three assemblies transferred to the pool per hour). The cooling system consists of a Seismic Category I spent fuel cooling circuit. The bulk temperature analysis assumes a 105<sup>0</sup>F coolant inlet temperature to the spent fuel pool heat exchanger for these refueling cases.

For the full core discharge, it is assumed that the total time period for the discharge of the full core is 64 hours (after 100 hours of shutdown time in the reactor). The discharge rate to the pool is assumed to be continuous and uniform.



For the 17 day back-to-back discharge mode, the following assumptions were made; 410 hours between the normal discharge and the full core discharge; 3288 hours between the normal discharge and the previous normal discharge; all the previous normal discharge were assumed double discharges (168 fuel assemblies) for conservatism.

The fuel assemblies are removed from the reactor after a maximum postulated time of 4.5 years of cumulative operating time. Since the decay heat load is a monotonically increasing function of the cumulative reactor operating time,  $\tau_0$ , it is conservatively assumed that every fuel assembly discharged has had the maximum postulated  $\tau_0$  of 4.5 years for the batch size of 84.

The water inventory in the reactor cavity cooled by the residual heat removal (RHR) heat exchanger exchanges heat with the fuel pool water mass through the refueling canal. This source of heat removal is neglected in the analysis. Thus, the results obtained for the normal refueling discharge, full core discharge and 17 day discharge mode are conservative.

The fuel pool cooling system (FC) consists of two independent trains, each consisting of one pump and heat exchanger. Either train is capable of providing sufficient cooling for the pool.

The following list identifies all relevant design data for the spent fuel pool heat exchangers:

o	Type	Tube and shell
---	------	----------------

- o Quantity 2
- o Performance data
  - Heat transferred  $15.833 \times 10^6$  Btu/hr

Tube Side

- Fluid flow  $2.23 \times 10^6$  lb/hr
- Pool water inlet temperature  $120^{\circ}\text{F}$
- Outlet temperature  $112.9^{\circ}\text{F}$
- Fouling factor .0005

Shell Side

- Fluid flow  $2.72 \times 10^6$  lb/hr
- Coolant inlet temperature  $105^{\circ}\text{F}$
- Outlet temperature  $110.82^{\circ}\text{F}$
- Fouling factor .0005

The above data enables complete characterization of the thermal performance of a fuel pool heat exchanger.

### 5.1.2 Model Description

Reference 1 is utilized to compute the heat dissipation requirements in the pool. The total decay heat consists of fission product and heavy element decay heat. Total decay heat,  $P$ , for a fuel assembly is given as a linear function of  $P_0$  and as an exponential function of  $\tau_0$  and  $\tau_s$ :

$$P = P_0 f(\tau_0, \tau_s) \quad (5.1-1)$$

where:

$P$  = total decay heat per fuel assembly, linear function of  $P_0$

$P_0$  = average operating power per fuel assembly

$\tau_0$  = cumulative exposure time of the fuel assembly in the reactor

$\tau_s$  = time elapsed since reactor shutdown

The appropriate uncertainty factor,  $K$ , was applied in accordance with NUREG-0800 (Ref. 1). Furthermore, the operating power,  $P_0$ , is taken equal to the rated power, even though the reactor may be operating at less than its rated power during much of the exposure period for the batch of fuel assemblies. Finally, the computations and results reported here are based on the discharge taking place when the inventory of fuel in the pool will be at its maximum resulting in an upper bound on the total decay heat rate.

Having determined the heat dissipation rate, the next task is to evaluate the time-dependent temperature of the pool water. Table 5.1 identifies the loading cases examined. The pool bulk temperature is determined using the first law of thermodynamics (conservation of energy).

A number of simplifying assumptions are made which render the analysis conservative, principally:

- o The heat exchangers are assumed to have maximum fouling. Thus, the temperature effectiveness,  $S$ , for the heat exchanger utilized in the analysis is the lowest postulated value:  $S = .3875$  for fuel pool cooler.  $S$  is calculated from heat exchanger technical data sheets. No heat loss is assumed to take place through the concrete floor.
- o No credit is taken for the improvement in the film coefficients of the heat exchanger as the operating temperature rises. Thus, the film coefficient used in the computations are lower bounds.
- o No credit is taken for heat loss by evaporation of the pool water.
- o No credit is taken for heat loss to pool walls and pool floor slab.

The basic energy conservation relationship for the pool heat exchanger system yields:

$$C_t \frac{dt}{d\tau} = Q_1 - Q_2 \quad (5.1-2)$$

where:

$C_t$  = Thermal capacity of stored water in the pool

$\tau_t$  = Temperature of pool water at time,  $\tau$

$Q_1$  = Heat generation rate due to stored fuel assemblies in the pool;  
 $Q_1$  is a known function of time,  $\tau$  from the preceding section.

$Q_2$  = Heat removed in the fuel pool cooler.

The pool has a total water inventory of approximately 63444.0 cubic feet when all racks are in place in the pool and every storage location is occupied.

### 5.1.3 Decay Heat Calculation Results

The calculations were performed for the pool, disregarding the additional thermal capacity and cooling system available in the transfer canal, and the reactor cavity.

For a specified coolant inlet temperature and flow rate, the quantity  $Q_2$  is shown to be a linear function of  $\tau$  in a recent paper by Singh (Ref. 3). As stated earlier,  $Q_1$  is an exponential function of  $\tau$ . Thus, Equation 5.1-2 can be integrated to determine  $t$  directly as a function of  $\tau$ . The results are plotted in Figures 5.1A through 5.2D. The results show that the pool water never approaches the boiling point even with the most adverse heat load, under normal operating conditions. These figures also give  $Q_1$  as a function of  $\tau$ . Four plots are generated for each case. The first and third plots for each case show temperature and power generation, respectively, for a period extending from  $\tau = 0$  to  $\tau = 2 \tau_n$  where  $\tau_n$  is the total time of fuel transfer. The second and fourth plots show the same quantities (i.e., temperature and power generation, respectively) over a longer period. The

long-term plots are produced to show the temperature drop with time. Summarized results are given in Table 5.2.

Finally, computations are made to determine the time interval to boiling after all heat dissipation paths are lost. Computations are made for each case under the following two assumptions:

- o All cooling systems lost at the instant pool bulk temperature reaches the maximum value.
- o All cooling systems lost at the instant the heat dissipation power reaches its maximum value in the pool.

Results are summarized in Table 5.3. Table 5.3 gives the bulk boiling vaporization rate for all cases at the instant the boiling commences. This rate will decrease with time due to reduced heat generation in the fuel. In all cases, adequate time exists to take corrective action.

## 5.2 THERMAL-HYDRAULIC ANALYSES FOR SPENT FUEL COOLING

This report section covers requirement III.1.5(3) of the NRC's "OT Position for Review and Acceptance of Spent Fuel Storage and Handling Applications," issued on April 14, 1978. Conservative methods have been used to calculate the maximum fuel cladding temperature as required therein. Also, it has been determined that nucleate boiling or voiding of coolant on the surface of the fuel rods occurs only at the locations where freshly discharged fuel assemblies are stored.



### 5.2.1 Basis

In order to determine an upper bound on the maximum fuel cladding temperature, a series of conservative assumptions are made. The most important assumptions are listed below:

- o As stated above, the fuel pool will contain spent fuel with varying time-after-shutdown ( $\tau_s$ ). Since the heat emission falls off rapidly with increasing  $\tau_s$ , it is obviously conservative to assume that all fuel assemblies are fresh ( $\tau_s = 100$  hours) and they all have had 4.5 years of operating time in the reactor for cases 1 and 2. The heat emission rate of each fuel assembly is assumed to be equal (Ref. 2).
- o As shown in Figure 2.1 in Section 2, the modules occupy an irregular floor space in the pool. For the hydrothermal analysis, a circle circumscribing the actual rack floor space is drawn. It is further assumed that the cylinder with this circle as its base is packed with fuel assemblies at the nominal pitch of 9.03 inches (see Figure 5.3).
- o The downcomer space around the rack module group varies, as shown in Figure 2.1. The nominal downcomer gap available in the pool is assumed to be the minimum gap available around the idealized cylindrical rack; thus, the maximum resistance to downward flow is incorporated into the analysis.
- o No downcomer flow is assumed to exist between the rack modules.

### 5.2.2 Model Description

In this manner, a conservative idealized model for the rack assemblage is obtained. The water flow is axisymmetric about the vertical axis of the circular rack assemblage, and thus, the flow is two-dimensional (axisymmetric three-dimensional). Figure 5.4 shows a typical "flow chimney" rendering of the thermal hydraulics model. The governing equation to characterize the flow field in the pool can now be written. The resulting integral equation can be solved for the lower plenum velocity field (in the radial direction) and axial velocity (in-cell velocity field), by using the method of collocation. It

should be added that the hydrodynamic loss coefficients which enter into the formulation of the integral equation are also taken from well-recognized sources (Ref. 4) and wherever discrepancies in reported values exist, the conservative values are consistently used. Reference 5 gives the details of mathematical analysis used in this solution process.

After the axial velocity field is evaluated, it is a straight-forward matter to compute the fuel assembly cladding temperature. The knowledge of the overall flow field enables pinpointing the storage location with the minimum axial flow (i.e., maximum water outlet temperature). This is called the most "choked" location. In order to find an upper bound on the temperature in a typical cell, it is assumed that it is located at the most choked location. Knowing the global plenum velocity field, the revised axial flow through this choked cell can be calculated by solving the Bernoulli's equation for the flow circuit through this cell. Thus, an absolute upper bound on the water exit temperature and maximum fuel cladding temperature is obtained. It is believed that, in view of the aforementioned assumptions, the temperatures calculated in this manner overestimate the temperature rise that will actually occur in the pool.

The maximum pool bulk temperature,  $t$ , is computed in Section 5.1.3 and reported in Table 5.2. The corresponding average power output from the hottest fuel assembly,  $q$ , is also reported in that table. The maximum radial peaking factor,  $F_{xy}$ , is 1.55 for the Byron Nuclear Power Station. Thus, it is conservative to assume that the maximum specific power of a fuel assembly,  $q_A$ , is given by:

$$q_A = q F_{xy}$$

(5.2-1)

where:

$$F_{xy} = 1.55$$

The maximum temperature rise of pool water in the most disadvantageously placed fuel assembly is given in Table 5.4 for all loading cases. Having determined the maximum local water temperature in the pool, it is now possible to determine the maximum fuel cladding temperature. It is conservatively assumed that the total peaking factor,  $F_Q$ , is 2.32. Thus, a fuel rod can produce 2.32 times the average heat emission rate over a small length. The axial heat dissipation in a rod is known to reach a maximum in the central region, and taper off at its two extremities. For the sake of added conservatism it is assumed that the peak heat emission occurs at the top where the local water temperature also reaches its maximum. Furthermore, no credit is taken for axial conduction of heat along the rod. The highly conservative model thus constructed leads to simple algebraic equations which directly give the maximum local cladding temperature,  $t_C$ .

### 5.2.3 Results

Table 5.4 gives the maximum local cladding temperature,  $t_C$ , at the instant the pool bulk temperature has attained its maximum value. It is quite possible, however, that the peak cladding temperature occurs at the instant of maximum value of  $q_A$ , the instant when the fuel assembly is first placed in a storage location. Table 5.5 gives the maximum local cladding temperature at  $\tau = 0$ .

The local boiling temperature near the top of the fuel cladding is 240<sup>0</sup>F. However, the cladding temperature must be somewhat higher than the boiling temperature to initiate and sustain nucleate boiling. The above considerations indicate that a comfortable margin against the initiation of localized boiling exists in case 1. For full core discharge (case 2 and case 3) under the described assumptions, the maximum cladding temperature will give rise to localized nucleate boiling, but not to bulk pool boiling (5.4).

REFERENCES TO SECTION 5

1. NUREG-0800 U.S. Nuclear Regulatory Commission, Standard Review Plan, Branch Technical Position ASB 9-2, Rev. 2, July 1981.
2. FSAR, Byron Nuclear Power Station.
3. Journal of Heat Transfer, Fundamental Transactions of the ASME, August 1981, Vol. 103, "Some Fundamental Relationships for Tubular Heat Exchanger Thermal Performance," K.P. Singh.
4. General Electric Corporation, R&D Data Books, "Heat Transfer and Fluid Flow," 1974 and updates.
5. 4th National Congress of the ASME, "A Method for Computing the Maximum Water Temperature in a Fuel Pool Containing Spent Nuclear Fuel," by K.P. Singh and A.I. Soler, Paper 83-NE-7, Portland, Oregon (June 1983).

Table 5.1  
LIST OF CASES ANALYZED

Case No.	Condition	No. of Fuel Assemblies Discharged, N	Total Time to Transfer Fuel Into the Pool $t_h$ , hrs	Decay Time Before Transfer Begins, hrs
1	Normal refueling discharge*	84	28	100
2	Full core* discharge	193	64	100
3	Back-to-back refueling	277	+	100

\* Discharge is assumed to be into a pool containing fuel from 17 previous discharges of 168 assemblies.

+ 28 hours for first discharge (84 assemblies), 64 hours for second discharge (full core).  
17 days between the discharges and 4-1/2 months to the previous discharge.



Table 5.2

MAXIMUM POOL BULK TEMPERATURE,  $t$ , COINCIDENT TOTAL POWER,  $Q_1$ , AND  
COINCIDENT SPECIFIC POWER,  $q$ , FOR THE HOTTEST ASSEMBLY

Case No.	No. of Assemblies	Time to Transfer Fuel Into Pool, hrs	Maximum Pool Bulk Temp., $t$ , °F	Coincident Time (After Initiation of Fuel Transfer), hrs	Coincident Specific Power, $q$ , Btu/sec	Coincident Total Power $Q_1$ ( $10^6$ ) Btu/hour	Notes
1	84	28	138	37.0	55.15	.1985	Normal discharge <sup>*</sup>
2	193	64	155	71.0	50.30	.1811	Full core discharge <sup>*</sup>
3	277	+	158	55.0	55.0	.1980	Abnormal discharge

<sup>\*</sup> Discharge is assumed to be into a pool containing fuel from 17 previous discharges of 168 assemblies.

<sup>+</sup> 28 hours for first discharge; 64 hours for the second discharge; 17 days between first and second discharge and 4-1/2 months to the previous discharge.

Table 5.3

## VAPORIZATION RATE FROM THE INSTANT ALL COOLING IS LOST

Case No.	CONDITION 1		CONDITION 2	
	Loss of Cooling at Maximum Pool Bulk Temperature		Loss of Cooling at Maximum Power Discharge	
	Time (Hrs) To Boil	Vap. Rate (lb/hr)	Time (Hrs) To Boil	Vap. Rate (lb/hr)
1	9	35329.0	9	35788.0
2	4	54233.0	4	54827.0
3	3.8	57560.0	3.8	58395.0

Table 5.4

MAXIMUM LOCAL POOL WATER TEMPERATURE AND LOCAL FUEL CLADDING TEMPERATURE AT INSTANT OF MAXIMUM POOL BULK TEMPERATURE

Case No.	Maximum Local Water Temperature, °F	Maximum Local Fuel Cladding Temperature, °F	Case Identified
1	194	239	84 assemblies
2	208	250	193 assemblies
3	227.4	275.1	277 assemblies

Table 5.5

POOL AND MAXIMUM CLADDING TEMPERATURE AT THE  
INSTANT FUEL ASSEMBLY TRANSFER BEGINS

Case No.	Cladding Temperature, °F	Coincident Pool Temperature, °F	
		Bulk	Local
1	236.6	122.6	186.0
2	236.6	122.8	186.2
3	236.6	122.8	186.2

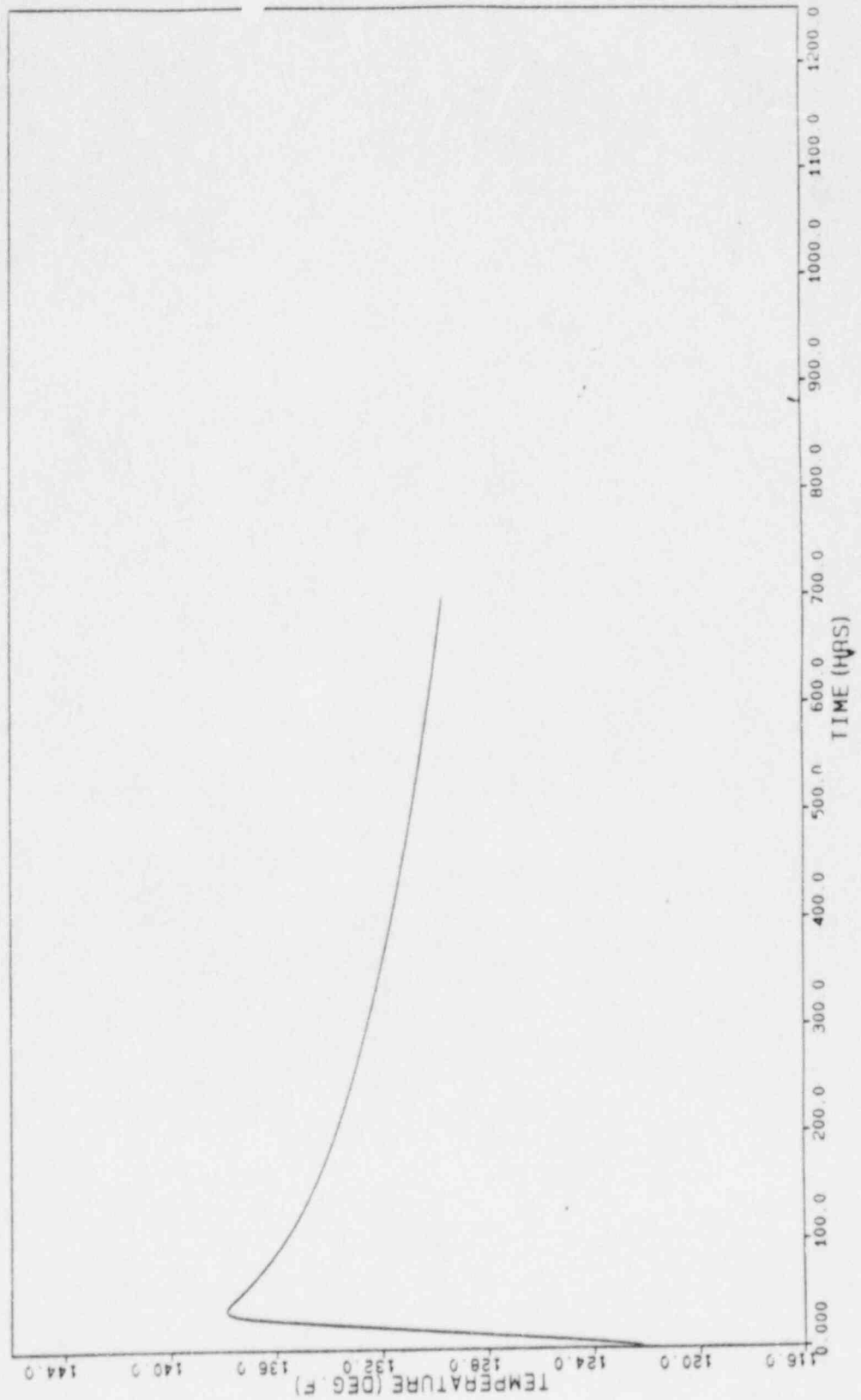


FIG. C.1A - SPENT FUEL POOL BULK TEMPERATURES (0-700 HOURS)

(NORMAL REFUELING DISCHARGE)

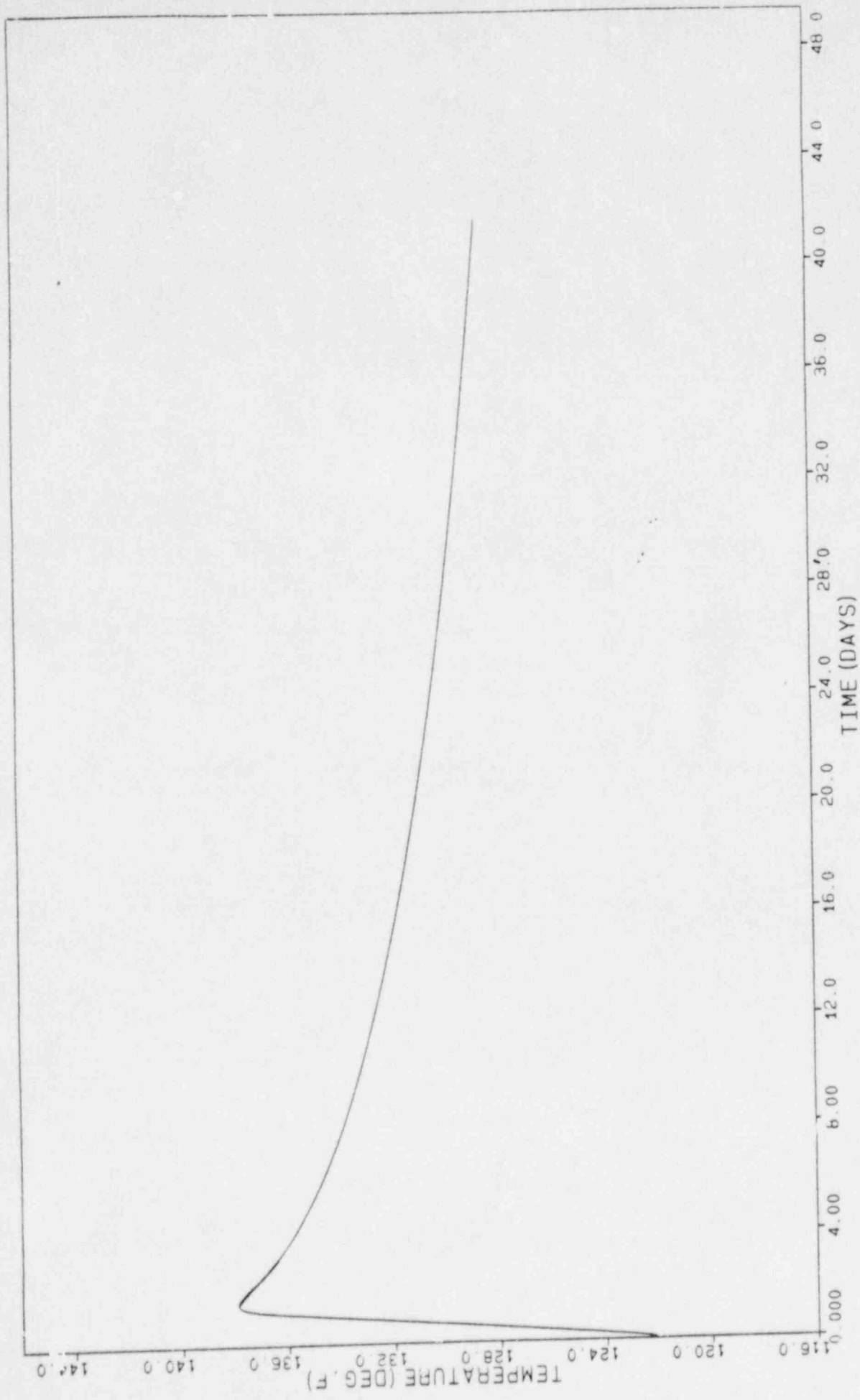


FIG. 5.1B SPENT FUEL POOL BULK TEMPERATURE (0-44 DAYS)

(NORMAL REFUELING DISCHARGE)



5-21

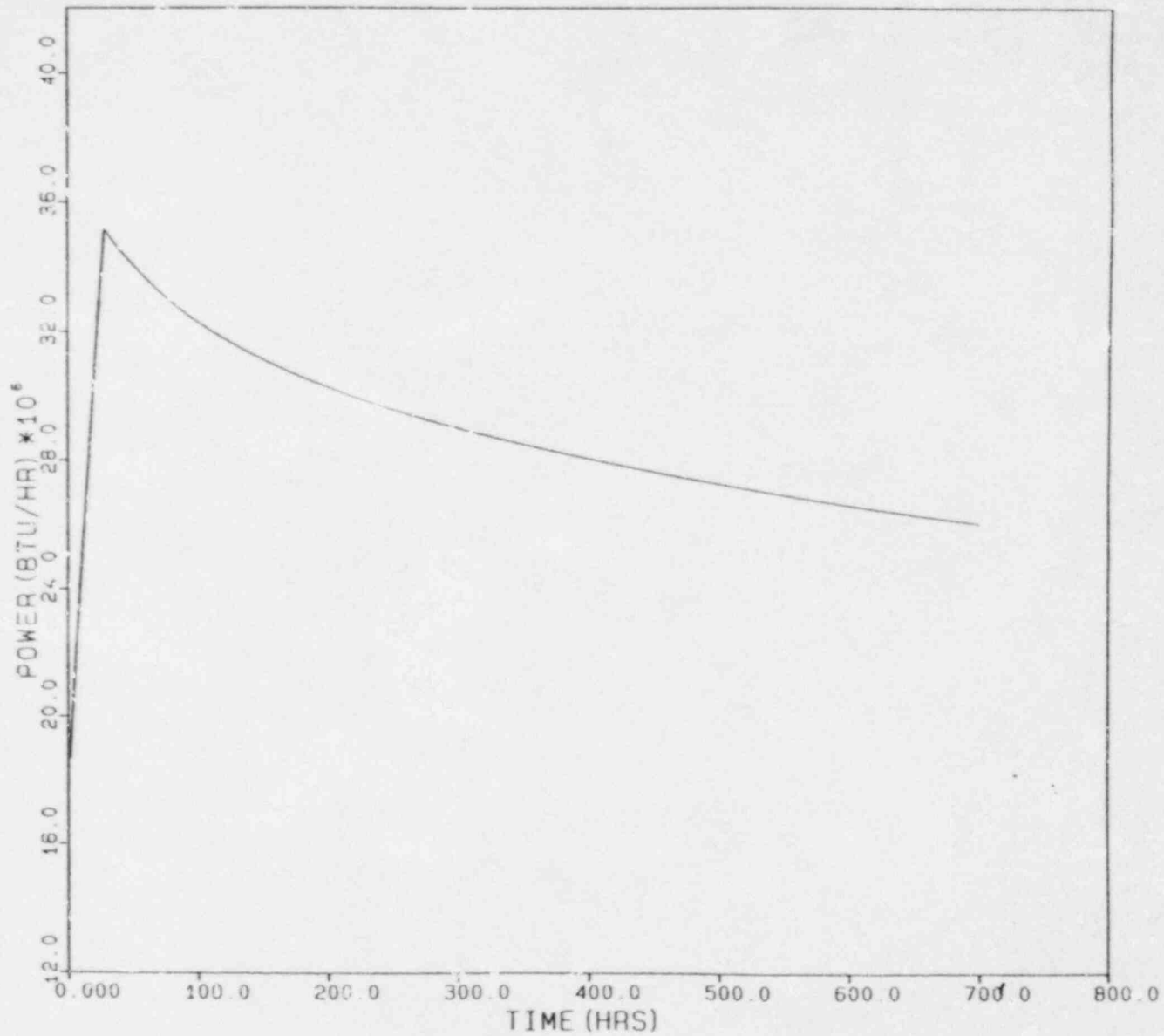


FIG. 5.1C POWER DISCHARGED IN SPENT FUEL POOL (0-700 HOURS)

(NORMAL REFUELING DISCHARGE)

5-22

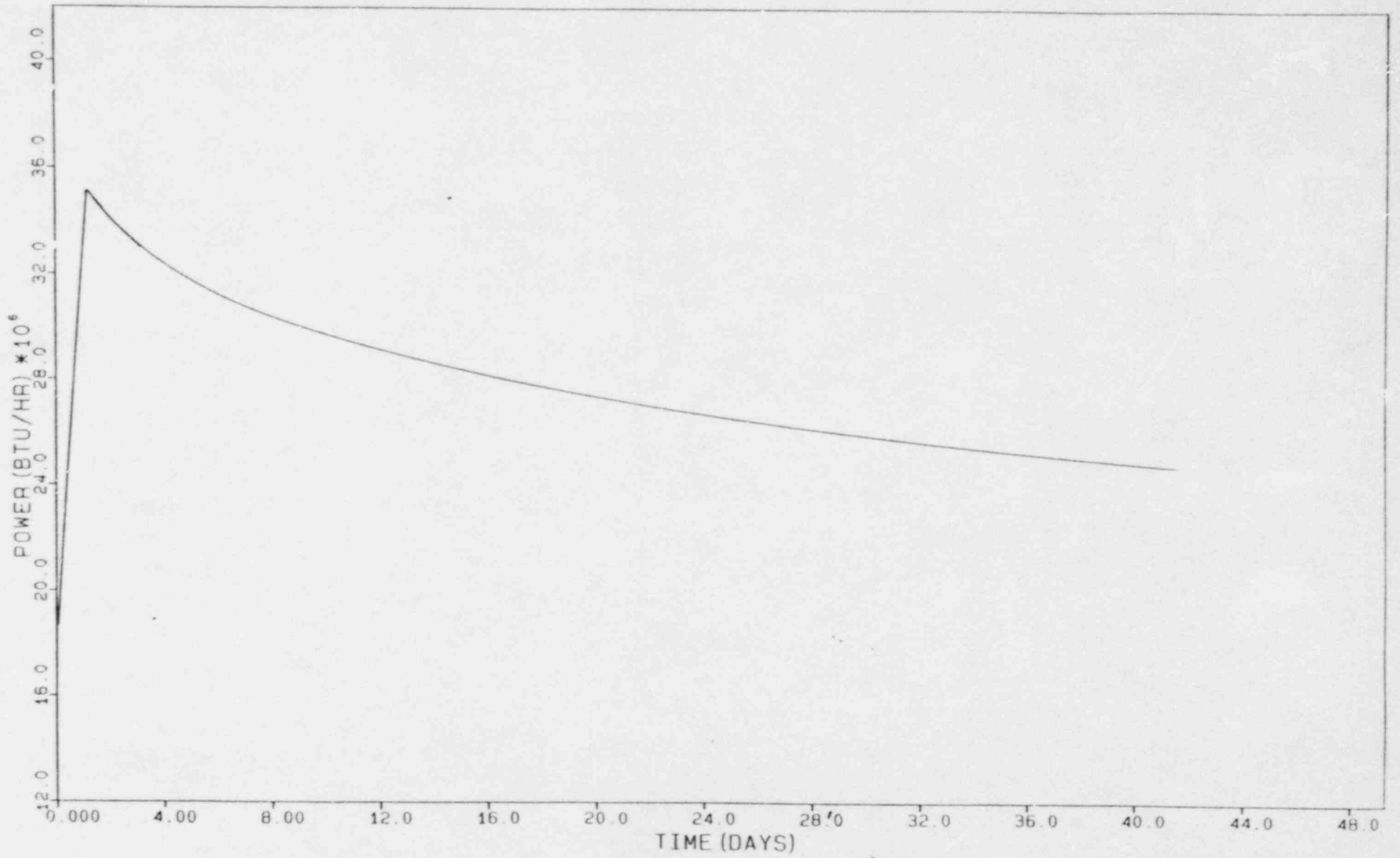


FIG. 5.1D POWER DISCHARGED IN SPENT FUEL POOL (0-44 DAYS)

(NORMAL REFUELING DISCHARGE)

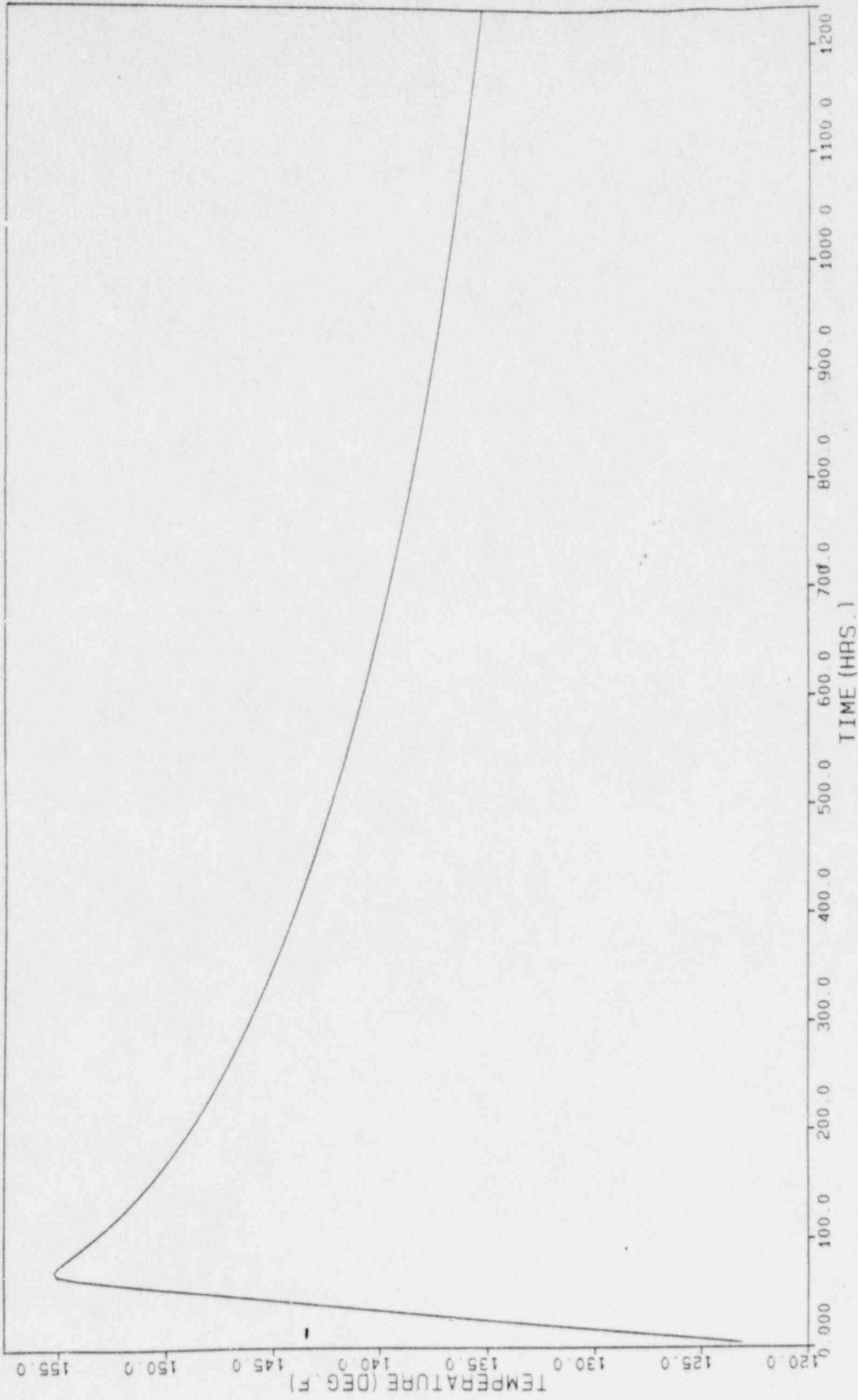


FIG. 5.2A SPENT FUEL POOL BULK TEMPERATURE (0-1200 HOURS)  
(FULL CORE DISCHARGE)

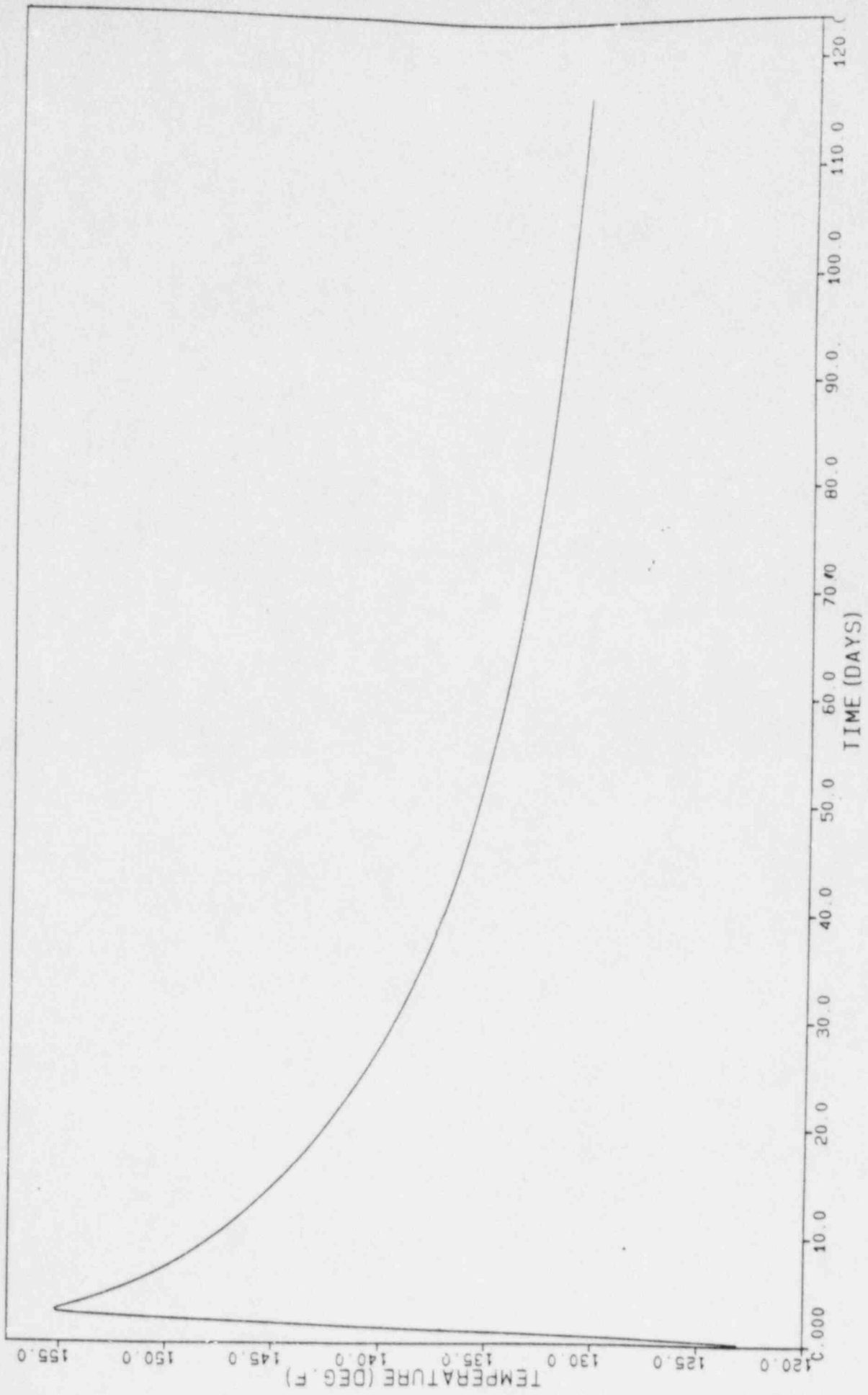
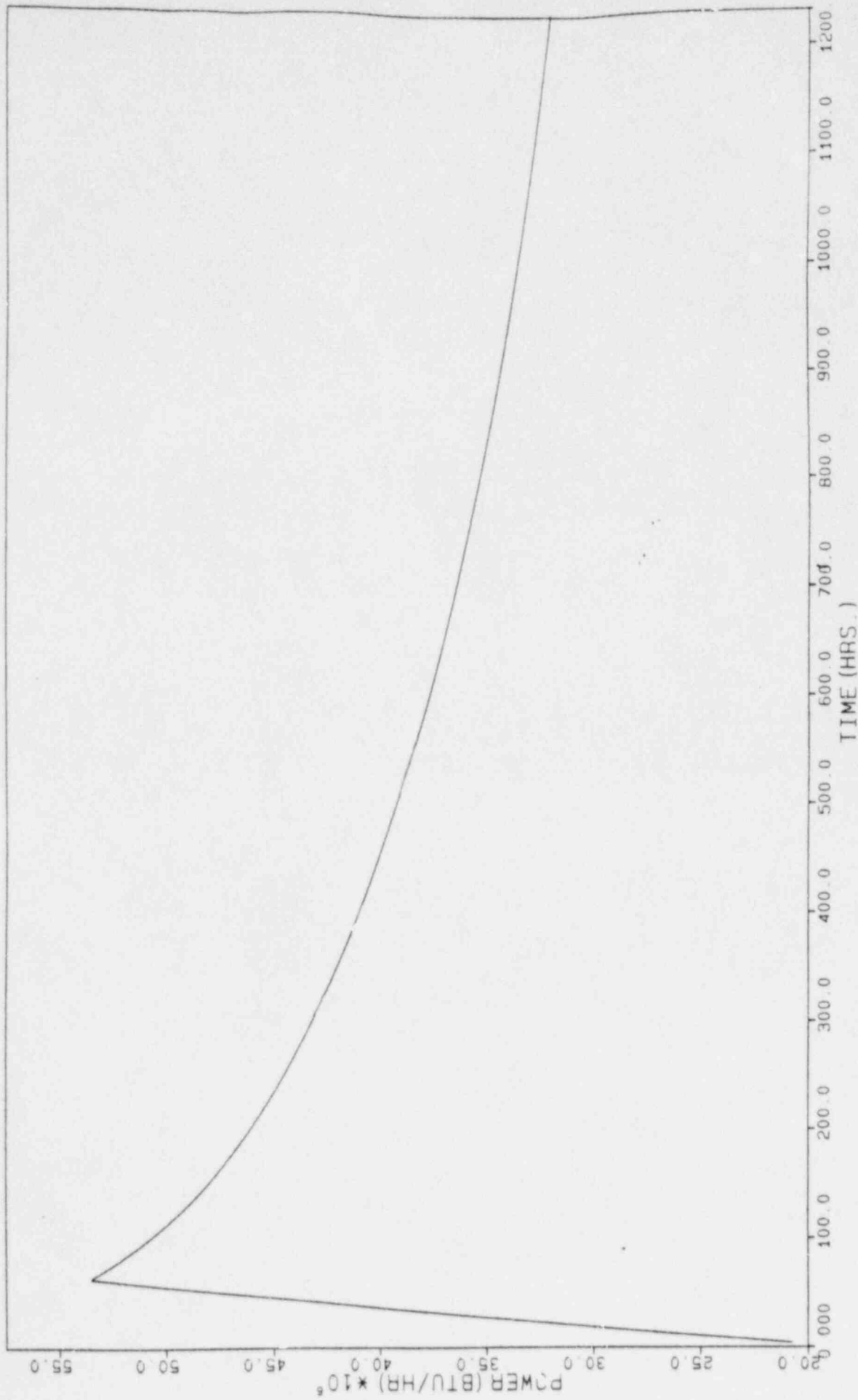


FIG. 5.2B SPENT FUEL POOL BULK TEMPERATURE (0-115 DAYS)  
(FULL CORE DISCHARGE)



**FIG. 5.2C POWER DISCHARGED IN SPENT FUEL POOL (0-1200 HOURS)  
(FULL CORE DISCHARGE)**

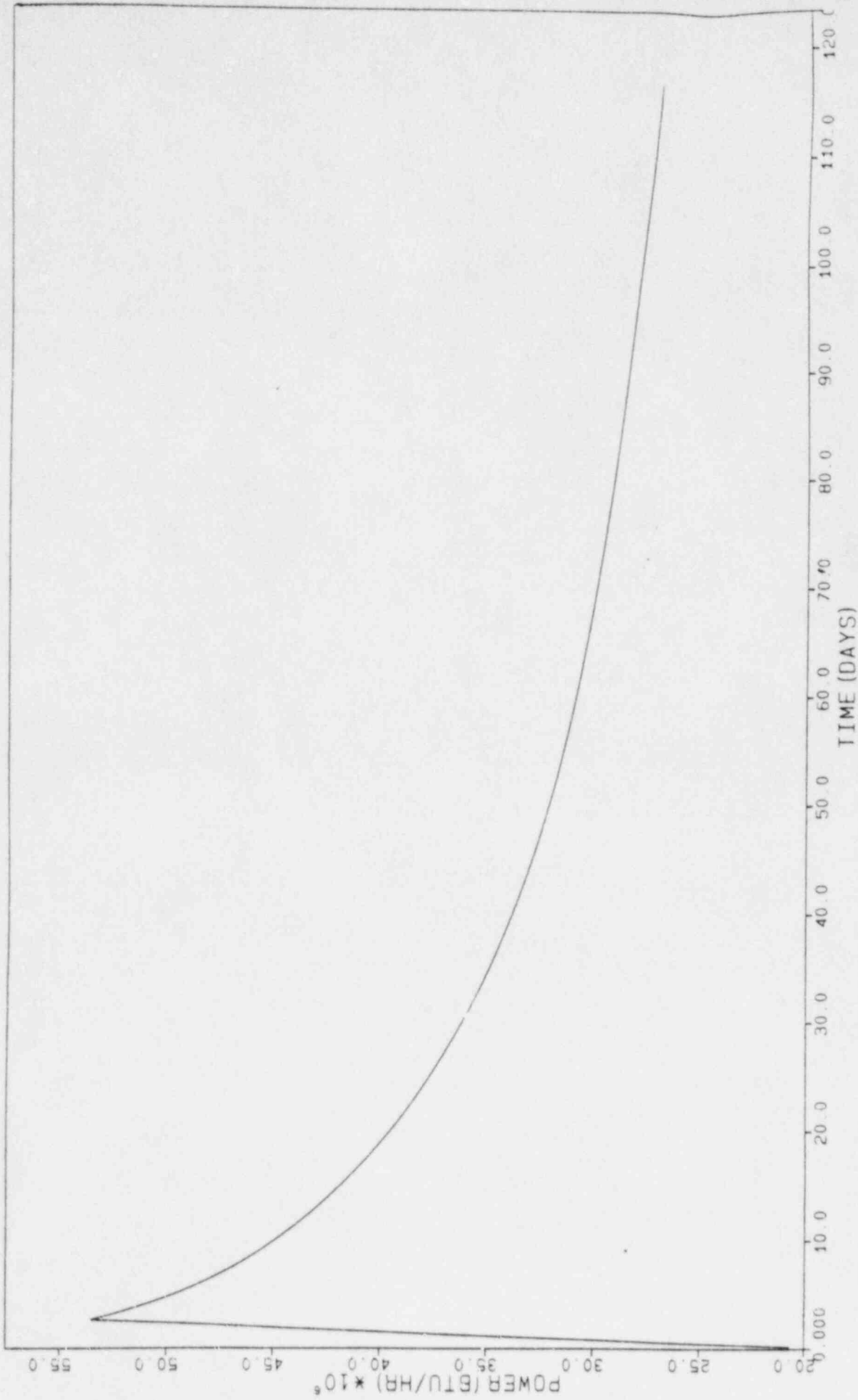


FIG. 6.2D POWER DISCHARGED IN SPENT FUEL POOL (0-115 DAYS)  
(FULL CORE DISCHARGE)



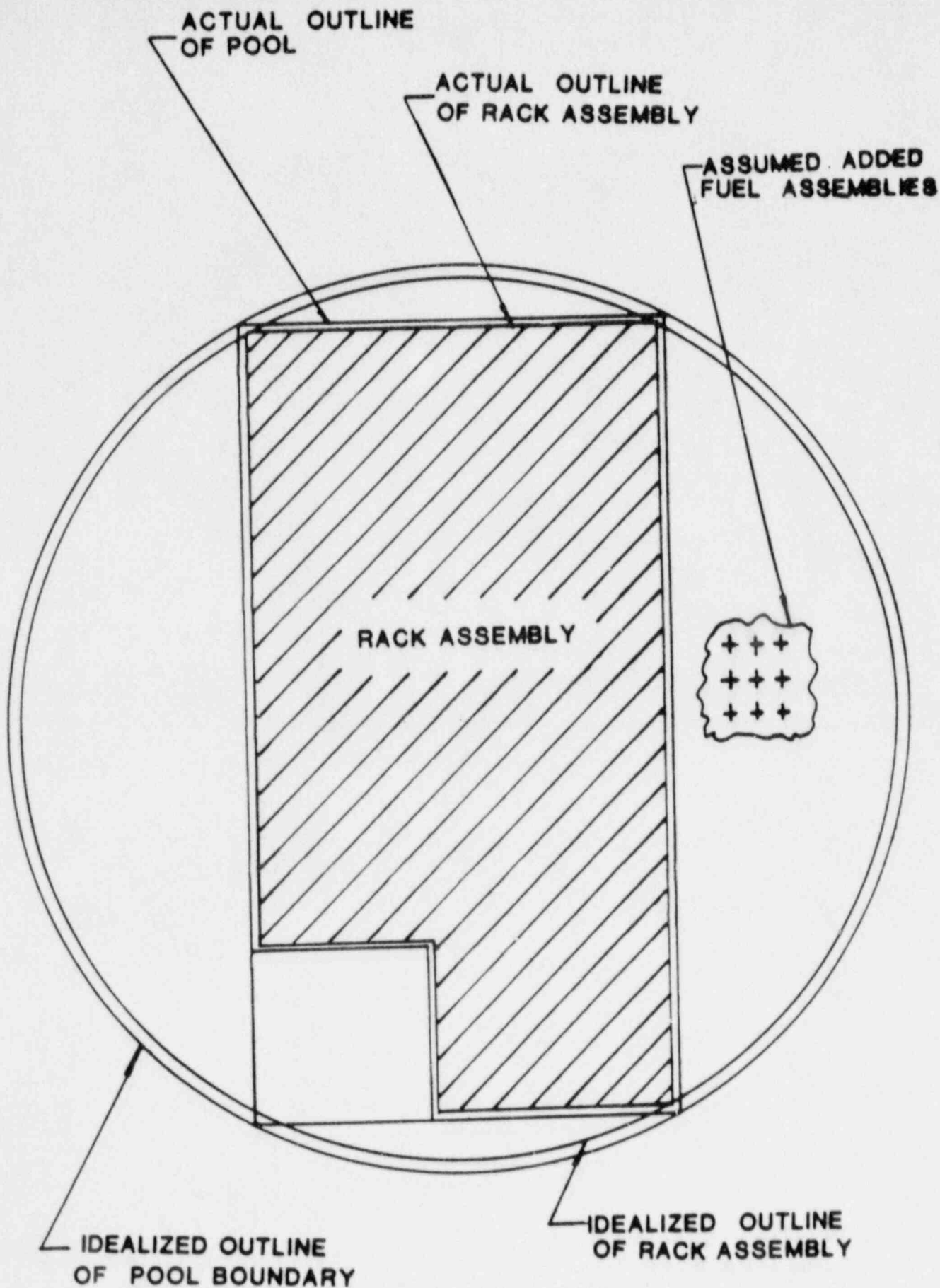


FIGURE 5.3 IDEALIZATION OF RACK ASSEMBLY

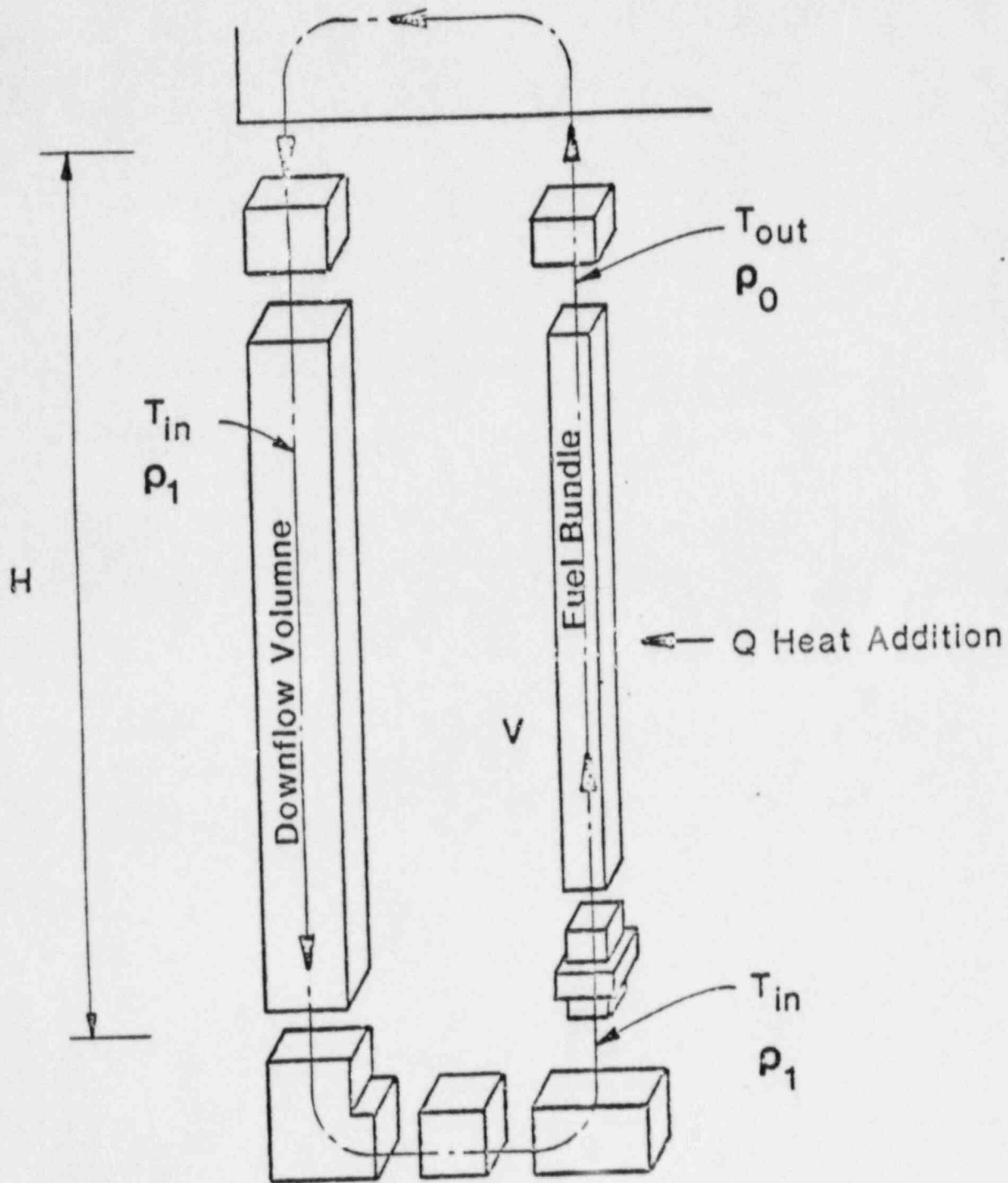


FIGURE 5.4 Thermal Chimney Flow Model

## 6.0 STRUCTURAL ANALYSIS

The purpose of this section is to demonstrate the structural adequacy of the spent fuel rack design under normal and accident loading conditions. The method of analysis presented herein uses a time-history integration method similar to that previously used in the Licensing Reports on High Density Fuel Racks for Fermi 2 (Docket No. 50-341), Quad Cities 1 and 2 (Docket Nos. 50-254 and 50-265), Rancho Seco (Docket No. 50-312), Grand Gulf Unit 1 (Docket No. 50-416), Oyster Creek (Docket No. 50-219), V.C. Summer (Docket No. 50-395), and Diablo Canyon 1 and 2 (Docket Nos. 50-275 and 50-323). The results show that the high density spent fuel racks are structurally adequate to resist the postulated stress combinations associated with level A, B, C, and D conditions as defined in References 1 and 2.

### 6.1 ANALYSIS OUTLINE

The spent fuel storage racks are Seismic Category I equipment. Thus, they are required to remain functional during and after a Safe Shutdown Earthquake (Ref. 3). As noted previously, these racks are neither anchored to the pool floor nor attached to the sidewalls. The individual rack modules are not interconnected. Furthermore, a particular rack may be completely loaded with fuel assemblies (which corresponds to greatest rack inertia), or it may be completely empty. The coefficient of friction,  $\mu$ , between the supports and pool floor is another indeterminate factor. According to Rabinowicz (Ref. 4) the results of 199 tests performed on austenitic stainless steel plates submerged in water show a mean value of  $\mu$  to be 0.503 with a standard deviation of 0.125. The upper and lower bounds (based on twice the standard deviation) are thus 0.753 and 0.253, respectively. Two separate analyses are performed for the rack assemblies with values of the coefficient of friction equal to 0.2 (lower limit) and 0.8 (upper limit), respectively. Analyses performed for the geometrically limiting rack modules focus on limiting values of the coefficient of friction, and the number of fuel assemblies stored. Cases studied are for the 12x14 rack, for the 7x14 rack, and for a special rack with 35 regular locations and 12 large storage cells. Typical simulations are:

- 0 Fully loaded rack (all storage locations occupied),  
 $\mu = 0.8; 0.2$  ( $\mu =$  coefficient of friction)
- 0 Rack half full,  $\mu = 0.8, 0.2$

The simulations were performed using a consolidated fuel weight of 3000# per cell. The case of nearly empty racks is found not to be critical.

The method of analysis employed is the time-history method. The pool slab acceleration data were developed from the response spectra provided by Sargent and Lundy Engineers, Chicago, Illinois.

The objective of the seismic analysis is to determine the structural response (stresses, deformation, rigid body motion, etc.) due to simultaneous application of the three statistically independent, orthogonal excitations. Thus, recourse to approximate statistical summation techniques such as the "Square-Root-of-the-Sum-of-the-Squares" method (Ref. 5) is avoided. For nonlinear analysis, the only practical method is simultaneous application.

Pool slab acceleration data are provided for two earthquakes: Operating Basis Earthquake (OBE) and Safe Shutdown Earthquake (SSE). Figures 6.1 - 6.3 show the time-histories corresponding to the SSE condition.

The seismic analysis is performed in three steps, namely:

1. Development of a nonlinear dynamic model consisting of inertial mass elements and gap and friction elements.
2. Generation of the equations of motion and inertial coupling and solution of the equations using the "component element time integration scheme" (References 6 and 7) to determine nodal forces and displacements.
3. Computation of the detailed stress field in the rack (at the critical location) and in the support legs using the nodal forces calculated in the previous step. These stresses are checked against the design limits given in Section 6.5.

A brief description of the dynamic model follows.

## 6.2 FUEL RACK - FUEL ASSEMBLY MODEL

Since the racks are not anchored to the pool slab or attached to the pool walls or to each other, they can execute a wide variety of rigid body motions. For example, the rack may slide on the pool floor (so-called "sliding condition"); one or more legs may momentarily lose contact with the liner ("tipping condition"); or the rack may experience a combination of sliding and tipping conditions. The structural model should permit simulation of these kinematic events with inherent built-in conservatism. Since the Byron racks are equipped with girdle bars to dissipate energy due to inter-rack impact (if it occurs), it is also necessary to model the inter-rack impact phenomena in a conservative manner. Similarly, lift off of the support legs and subsequent impacts must be modelled using appropriate impact elements, and Coulomb friction between the rack and the pool liner must be simulated by appropriate piecewise linear springs. These special attributes of the rack dynamics require a strong emphasis on the modeling of the linear and nonlinear springs, dampers, and stop elements. The model outline in the remainder of this section, and the model description in the following section describe the detailed modeling technique to simulate these effects, with emphasis placed on the nonlinearity of the rack seismic response.

### 6.2.1 Outline of Model

- a. The fuel rack structure is a folded metal plate assemblage welded to a baseplate and supported on four legs. The rack structure itself is a very rigid structure. Dynamic analysis of typical multicell racks has shown that the motion of the structure is captured almost completely by the behavior of a six degrees-of-freedom structure; therefore, the movement of the rack cross-section at any height is described in terms of the six degrees-of-freedom of the rack base. The rattling fuel is modelled by five lumped masses located at  $H$ ,  $.75H$ ,  $.5H$ ,  $.25H$ , and at the rack base. Fuel mass connectivity is included to model the fuel assembly stiffness.
- b. The seismic motion of a fuel rack is characterized by random rattling of fuel assemblies in their individual storage locations. Assuming that all assemblies vibrate in phase obviously exaggerates the computed dynamic loading on the rack structure. This assumption, however, greatly reduces the required degrees-of-freedom needed to model the fuel assemblies which are represented by five lumped masses located at different levels of the rack. The centroid of each fuel assembly mass can be located, relative to the rack structure centroid at that level, so as to simulate a partially loaded rack.



- c. The local flexibility of the rack-support interface is modeled conservatively in the analysis.
- d. The rack base support may slide or lift off the pool floor.
- e. The pool floor has a specified time-history of seismic accelerations along the three orthogonal directions.
- f. Fluid coupling between rack and assemblies, and between rack and adjacent racks, is simulated by introducing appropriate inertial coupling into the system kinetic energy. Inclusion of these effects uses the methods of References 4 and 6 for rack/assembly coupling and for rack/rack coupling (see Section 6.2.3 of this report).
- g. Potential impacts between rack and assemblies are accounted for by appropriate "compression only" gap elements between masses involved.
- h. Fluid damping between rack and assemblies, and between rack and adjacent rack, is conservatively neglected.
- i. The supports are modeled as "compression only" elements for the vertical direction and as "rigid links" for dynamic analysis. The bottom of a support leg is attached to a frictional spring as described in Section 6.3. The cross-section inertial properties of the support legs are computed and used in the final computations to determine support leg stresses.
- j. The effect of sloshing can be shown to be negligible at the bottom of a pool and is hence neglected.
- k. Inter-rack impact, if it occurs, is simulated by a series of gap elements at the top and bottom of the rack in the two horizontal directions. The most conservative case of adjacent rack movement is assumed; each adjacent rack is assumed to move completely out of phase with the rack being analyzed. The effect of misalignment is also considered. The rack is assumed misaligned so that the rack has a gap that varies linearly from 0 inch at one corner to 0.25 inch at the other corner along each side. Two different configurations are considered:
  - 1) All four adjacent racks are rotated in the same direction (configuration 1).
  - 2) Three of four adjacent racks are rotated in the same direction and the fourth one is rotated in the opposite direction (configuration 2).
- l. The form drag opposing the motion of the fuel assemblies in the storage locations is conservatively neglected in the results reported herein.
- m. The form drag opposing the motion of the fuel rack in the water is also conservatively neglected in the results reported herein.



n. The rattling of the fuel assemblies inside the storage locations causes the "gap" between the fuel assemblies and the cell wall to change from a maximum of twice the nominal gap to a theoretical zero gap. However, the fluid coupling coefficients (Ref. 8) utilized are based on linear vibration theory (Ref. 9). Studies in the literature show that inclusion of the nonlinear effect (viz. vibration amplitude of the same order of magnitude as the gap) drastically lowers the equipment response (Ref. 10).

Figure 6.4 shows a schematic of the model. Six degrees-of-freedom are used to track the motion of the rack structure. Figures 6.5 and 6.6, respectively, show the inter-rack impact springs and fuel assembly/storage cell impact springs at a particular level.

As shown in Figure 6.4, the model for simulating fuel assembly motion incorporates five lumped masses. The five rattling masses are located at the baseplate, at quarter height, at half height, at three quarter height, and at the top of the rack. Two degrees-of-freedom are used to track the motion of each rattling mass in the horizontal plane. The vertical motion of each rattling mass is assumed to be the same as the rack base.

### 6.2.2 Model Description

The absolute degrees-of-freedom associated with each of the mass locations are identified in Figure 6.4 and Table 6.1. The rattling masses (nodes 1\*, 2\*, 3\*, 4\*, 5\*) are described by translational degrees-of-freedom q7-q16.

$U_i(t)$  is the pool floor slab displacement seismic time-history. Thus, there are sixteen degrees-of-freedom in the system. Not shown in Fig. 6.4 are the gap elements used to model the support legs and the impacts with adjacent racks.

### 6.2.3 Fluid Coupling

An effect of some significance requiring careful modeling is the so-called "fluid coupling effect". If one body of mass ( $m_1$ ) vibrates adjacent to another body (mass  $m_2$ ), and both bodies are submerged in a frictionless fluid medium, then Newton's equations of motion for the two bodies have the form:

$$(m_1 + M_{11}) \ddot{X}_1 - M_{12} \ddot{X}_2 = \text{applied forces on mass } m_1$$

$$-M_{21} \ddot{X}_1 + (m_2 + M_{22}) \ddot{X}_2 = \text{applied forces on mass } m_2$$

$\ddot{X}_1, \ddot{X}_2$  denote absolute accelerations of mass  $m_1$  and  $m_2$ , respectively.

$M_{11}, M_{12}, M_{21},$  and  $M_{22}$  are fluid coupling coefficients which depend on the shape of the two bodies, their relative disposition, etc. Fritz (Ref. 9) gives data for  $M_{ij}$  for various body shapes and arrangements. It is to be noted that the above equation indicates that the effect of the fluid is to add a certain amount of mass to the body ( $M_{11}$  to body 1), and an external force which is proportional to the acceleration of the adjacent body (mass  $m_2$ ). Thus, the acceleration of one body affects the force field on another. This force is a strong function of the interbody gap, reaching large values for very small gaps. This inertial coupling is called fluid coupling. It has an important effect in rack dynamics. The lateral motion of a fuel assembly inside the storage location will encounter this effect. So will the motion of a rack adjacent to another rack. These effects are included in the equations of motion. For example, the fluid coupling is between nodes 2 and 2\* in Figure 6.4. Furthermore, the rack equations contain coupling terms which model the effect of fluid in the gaps between adjacent racks. The coupling terms modeling the effects of fluid flowing between adjacent racks are computed assuming that all adjacent racks are vibrating  $180^\circ$  out of phase from the rack being analyzed. Therefore, only one rack is considered surrounded by a hydrodynamic mass computed as if there were a plane of symmetry located in the middle of the gap region.

Finally, fluid virtual mass is included in the vertical direction vibration equations of the rack; virtual inertia is also added to the governing equation corresponding to the rotational degree-of-freedom,  $q_6(t)$ .

#### 6.2.4 Damping

In reality, damping of the rack motion arises from material hysteresis (material damping), relative intercomponent motion in structures (structural damping), and fluid drag effects (fluid damping). In the analysis, a maximum of 4% structural damping is imposed on elements of the rack structure during SSE seismic simulations. This is in accordance with the FSAR and NRC guidelines (Ref. 11). Material and fluid damping are conservatively

neglected. The dynamic model has the provision to incorporate fluid damping effects; however, no fluid damping has been used for this analysis.

#### 6.2.5 Impact

Any fuel assembly node (e.g. 2\*) may impact the corresponding structural mass node 2. To simulate this impact, four compression-only gap elements around each rattling fuel assembly node are provided (see Figure 6.6). As noted previously, fluid dampers may also be provided in parallel with the springs. The compressive loads developed in these springs provide the necessary data to evaluate the integrity of the cell wall structure and stored array during the seismic event. Figure 6.5 shows the location of the impact springs used to simulate any potential for inter-rack impacts. Section 6.4.2 gives more details on these additional impact springs.

### 6.3 ASSEMBLY OF THE DYNAMIC MODEL

The cartesian coordinate system associated with the rack has the following nomenclature:

- 0 x = Horizontal coordinate along the short direction of rack rectangular platform
- 0 y = Horizontal coordinate along the long direction of the rack rectangular platform
- 0 z = Vertically upward

As described in the preceding section, the rack, along with the base, supports, and stored fuel assemblies, is modeled for the general three-dimensional (3-D) motion simulation by a sixteen degree-of-freedom model. To simulate the impact and sliding phenomena expected, 64 nonlinear gap elements and 16 nonlinear friction elements are used. Gap and friction elements, with their connectivity and purpose, are presented in Table 6.2.

A descriptive model restricted to two dimensions (one horizontal motion plus vertical motion) of the simulated structure which includes gap and friction elements is shown in Figure 6.7. Note that only the top rattling mass is shown for clarity.

The impacts between fuel assemblies and rack show up in the gap elements, having local stiffness  $K_1$ , in Figure 6.7. In Table 6.2, gap elements 5 through 8 are for the vibrating mass at the top of the rack. The support leg spring rates  $K_s$  are modeled by elements 1 through 4 in Table 6.2. Note that the local compliance of the concrete floor is included in  $K_s$ . To simulate sliding potential, friction elements 2 plus 8 and 4 plus 6 (Table 6.2) are shown in Figure 6.7. The friction of the support/liner interface is modeled by a piecewise linear spring with a suitably large stiffness  $K_f$  up to the limiting lateral load,  $\mu N$ , where  $N$  is the current compression load at the interface between support and liner. At every time step during the transient analysis, the current value of  $N$  (either zero for liftoff condition, or a compressive finite value) is computed. Finally, the support rotational friction springs  $K_R$  reflect any rotational restraint that may be offered by the foundation. This spring rate is calculated using a modified Boussinesq equation (Ref. 4) and is included to simulate the resistive moment of the support to counteract rotation of the rack leg in a vertical plane. This rotation spring is also nonlinear, with a zero spring constant value assigned after a certain limiting condition of slab moment loading is reached.

The nonlinearity of these springs (friction elements 9, 11, 13, and 15 in Table 6.2) reflects the edging limitation imposed on the base of the rack support legs. In this analysis, this effect is neglected; any support leg bending, induced by liner/baseplate friction forces, is resisted by the leg acting as a beam cantilevered from the rack baseplate.

The spring rate  $K_s$  modeling the effective compression stiffness of the structure in the vicinity of the support, is computed from the equation:

$$\frac{1}{K_s} = \frac{1}{K_1} + \frac{1}{K_2} + \frac{1}{K_3}$$

where:

$K_1$  = spring rate of the support leg treated as a tension-compression member =  $E_{\text{SUPPORT}} * A_{\text{SUPPORT}}/h$   
(h = length of support leg)

$K_2 = 1.05E_C B/(1 - \nu^2)$  = local spring rate of pool slab ( $E_C$  = Young's modulus of concrete, and B = length of bearing surface)

$K_3$  = spring rate of folded plate cell structure above support leg (same form as  $K_2$  with E chosen to reflect the local stiffness of the honeycomb structure above the leg)

For the 3-D simulation, all support elements (listed in Table 6.2) are included in the model. Coupling between the two horizontal seismic motions is provided both by the offset of the fuel assembly group centroid which causes the rotation of the entire rack and by the possibility of liftoff of one or more support legs. The potential exists for the rack to be supported on one or more support legs or to liftoff completely during any instant of a complex 3-D seismic event. All of these potential events may be simulated during a 3-D motion.

## 6.4 TIME INTEGRATION OF THE EQUATIONS OF MOTION

### 6.4.1 Time-History Analysis Using Multi-Degree of Freedom Rack Model

Having assembled the structural model, the dynamic equations of motion corresponding to each degree-of-freedom are written by using Lagrange's Formulation. The system kinetic energy can be constructed including contributions from the solid structures and from the trapped and surrounding fluid. A single rack is modelled in detail. The system of equations can be represented in matrix notation as:

$$[M] \{\ddot{q}\} = \{Q\} + \{G\}$$

where the vector  $\{Q\}$  is a function of nodal displacements and velocities, and  $\{G\}$  depends on the coupling inertia and the ground acceleration. Premultiplying the above equations by  $[M]^{-1}$  renders the resulting equation uncoupled in mass.

We have: 
$$\{\ddot{q}\} = [M]^{-1} \{Q\} + [M]^{-1} \{G\}$$

As noted earlier, in the numerical simulations run to verify structural integrity during a seismic event, all elements of the fuel assemblies are assumed to move in phase. This will provide maximum impact force level, and induce additional conservatism in the time-history analysis.

This equation set is mass uncoupled, displacement coupled, and is ideally suited for numerical solution using a central difference scheme. The computer program "DYNARACK"\* is utilized for this purpose.

Stresses in various portions of the structure are computed from known element forces at each instant of time.

Dynamic analysis of typical multicell racks has shown that the motion of the structure is captured almost completely by the behavior of a six-degree-of-freedom structure; therefore, in this analysis model, the movement of the rack cross-section at any height is described in terms of the rack base degrees-of-freedom ( $q_1(t), \dots, q_6(t)$ ). The remaining degrees-of-freedom are associated with horizontal movements of the fuel assembly masses. In this dynamic model, five rattling masses are used to represent fuel assembly movement in the horizontal plane. Therefore, the final dynamic model consists of six degrees-of-freedom for the rack plus ten additional mass degrees-of-freedom for the five rattling masses. The totality of fuel mass is included in the simulation and is distributed among the five rattling masses.

---

\*This code has been previously utilized in licensing of similar racks for Fermi 2 (Docket No. 50-341), Quad Cities 1 and 2 (Docket Nos. 50-254 and 265), Rancho Seco (Docket No. 50-312), Oyster Creek (Docket No. 50-219), V.C. Summer (Docket No. 50-395), and Diablo Canyon 1 and 2 (Docket Nos. 50-275 and 50-323).



#### 6.4.2 Evaluation of Potential for Inter-Rack Impact

Since the racks are closely spaced, the simulation includes impact springs to model the potential for inter-rack impact, especially for low values of the friction coefficient between the support and the pool liner. To account for this potential, yet still retain the simplicity of simulating only a single rack, gap elements were located on the rack at the top and at the baseplate level. Figure 6.5 shows the location of these gap elements. Loads in these elements, computed during the dynamic analysis, are used to assess rack integrity if inter-rack impact occurs.

#### 6.5 STRUCTURAL ACCEPTANCE CRITERIA

There are two sets of criteria to be satisfied by the rack modules:

##### a. Kinematic Criterion

This criterion seeks to ensure that the rack is a physically stable structure. Byron racks are designed to sustain certain inter-rack impact at designated locations in the rack modules. Therefore, physical stability of the rack is considered along with the localized inter-rack impacts. Localized permanent deformation of the module is permissible, so long as the subcriticality of the stored fuel array is not violated.

##### b. Stress Limits

The stress limits of the ASME Code, Section III, Subsection NF, 1983 Edition are used since this code provides the most appropriate and consistent set of limits for various stress types and various loading conditions. The following loading combinations are applicable (Ref. i).



<u>Loading Combination</u>	<u>Stress Limit</u>
D + L D + L + T <sub>o</sub> D + L + T <sub>c</sub> + E	Level A service limits
D + L + T <sub>a</sub> + E D + L + T <sub>o</sub> + P <sub>f</sub>	Level B service limits
D + L + T <sub>a</sub> + E' D + L + F <sub>d</sub>	Level D service limits The functional capability of the fuel racks should be demonstrated.

where:

- D = Dead weight-induced stresses (including fuel assembly weight)
- L = Live Load (0 for the structure, since there are no moving objects in the rack load path).
- F<sub>d</sub> = Force caused by the accidental drop of the heaviest load from the maximum possible height.
- P<sub>f</sub> = Upward force on the racks caused by postulated stuck fuel assembly
- E = Operating Basis Earthquake
- E' = Safe Shutdown Earthquake
- T<sub>o</sub> = Differential temperature induced loads (normal or upset condition)
- T<sub>a</sub> = Differential temperature induced loads (abnormal design conditions)

The conditions T<sub>a</sub> and T<sub>o</sub> cause local thermal stresses to be produced. The worst situation will be obtained when an isolated storage location has a fuel assembly which is generating heat at the maximum postulated rate. The surrounding storage locations are assumed to contain no fuel. The heated water makes unobstructed contact with the inside of the storage walls, thereby producing the maximum possible temperature difference between the adjacent cells. The secondary stresses thus produced are limited to the body of the rack; that is, the support legs do not experience the secondary (thermal) stresses.

## 6.6 MATERIAL PROPERTIES

The data on the physical properties of the rack and support materials, obtained from the ASME Boiler & Pressure Vessel Code, Section III, appendices, and supplier's catalog, are listed in Tables 6.3 and 6.4. Since the maximum pool bulk temperature (except for the full core discharge case) is  $150^{\circ}$ , this is used as the reference design temperature for evaluation of material properties.

## 6.7 STRESS LIMITS FOR VARIOUS CONDITIONS

The following stress limits are derived from the guidelines of the ASME Code, Section III, Subsection NF, in conjunction with the material properties data of the preceding section.

### 6.7.1 Normal and Upset Conditions (Level A or Level B)

- a. Allowable stress in tension on a net section  
 $= F_t = 0.6 S_y$  or
- $$F_t = (0.6) (23,150) = 13,890 \text{ psi (rack material)}$$
- $F_t$  = is equivalent to primary membrane stresses
- $$F_t = (.6) (27,500) = 16,500 \text{ psi (upper part of support feet)}$$
- $$= (.6) (62,400) = 37,440 \text{ psi (lower part of support feet)}$$
- b. On the gross section, allowable stress in shear is:
- $$F_v = .4 S_y$$
- $$(.4)^y (23,150) = 9,260 \text{ psi (main rack body)}$$
- $$F_v = (.4) (27,500) = 11,000 \text{ psi (upper part of support feet)}$$
- $$= (.4) (62,400) = 24,960 \text{ psi (lower part of support feet)}$$

c. Allowable stress in compression,  $F_a$ :

$$F_a = S_y \left[ 1 - \frac{1}{2} \left( \frac{k_1}{r C_c} \right)^2 \right] / \left[ \frac{5}{3} + \left( \frac{3}{8} \frac{k_1}{r C_c} \right) - \frac{1}{8} \left( \frac{k_1}{r C_c} \right)^3 \right]$$

where:

$$C_c = \left( \frac{2\pi^2 E}{S_y} \right)^{0.5}$$

$k_1/r$  for the main rack body is based on the full height and cross section of the honeycomb region. Substituting numbers, we obtain, for both support leg and honeycomb region:

$$\begin{aligned} F_a &= 13,890 \text{ psi (main rack body)} \\ F_a &= 16,500 \text{ psi (upper part of support feet)} \\ F_a &= 37,440 \text{ psi (lower part of support feet)} \end{aligned}$$

d. Maximum allowable bending stress at the outermost fiber due to flexure about one plane of symmetry:

$$\begin{aligned} F_b &= 0.60 S_y = 13,890 \text{ psi (rack body)} \\ F_b &= 16,500 \text{ psi (upper part of support feet)} \\ F_b &= 37,440 \text{ psi (lower part of support feet)} \end{aligned}$$

e. Combined flexure and compression:

$$\frac{f_a}{F_a} + \frac{C_{mx} f_{bx}}{D_x F_{bx}} + \frac{C_{my} f_{by}}{D_y F_{by}} < 1$$

where:

$$\begin{aligned} f_a &= \text{Direct compressive stress in the section} \\ f_{bx} &= \text{Maximum flexural stress about x-axis} \\ f_{by} &= \text{Maximum flexural stress about y-axis} \\ C_{mx} &= C_{my} = 0.85 \end{aligned}$$

$$D_x = 1 - \frac{f_a}{F'_{ex}}$$

$$D_y = 1 - \frac{f_a}{F'_{ey}}$$

where:

$$F'_{ex,ey} = \frac{12\pi^2 E}{23 \left( \frac{k_1}{r_{bx,y}} \right)^2}$$

and the subscripts x,y reflect the particular bending plane of interest.

f. Combined flexure and compression (or tension):

$$\frac{f_a}{0.6S_y} + \frac{f_{bx}}{F_{bx}} + \frac{f_{by}}{F_{by}} < 1.0$$

The above requirement should be met for both the direct tension or compression case.

#### 6.7.2 Level D Service Limits

F-1370 (Section III, Appendix F), states that the limits for the Level D condition are the minimum of 1.2 ( $S_y/F_t$ ) or 0.7( $S_u/F_t$ ) times the corresponding limits for Level A condition. Since 1.2  $S_y$  is less than 0.7  $S_u$  for the rack material, and for the upper part of the support feet, the multiplying factor for the limits is 2.0 for the SSE condition for the upper section. The factor is 1.68 for the lower section under SSE conditions.

Instead of tabulating the results of these six different stresses as dimensioned values, they are presented in a dimensionless form. These so-called stress factors are defined as the ratio of the actual developed stress to its specified limiting value. With this definition, the limiting value of each stress factor is 1.0 for OBE and 2.0 or 1.68 for the SSE condition.

#### 6.8 RESULTS

Figures 6.1; 6.2, and 6.3 show the pool slab motion in horizontal x, horizontal y, and vertical directions. This motion is for the SSE earthquake.

Results are abstracted here for a 12x14 module (the largest module) and for a 7 x 14 module (largest aspect ratio) next to the cask pit. Results are also presented for the J1 rack which has a special configuration.

A complete synopsis of the analysis of the 12x14, the 7x14 module, and the J1 module, subject to the SSE earthquake motions are presented in summary Tables 6.5a through 6.5l which gives the bounding values of stress factors  $R_i$  ( $i = 1, 2, 3, 4, 5, 6$ ). The stress factors are defined as:

- $R_1$  = Ratio of direct tensile or compressive stress on a net section to its allowable value (note support feet only support compression)
- $R_2$  = Ratio of gross shear on a net section to its allowable value
- $R_3$  = Ratio of maximum bending stress due to bending about the x-axis to its allowable value for the section
- $R_4$  = Ratio of maximum bending stress due to bending about the y-axis to its allowable value
- $R_5$  = Combined flexure and compressive factor (as defined in 6.7.1e above)
- $R_6$  = Combined flexure and tension (or compression) factor (as defined in 6.7.1f above)

As stated before, the allowable value of  $R_i$  ( $i = 1, 2, 3, 4, 5, 6$ ) is 1 for the OBE condition, and 2 for the SSE (except for the lower section of the support where the factor is 1.68)

The dynamic analysis gives the maximax (maximum in time and in space) values of the stress factors at critical locations in the rack module. Values are also obtained for maximum rack displacements and for critical impact loads. Tables 6.5a through 6.5l presents the results of the dynamic analyses. The fuel load in each case was assumed to be consolidated, with weight of 3000# per assembly.

It is found that the results corresponding to SSE are most critical vis-a-vis the corresponding allowable limits. The results given herein are for the SSE. The maximum stress factors ( $R_i$ ) are below the limiting value for the SSE condition for all sections. It is noted that the critical load factors reported for the support feet are all for the upper segment of the foot and are to be compared with the limiting value of 2.0.

Analyses (not included here) have been carried out to show that significant margins of safety exist against local deformation of the fuel storage cell due to rattling impact of fuel assemblies and against local overstress of impact bars due to inter-rack impact.

Benchmark analyses (not presented here) have also been carried out for the OBE condition. Comparison between OBE and SSE shown that the SSE condition controls the design of the fuel racks.

## 6.9 IMPACT ANALYSES

### 6.9.1 Impact Loading Between Fuel Assembly and Cell Wall

The local stress in a cell wall is estimated from peak impact loads obtained from the dynamic simulations. Plastic analysis is used to obtain the limiting impact load that can be tolerated. Including a safety margin of 2.0, we find that the total limit load for the number of cells (NC) is:

$$QL = 9030 \text{ NC}$$

### 6.9.2 Impacts Between Adjacent Racks

All of the dynamic analyses assume, conservatively, that adjacent racks move completely out of phase. Thus, the highest potential for inter-rack impact is achieved. Based on the dynamic loads obtained in the gap elements simulating adjacent racks, we can study rack integrity in the vicinity of the impact point. The use of framing material around the top of the rack allows us to withstand impact loads. It is shown that rack-to-rack impact loads can be accommodated with the load levels shown in Tables 6.5i and 6.5k without causing any permanent deformation in the active fuel region. Thus, impacts between racks can be accommodated without violating rack integrity.

## 6.10 WELD STRESSES

Critical weld locations under seismic loading are at the bottom of the rack at the baseplate connection and at the welds on the support legs. Results from the dynamic analysis using the simulation codes are surveyed and the maximum loading is used to qualify the welds on these locations.

### 6.10.1 Baseplate to Rack Welds and Cell-to-Cell Welds

Section NF permits, for the SSE condition, an allowable weld stress  $\tau = .42 S_u = 28,600$  psi. The calculated weld stress, based on the highest load factor, is 7735 psi for the baseplate to rack welds.

The critical area that must be considered for cell-to-cell welds is the weld between gap channels and tubes. Where skip welding is used, this weld is continuous near the baseplate but is a skip weld (2" on 10.25" spacing) as we move up the tube. The critical shear stress in this area for the SSE condition is less than 14000 psi where account is taken of the skip welds or spot welds used in this region. Near the bottom of the rack where this shear stress dominates, there are no other stresses on the weld which need be considered.

Stresses in the channel-to-cell welds may also develop due to fuel assembly impact with the cell wall near the top of the rack. This will occur if fuel assemblies in adjacent tubes are moving out of phase with one another so that impact loads in two adjacent cells are in opposite directions which would tend to separate the channel from the tube at the weld. Our analysis shows that the maximum weld shear stress in this area is less than 8000 psi.

### 6.10.2 Heating of an Isolated Cell

Weld stresses due to heating of an isolated hot cell are also computed. The assumption used is that a single cell is heated, over its entire length, to a temperature above the value associated with all surrounding cells. No thermal gradient in the vertical direction is assumed so that the results are conservative. Using the temperatures associated with this unit, we show that the skip welds along the entire cell length do not exceed the allowable value for a thermal loading condition.



The mathematical model constructed to determine the impact velocity of falling objects is based on several conservative assumptions, such as:

1. The virtual mass (see Ref. 8-10 for further material on this subject) of the body is conservatively assumed to be equal to its displaced fluid mass. Evidence in the literature (Ref. 12), indicates that the virtual mass can be many times higher.
2. The minimum frontal area is used for evaluating the drag coefficient.
3. The drag coefficients utilized in the analysis are the lower bound values reported in the literature (Ref. 13). In particular, at the beginning of the fall when the velocity of the body is small, the corresponding Reynolds number is low, resulting in a large drag coefficient.
4. The falling bodies are assumed to be rigid for the purposes of impact stress calculation on the rack. The solution of the immersed body motion problem is found analytically. The impact velocity thus computed is used to determine the maximum stress generated due to stress wave propagation.

With this model, the following analyses are performed:

a. Dropped Fuel Accident I

A fuel assembly (weight = 1616 pounds) is dropped from 36 inches above the module and impacts the base. The final velocity of the dropped fuel assembly (just prior to impact) is calculated and, thus, the total energy at impact is known. To study baseplate integrity, we assume that this energy is all directed toward punching of the baseplate in shears and thus transformed into work done by the supporting shear stresses. It is determined that shearing deformation of the baseplate is less than the thickness of the baseplate so that we conclude that local piercing of the baseplate will not occur. Direct impact with the pool liner does not occur. The subcriticality of the adjacent fuel assemblies is not violated.

b. Dropped Fuel Accident II

One fuel assembly drops from 36 inches above the rack and hits the top of the rack. Permanent deformation of the rack is found to be limited to the top region such that the rack cross-sectional geometry at the level of the top of the active fuel (and below) is not altered. The region of local permanent deformation does not extend below 6 inches from the rack top. An energy balance approach is used here to obtain the results.

c. Jammed Fuel-handling Equipment

A 4400-pound uplift force is applied at the top of the rack at the "weakest" storage location; the force is assumed to be applied on one wall of the storage cell boundary as an upward shear force. The plastic deformation is found to be limited to the region well above the top of the active fuel.

These analyses prove that the rack modules are engineered to provide maximum safety against all postulated abnormal and accident conditions.

6.12 DEFINITION OF TERMS USED IN SECTION 6

S1, S2, S3, S4	Support designations
$P_i$	Absolute degree-of-freedom number $i$
$q_i$	Relative degree-of-freedom number $i$
$\mu$	Coefficient of friction
$U_i$	Pool floor slab displacement time history in the $i$ -th direction
$x, y$ coordinates	horizontal direction
$z$ coordinate	vertical direction
$K_I$	Impact spring between fuel assemblies and cell
$K_f$	Linear component of friction spring
$K_s$	Axial spring of support leg locations
$N$	Compression load in a support foot
$K_R$	Rotational spring provided by the pool slab
Subscript $i$	When used with $U$ or $X$ indicates direction ( $i = 1$ x-direction, $i = 2$ y-direction, $i = 3$ z-direction)

## REFERENCES TO SECTION 6

1. USNRC Standard Review Plan, NUREG-0800 (1981).
2. ASME Boiler & Pressure Vessel Code, Section III, Subsection NF (1983).
3. USNRC Regulatory Guide 1.29, "Seismic Design Classification," Rev. 3, 1978.
4. "Friction Coefficients of Water Lubricated Stainless Steels for a Spent Fuel Rack Facility," Prof. Ernest Rabinowicz, MIT, a report for Boston Edison Company, 1976.
5. USNRC Regulatory Guide 1.92, "Combining Modal Responses and Spatial Components in Seismic Response Analysis," Rev. 1, February, 1976.
6. "The Component Element Method in Dynamics with Application to Earthquake and Vehicle Engineering," S. Levy and J.P.D. Wilkinson, McGraw Hill, 1976.
7. "Dynamics of Structures," R.W. Clough and J. Penzien, McGraw Hill (1975).
8. "Mechanical Design of Heat Exchangers and Pressure Vessel Components," Chapter 16, K.P. Singh and A.I. Soler, Arcturus Publishers, Inc., 1984.
9. R.J. Fritz, "The Effects of Liquids on the Dynamic Motions of Immersed Solids," Journal of Engineering for Industry, Trans. of the ASME, February 1972, pp 167-172.
10. "Dynamic Coupling in a Closely Spaced Two-Body System Vibrating in Liquid Medium: The Case of Fuel Racks," K.P. Singh and A.I. Soler, 3rd International Conference on Nuclear Power Safety, Keswick, England, May 1982.
11. USNRC Regulatory Guide 1.61, "Damping Values for Seismic Design of Nuclear Power Plants," 1973.
12. "Flow Induced Vibration," R.D. Blevins, VonNostrand (1977).
13. "Fluid Mechanics," M.C. Potter and J.F. Foss, Ronald Press, p 459 (1975).

Table 6.1  
DEGREES OF FREEDOM

Location (Node)	Displacement			Rotation		
	$U_x$	$U_y$	$U_z$	$\theta_x$	$\theta_y$	$\theta_z$
1	$p_1$	$p_2$	$p_3$	$q_4$	$q_5$	$q_6$
2	Point 2 is assumed attached to rigid rack at the top most point.					
2*	$p_7$	$p_8$				
3*	$p_9$	$p_{10}$				
4*	$p_{11}$	$p_{12}$				
5*	$p_{13}$	$p_{14}$				
1*	$p_{15}$	$p_{10}$				

where:

$$\begin{aligned}
 p_i &= q_i(t) + U_1(t) & i &= 1, 7, 9, 11, 13, 15 \\
 &= q_i(t) + U_2(t) & i &= 2, 8, 10, 12, 14, 16 \\
 &= q_i(t) + U_3(t) & i &= 3
 \end{aligned}$$

$U_i(t)$  are the 3 known earthquake displacements.

Table 6.2

## NUMBERING SYSTEM FOR GAP ELEMENTS AND FRICTION ELEMENTS

I. Nonlinear Springs (Gap Elements) (60 Total)

<u>Number</u>	<u>Node Location</u>	<u>Description</u>
1	Support S1	Z compression only element
2	Support S2	Z compression only element
3	Support S3	Z compression only element
4	Support S4	Z compression only element
5	2,2	X rack/fuel assembly impact element
6	2,2*	X rack/fuel assembly impact element
7	2,2*	Y rack/fuel assembly impact element
8	2,2*	Y rack/fuel assembly impact element
9-24	Other rattling masses	
25	Bottom cross-section of rack (around edge)	Inter-rack impact elements
.		Inter-rack impact elements
.		Inter-rack impact elements
.		Inter-rack impact elements
.		Inter-rack impact elements
.		Inter-rack impact elements
44		Inter-rack impact elements
45	Top cross-section of rack (around edge)	Inter-rack impact elements
.		Inter-rack impact elements
.		Inter-rack impact elements
.		Inter-rack impact elements
.		Inter-rack impact elements
.		Inter-rack impact elements
.		Inter-rack impact elements
64		Inter-rack impact elements

Table 6.2 (continued)

## NUMBERING SYSTEM FOR GAP ELEMENTS AND FRICTION ELEMENTS

II. Friction Elements (16 total)

---

<u>Number</u>	<u>Node Location</u>	<u>Description</u>
1	Support S1	X direction support friction
2	Support S1	Y direction friction
3	Support S2	X direction friction
4	Support S2	Y direction friction
5	Support S3	X direction friction
6	Support S3	Y direction friction
7	Support S4	X direction friction
8	Support S4	Y direction friction
9	S1	X Slab moment
10	S1	Y Slab moment
11	S2	X Slab moment
12	S2	Y Slab moment
13	S3	X Slab moment
14	S3	Y Slab moment
15	S4	X Slab moment
16	S4	Y Slab moment

---

Table 6.3  
RACK MATERIAL DATA

Material	Young's Modulus E (psi)	Yield Strength S <sub>y</sub> (psi)	Ultimate Strength S <sub>u</sub> (psi)
304L S.S.	27.9 x 10 <sup>6</sup>	23150	68100
Section III Reference	Table I-6.0	Table I-2.2	Table I-3.2

Table 6.4  
SUPPORT MATERIAL DATA

Material	Young's Modulus E (psi)	Yield Strength S <sub>y</sub> (psi)	Ultimate Strength S <sub>u</sub> (psi)
1 SA-351-CF3 (upper part of support feet)	27.9 x 10 <sup>6</sup>	27,500	68,100
2 SA-217-CA15 (lower part of support feet)	27.9 x 10 <sup>6</sup>	62,400	90,000



Table 6.5a  
 RACK SUMMARY M1 (7x14)

Run #	Fuel Assembly to Cell Impact Load (#)	Rack/Rack Impact Load GB/BP	Rack/Wall Impact Load GB/BP
M12	$4.035 \times 10^4$	$8.343 \times 10^4$ <hr/> $6.165 \times 10^4$	0./0.
M18	$4.354 \times 10^4$	$2.062 \times 10^5$ <hr/> $1.247 \times 10^5$	0./0.
M28a	$3.30 \times 10^4$	$9.757 \times 10^4$ <hr/> $2.662 \times 10^4$	0./0.

\* GB = Girdle bar

BP = Baseplate

Table 6.5b  
 RACK SUMMARY M1 (7x14)

STRESS FACTORS

(Upper values for rack base - Lower values for support feet)

Run #	R <sub>1</sub>	R <sub>2</sub>	R <sub>3</sub>	R <sub>4</sub>	R <sub>5</sub>	R <sub>6</sub>
M12	.264	.054	.280	.347	.636	.715
	.573	.142	.255	.251	.621	.806
M18	.240	.204	.455	.683	.933	1.057
	.791	.559	1.001	.860	1.416	1.692
M28a	.104	.083	.246	.255	.394	.446
	.332	.278	.457	.495	.643	.771

Table 6.5c

## RACK SUMMARY M1 (7x14)

Run #	Remarks	Max. Disp. DX (in)	Max. Disp. DY (in)	Max. Vert. Disp. (in)
M12	$\mu = .2$ Full Load of Fuel Assemblies	.5218	.7385	.075
M18	$\mu = .8$ Full Load of Fuel Assemblies	1.822	.322	.209
M28a	$\mu = .8$ - 1% fuel load 1 positive x-half	.4936	.2011	.0343

Table 6.5d

## RACK SUMMARY M1 (7x14)

Run #	Remarks	Max. Floor Load (#) 4 Feet	Max. Floor* Load (#) Vertical/Shear
M12	$\mu = .2$ Full Load of fuel assemblies	$8.376 \times 10^5$	233593./44954.
M18	$\mu = .8$ Full Load of fuel assemblies	$7.437 \times 10^5$	722164./184918.
M28a	$\mu = .8$ 50% fuel load in positive x-half	$3.217 \times 10^5$	134546./83986.

---

\* Vertical = vertical load  
Shear = shear load

---

Table 6.5e

## RACK SUMMARY C1 12x14; C3 RACK

Run #	Remarks	Max. Disp. DX (in)	Max. Disp. DY (in)	Max. Vert. Disp. (in)
C28	C1 rack, $\mu = .8$ Fuel centroid at $x = 27.17''$ (1/2 full)	.346	.484	.076
C18d	C1 rack, $\mu = .8$ 168 cells have fuel assemblies	.346	.425	.116
C12	C1 rack, $\mu = .2$ 168 cells have fuel assemblies	.318	.363	.126
C51	C3 rack, $\mu = .8$ 168 cells with fuel; adjacent racks per configuration #1	.1239	.1318	.144
C53	C3 rack, $\mu = .8$ 168 cells with fuel; adjacent racks per configuration #2	.1375	.1321	.144

Table 6.5f

## RACK SUMMARY C1 12x14; C3 RACK

Run #	Remarks	Max. Floor Load (#) 4 Feet	Max. Floor* Load (#) Vertical/Shear
C28	C1 rack, $\mu = .8$ Fuel centroid at $x = 27.17''$ (1/2 full)	$6.221 \times 10^5$	$2.297 \times 10^5$ <hr/> $1.511 \times 10^5$
C18d	C1 rack, $\mu = .8$ 168 cells have fuel assemblies	$1.013 \times 10^6$	$3.831 \times 10^5$ <hr/> $1.831 \times 10^5$
C12	C1 rack, $\mu = .2$ 168 cells have fuel assemblies	$1.131 \times 10^6$	$3.585 \times 10^5$ <hr/> $.717 \times 10^5$
C51	C3 rack, $\mu = .8$ 168 cells with fuel; adjacent racks per configuration #1	$9.967 \times 10^5$	$2.724 \times 10^5$ <hr/> $.8319 \times 10^5$
C53	C3 rack, $\mu = .8$ 168 cells with fuel; adjacent racks per configuration #2	$9.767 \times 10^5$	$2.724 \times 10^5$ <hr/> $.9628 \times 10^5$

\* Vertical = vertical load  
Shear = shear load

Table 6.5g  
RACK SUMMARY J1

Run #	Remarks	Max. Disp. DX (in)	Max. Disp. DY (in)	Max. Vert. Disp. (in)
J101	$\mu = .8$ , 35 cells filled with 3000# assemblies	.5722	.3601	.0395
J201	$\mu = .2$ , 35 cells filled with 3000# assemblies	.492	2.0788	.043
J111	$\mu = .8$ , 70 cells filled with 3000# assemblies	1.214	.383	.185
J112	$\mu = .2$ , 70 cells filled with 3000# assemblies	.2893	.3348	.073
J150	$\mu = .8$ , 12 large cells with 10000# assemblies	.977	.628	.164
J151	$\mu = .2$ , 12 large cells with 10000# assemblies	.5923	.3023	.015



Table 6.5h  
RACK SUMMARY J1

Run #	Remarks	Max. Floor Load (#) 4 Feet	Max. Floor* Load (#) Vertical/Shear
J101	$\mu = .8$ , 35 cells filled with 3000# assemblies	$2.057 \times 10^5$	$\frac{118970.}{94444.}$
J201	$\mu = .2$ , 35 cells filled with 3000# assemblies	$2.392 \times 10^5$	$\frac{125000.}{24990.}$
J111	$\mu = .8$ , 70 cells filled with 3000# assemblies	$5.163 \times 10^5$	$\frac{226652.}{109011.}$
J112	$\mu = .2$ , 70 cells filled with 3000# assemblies	$4.866 \times 10^5$	$\frac{195021.}{38439.}$
J150	$\mu = .8$ , 12 large cells with 10000# assemblies	$3.744 \times 10^5$	$\frac{166930.}{86890.}$
J151	$\mu = .2$ , 12 large cells with 10000# assemblies	$2.163 \times 10^5$	$\frac{105420.}{21084.}$

\* Vertical = vertical load  
Shear = shear load

Table 6.5i

## RACK SUMMARY J1

Run #	Fuel Assembly to Cell Impact Load (#)	Rack/Rack Impact Load GB/BP	Rack/Wall Impact Load GB/BP*
J101	$6.761 \times 10^4$	$7.28 \times 10^4$ <hr/> 0.	0./0.
J201	$5.361 \times 10^4$	$6.827 \times 10^4$ <hr/> $2.261 \times 10^4$	0./0.
J111	$8.421 \times 10^4$	$1.099 \times 10^5$ <hr/> $2.749 \times 10^4$	0./0.
J112	$6.738 \times 10^4$	$6.115 \times 10^4$ <hr/> 0.	0./0.
J150	$1.002 \times 10^5$ (at bottom)	$7.362 \times 10^4$ <hr/> $3.555 \times 10^4$	0./0.
J151	$9.583 \times 10^4$ (at bottom)	$2.863 \times 10^4$ <hr/> $3.794 \times 10^4$	0./0.

\* GB = Girdle bar

BP = Baseplate

Table 6.5j  
RACK SUMMARY J1

Run #	STRESS FACTORS					
	(Upper values for rack base - Lower values for support feet)					
	R <sub>1</sub>	R <sub>2</sub>	R <sub>3</sub>	R <sub>4</sub>	R <sub>5</sub>	R <sub>6</sub>
J101	.092	.086	.242	.271	.448	.512
	.293	.327	.604	.335	.741	.884
J201	.109	.028	.341	.212	.489	.559
	.308	.082	.137	.151	.350	.454
J111	.233	.164	.375	.550	.684	.767
	.558	.347	.524	.640	.969	1.182
J112	.216	.056	.320	.292	.530	.582
	.480	.136	.250	.238	.539	.698
J150	.155	.148	.324	.308	.427	.490
	.411	.320	.590	.549	.707	.855
J151	.089	.023	.222	.191	.309	.351
	.260	.074	.136	.129	.295	.383

Table 6.5k  
RACK SUMMARY C1, C3 RACK

Run #	Fuel Assembly to Cell Impact Load (#)	Rack/Rack Impact Load GB/BP*	Rack/Wall Impact Load GB/BP*
C28	37570.	93410 ----- 0.	0./0.
C18d	70340.	101000 ----- 0.	0./0.
C12	70600	67310 ----- 46620	0./0.
C51	69830.	1.31x10 <sup>5</sup> ----- 8654.	N.A.
C53	69870.	1.331x10 <sup>5</sup> ----- 8727.	N.A.

\* GB = girdle bar      BP = baseplate

Table 6.51  
RACK SUMMARY C1, C3 RACK

<u>STRESS FACTORS</u>						
(Upper values for rack base - Lower values for support feet)						
Run #	R <sub>1</sub>	R <sub>2</sub>	R <sub>3</sub>	R <sub>4</sub>	R <sub>5</sub>	R <sub>6</sub>
C28	.118	.076	.325	.310	.433	.494
	.564	.474	.756	.807	1.171	1.403
C13d	.193	.102	.385	.264	.607	.679
	.940	.673	1.205	.967	1.402	1.675
C12	.215	.061	.250	.274	.483	.549
	.880	.241	.431	.399	.991	1.286
C51	.187	.052	.111	.087	.266	.281
	.669	.295	.366	.528	.834	1.042
C53	.187	.053	.110	.091	.266	.281
	.669	.319	.473	.571	.813	1.001

BYRON FUEL RACK - SSE EAST/WEST

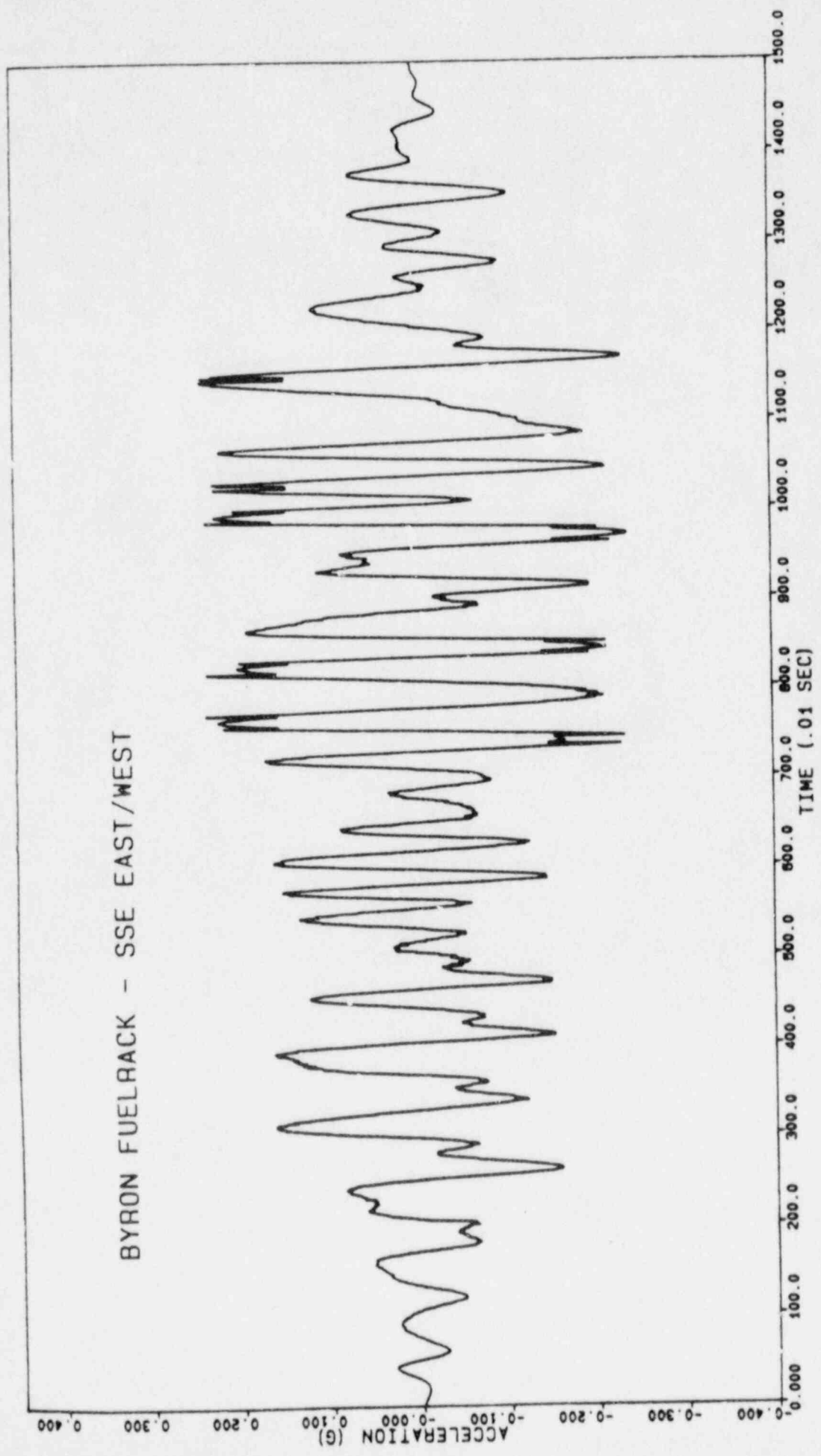


FIG. 6.1

BYRON FUEL RACK - SSE NORTH/SOUTH

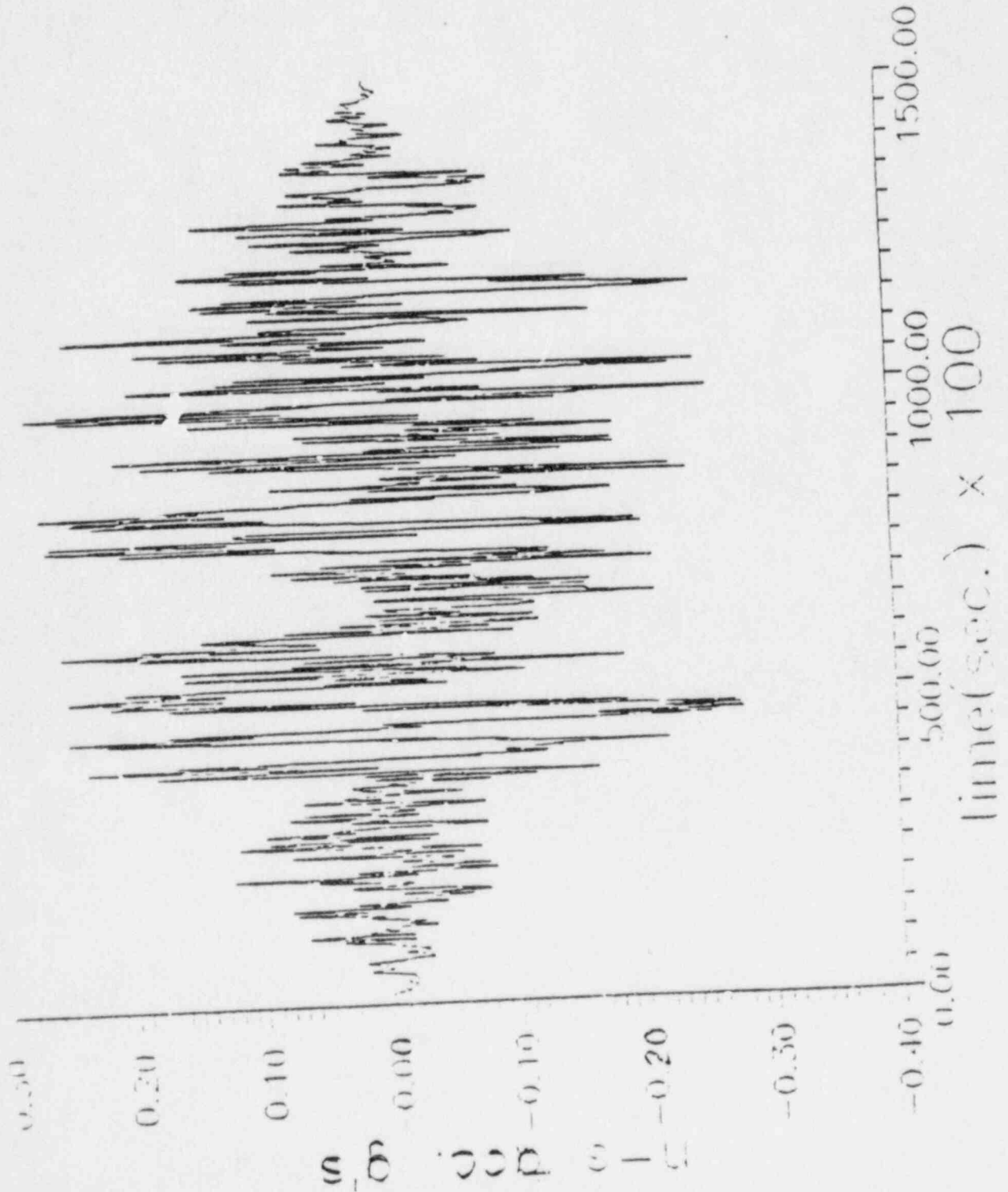
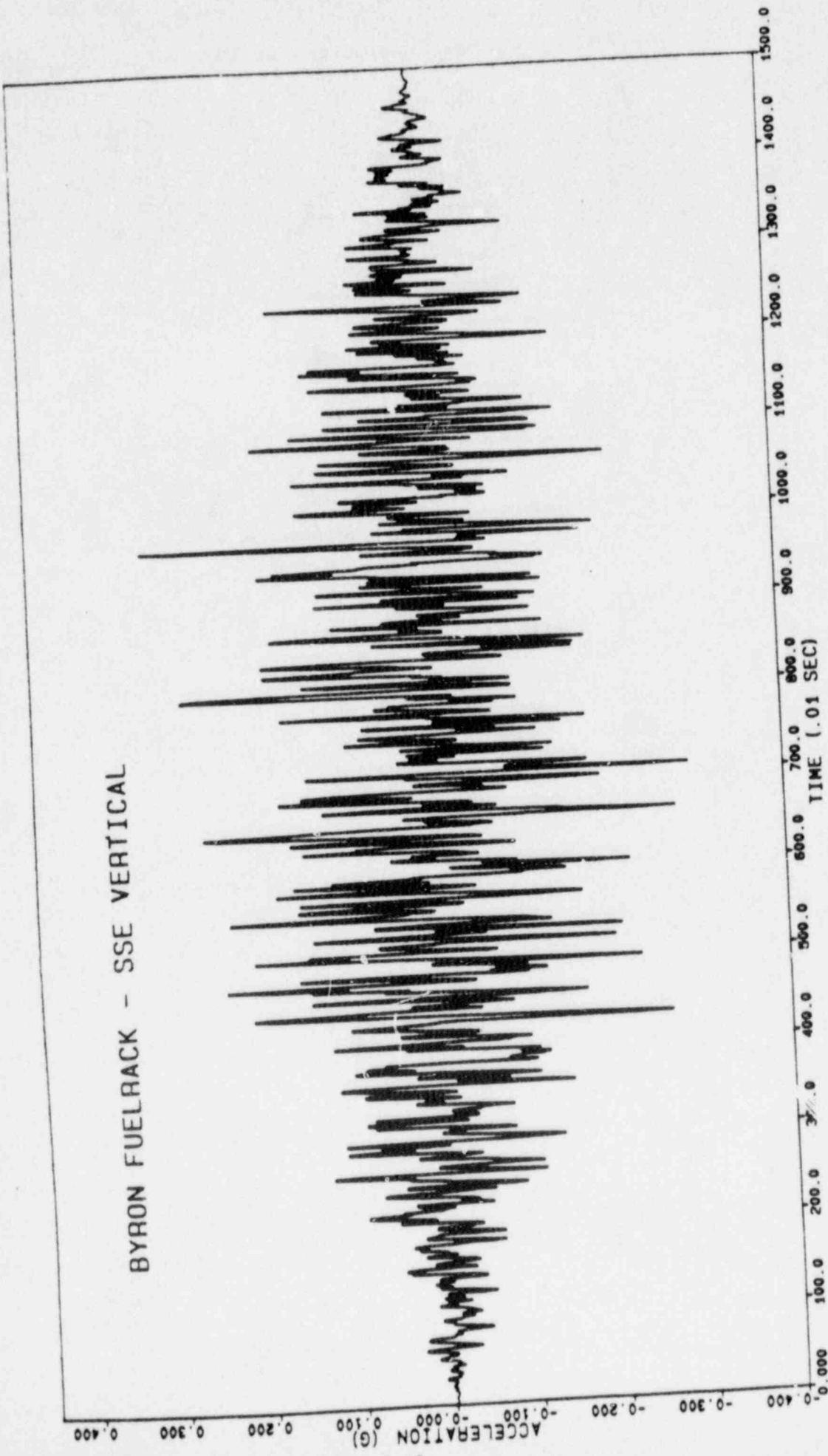


Fig. 6.2





BYRON

FIG. 6.3

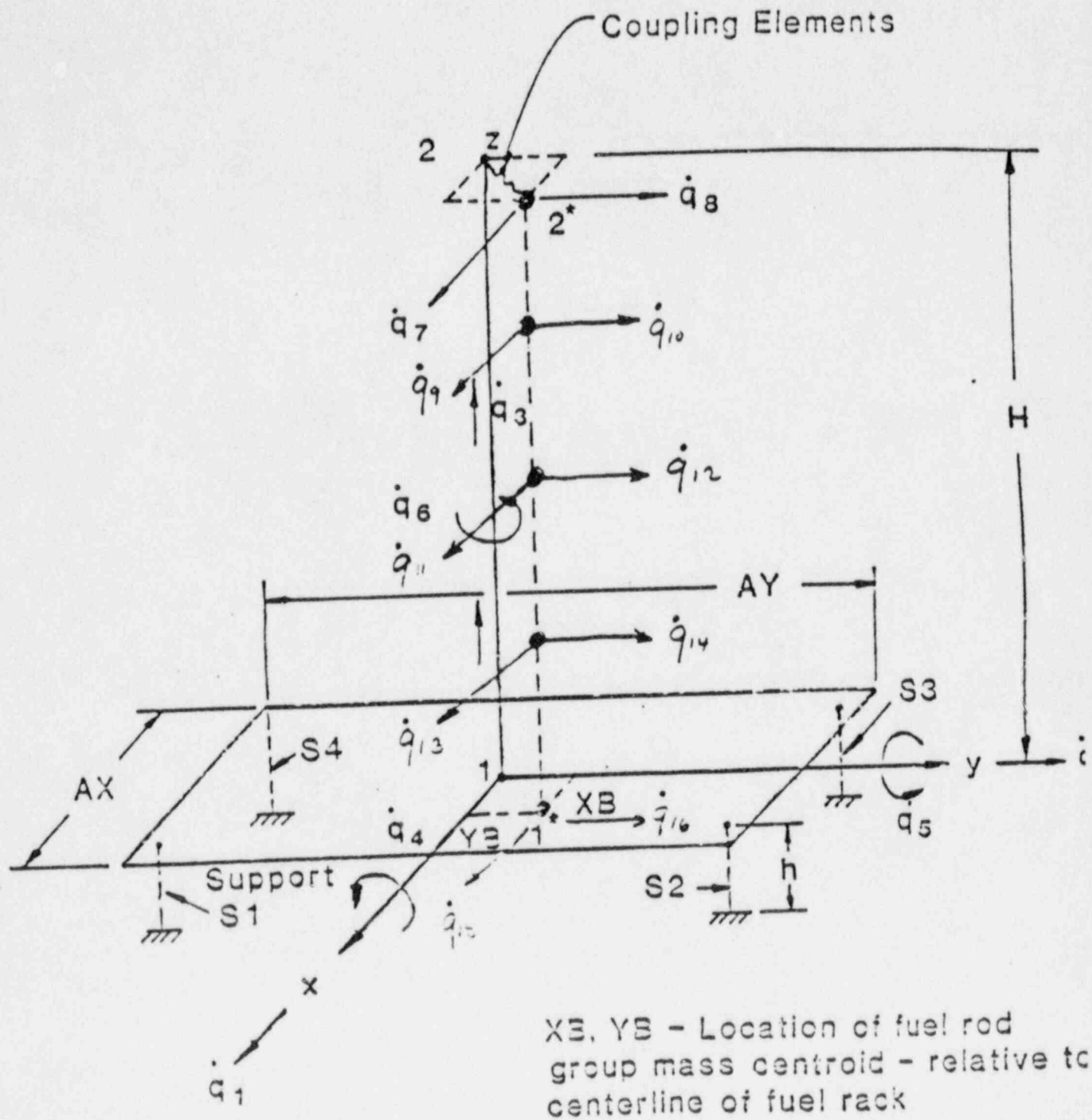


FIGURE 6.4 Dynamic Model

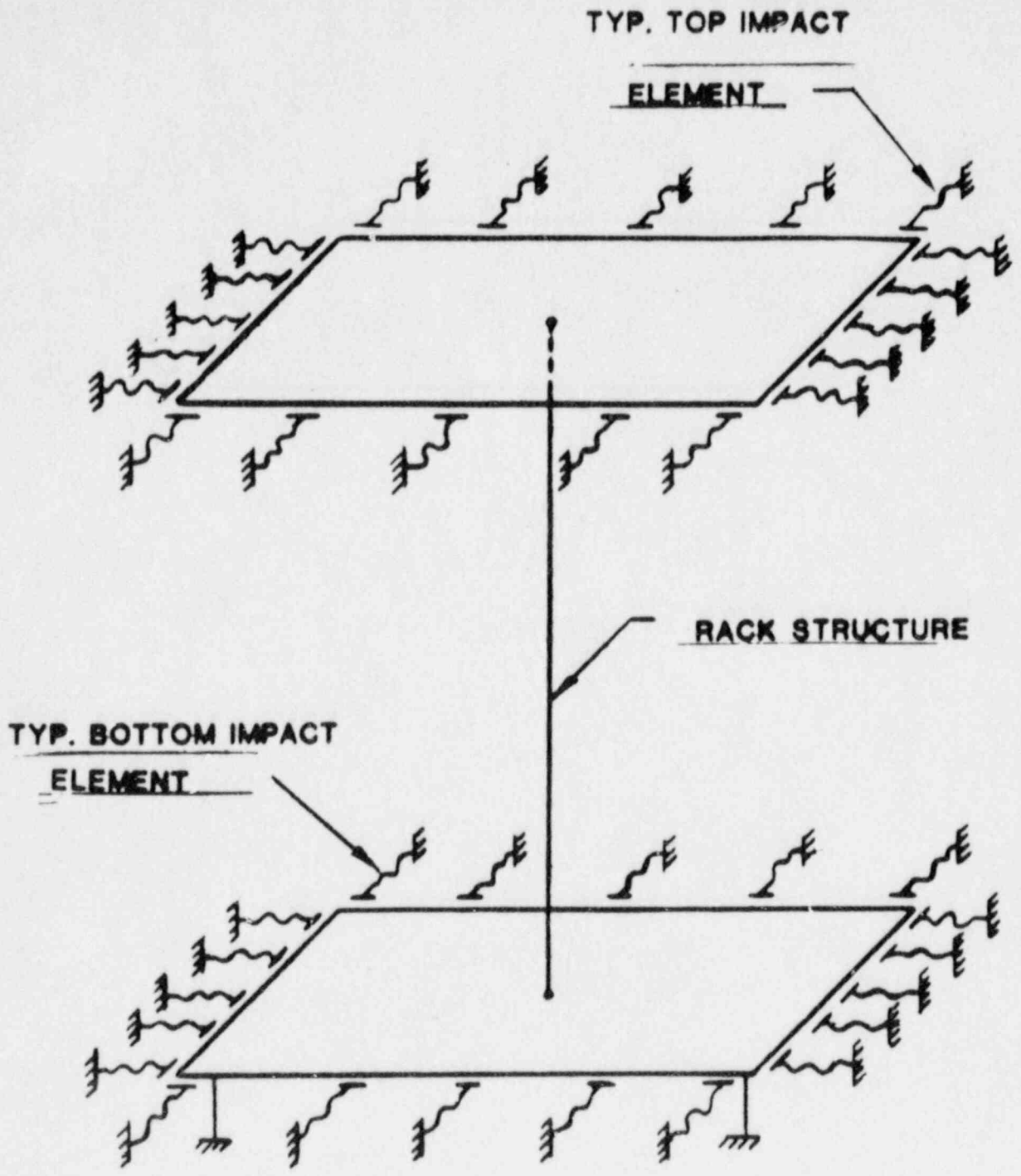


FIG. 6.5 GAP ELEMENTS TO SIMULATE INTER-RACK IMPACTS

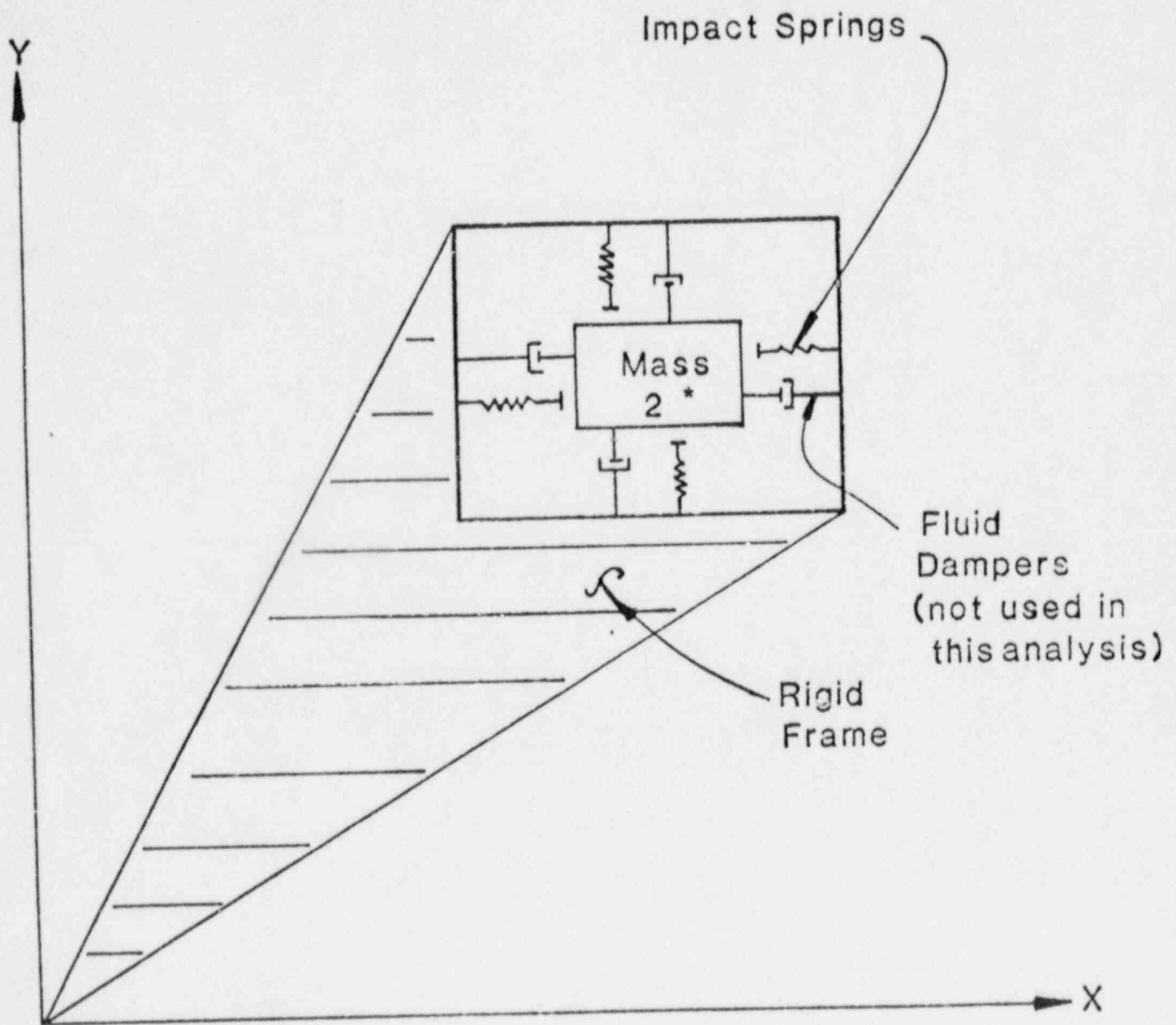


FIGURE 6.6 IMPACT SPRINGS AND FLUID DAMPERS

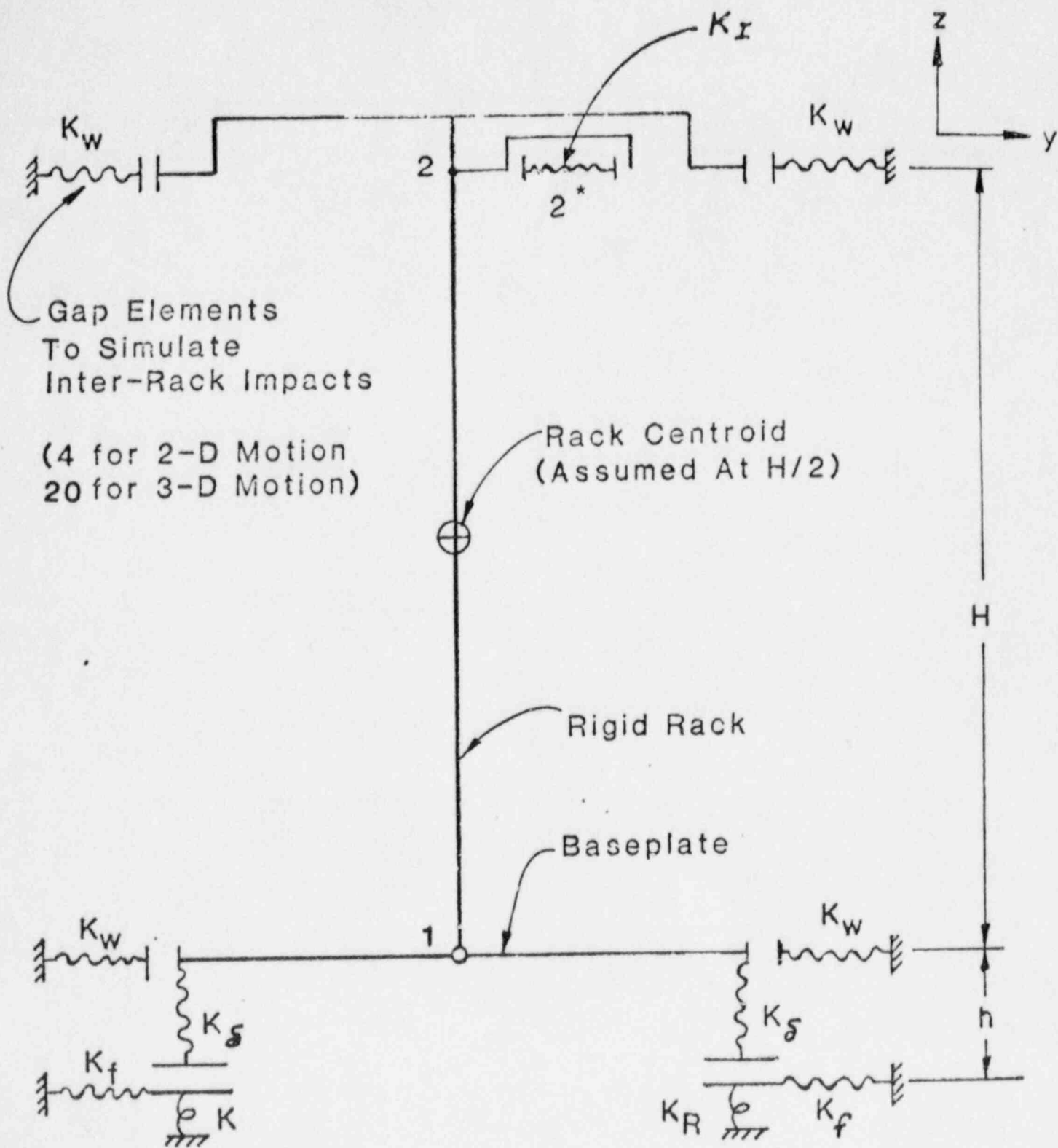


FIGURE 6.7 Spring Mass Simulation For Two-Dimensional Motion

## 7.0 ENVIRONMENTAL EVALUATION

### 7.1 SUMMARY

Installation of high density spent fuel storage racks at the Byron Nuclear Power Station will increase the licensed storage capacity of the spent fuel pool from 1060 to a maximum of 2870 assemblies. Radiological consequences of expanding the capacity have been evaluated with the objective of determining if there is a significant additional onsite or offsite radiological impact relative to that previously reviewed and evaluated (Ref. 1). In addition, radiological impact to operating personnel has been evaluated to ensure that exposures remain as low as is reasonably achievable (ALARA).

The decay heat loading and the radiological burden to the spent fuel pool water are determined almost entirely by refueling operations. The frequency of refueling operations and the conduct of refueling are independent of the increased capacity of the storage pool, except that the increased capacity should reduce fuel movement and allow continued normal operation. Since the fuel assemblies which will utilize the bulk of the storage capacity (and will ultimately fill all incremental capacity above that of the existing design) are aged, their contribution to either the peak decay-heat load or the increased radiological impact, in terms of increased doses, is negligible. A study performed by the NRC (Ref. 2) supports this conclusion. Consequently, the increase in the storage capacity of the spent fuel pool will neither significantly alter the operating characteristics of the current pool nor result in a measurable change in impact on the environment.

### 7.2 CHARACTERISTICS OF STORED FUEL

Because of radioactive decay, the heat generation rate and the intensity of gamma radiation from the spent fuel assemblies decreases substantially with decay time. After a cooling time of about 4 years (Ref. 3), the decay heat generation rate is less than 2% of the rate at 7 days, the nominal time at which depleted fuel assemblies are transferred to the spent fuel pool. The intensity of gamma radiation is very nearly proportional to the decay heat and decreases with cooling time in a similar manner.



The bulk of the heat load is due to freshly discharged fuel; aged fuel contributes relatively little to the total heat load. Therefore, this expansion will not significantly increase the thermal dissipation to the environment. Since the intensity of gamma radiation follows the decline in decay heat generation rate, it is similarly concluded that there will be no significant increase in gamma radiation beyond the pool environment due to the expanded storage.

It is important to note that the aged fuel in the expanded storage capacity will not contain significant amounts of radioactive iodine or short-lived gaseous fission products, since these would have decayed during the storage period. The Krypton-85 which might escape from defective fuel assemblies has been shown to do so quickly (Ref. 2) (i.e., within a short time after discharge from the core). Further, the residual Krypton-85 will be contained within the fuel pellet matrix and hence any leakage would occur at very low rates (Ref. 2). Cesium 134/137 (Ref. 2) is strongly bound within the fuel pellet matrix and its dissolution rate in water is extremely small. Any Cesium dissolved in the pool water is easily controllable in the cleanup system (demineralizer-ion exchanger resin bed) (Ref. 2). Thus, the planned storage expansion will not significantly increase the release of gaseous radionuclides.

### 7.3 RELATED INDUSTRY EXPERIENCE

Experience with storing spent fuel underwater has been substantial (Refs. 2, 3, and 4). These references show that the pool water activity, normally low, experiences small increase during refueling periods, which then decays rapidly with time. Typical concentrations (Ref. 5) of radionuclides in spent fuel pool water range from  $10^{-4}$   $\mu\text{Ci/ml}$  to  $10^{-3}$   $\mu\text{Ci/ml}$ , with the higher value associated with refueling operations. References 2 and 5 also state that the increase in pool water activity during refueling can be attributed to:

- 0 Dislodging (sloughing off) of corrosion products on the fuel assembly during transfer and handling operations.
- 0 The possible short-term exposure of fuel pellets to pool water via a cladding defect.



- 0 Mixing of the spent fuel pool water with the higher activity reactor coolant. Upon cessation of the refueling operations, the fuel pool water and the reactor coolant system would be isolated from each other, thereby terminating transports of corrosion products from the reactor coolant system. Thus, deposition of crud is a function of refueling operations and is not impacted by the expanded storage.
- 0 Furthermore, it has been shown (Ref. 6) that release of fission products from failed fuel decreases rapidly after shutdown to essentially negligible levels. The dissolution of exposed fuel pellets (made of  $UO_2$ ) is very slow in water at fuel pool temperatures and the corrosion of the cladding (Zircaloy 4) at spent fuel pool water temperatures is virtually nil (Refs. 2 and 5). Another mechanism available for the release of the gaseous fission products is diffusion through the  $UO_2$  pellet. It has been shown that at low water temperatures ( $<150^\circ F$ ), the diffusion coefficient is extremely small (Ref. 7). Therefore, the small increase in activity of the spent fuel pool water is due to either crud transport, fission products release, or cross-flow from the reactor coolant system, and is only a function of refueling operations. The expansion of fuel pool storage capacity will not cause a significant increase in doses either onsite or offsite.

The corrosion properties of irradiated Zircaloy cladding have been reviewed in References 2 and 4 and the conclusion is drawn that the corrosion of the cladding in spent fuel pool water is negligible. The minor incremental heating of pool water, due to the expansion of storage capacity, is far too small to materially affect the corrosion properties of Zircaloy cladding.

#### 7.4 BYRON NUCLEAR POWER STATION EXPERIENCE

At present, there is one spent (normal core offload) batch of spent fuel assemblies stored in the spent fuel pool.

#### 7.5 SPENT FUEL POOL COOLING AND CLEANUP SYSTEM

It has been shown previously in Section 5 of this licensing report that the cooling system at Byron is adequate to handle the expected heat loads and maintain the pool temperature peaks within acceptable limits. It has been shown in Section 5 that the small increase in heat load due to the storage capacity expansion will neither significantly increase the thermal dissipation to the environment nor increase the propensity for corrosion of the cladding.

It has also been shown that the crud deposition in the spent fuel pool water occurs during refueling outages and that the planned expansion will not

increase long-term crud deposition. The fuel pool cleanup system (filter and demineralizer) is designed to maintain fuel pool water clarity and is operated and maintained in accordance with the Byron operating procedures. The cleanup system takes a surface skim from the fuel pool and cleans it through a process of filtration and demineralization to prevent crud buildup on the fuel pool walls at the water-to-air interface.

The spent fuel pool water is sampled and analyzed periodically to confirm proper operation of the pool cleanup system. The spent fuel pool modification will not result in a significantly higher quantity of solid radwaste.

## 7.6 FUEL POOL RADIATION SHIELDING

### 7.6.1 Source Terms

The spent fuel gamma source terms used for the fuel pool shielding evaluation were generated using the point reactor fission product inventory code RIBD. The following assumptions were used in the analysis:

- 0 Initial fuel enrichment = 4.2%
- 0 Net Reactor core power level = 3565 MWt
- 0 Average assembly discharge burnup = 45,750 MWD/MTU
- 0 Power level for average assembly = 17.67 MWt
- 0 Power level for peak power assembly = 29.16 MWt  
(peaking factor of 1.65)
- 0 Burnup for peak power assembly = 33,000 MWD/MTU  
(one 18-month cycle at maximum power)
- 0 Start of Refueling Process = 100 hours after shutdown
- 0 Time after shutdown for dose rate calculation = 9 days

The peaking factor of 1.65 and burnup for peak power assembly of 33,000 MWD/MTU for one cycle were chosen to produce the highest possible gamma source term attainable under operational conditions. The average assembly burnup and power level were chosen to represent a conservative gamma source term for the spent fuel. The 100-hour decay time is the minimum permitted period before

refueling can begin per the Technical Specifications.

The photon energy production rates of an average spent fuel assembly is given in Table 7.1.

#### 7.6.2 Radiation Shielding

For an equilibrium refueling cycle 84 fuel assemblies will be discharged into the pool starting no earlier than 100 hours after reactor shutdown at a rate of 1 fuel assembly per hour. For a full core discharge, 193 assemblies are discharged.

To evaluate the adequacy of the shielding capability of the spent fuel pool walls, the radiation dose from all racks filled to capacity with assemblies decayed 9 days after shutdown. It was found that only the first row of racks closest to the wall contributes significantly to the dose rate on the other side of the wall due to self-shielding. Only the "first row" results were used.

The north and south perimeter walls of the spent fuel pool are 5 feet thick. The east and west perimeter walls of the pool are 6 feet thick. The wall separating the spent fuel pool from the transfer canal is 5 feet 6 inches thick. These walls, together with the water and fuel storage racks are incorporated in the dose rate calculations for the adjacent areas. The results of the calculations are provided in Table 7.2.

Except for the area immediately adjacent to the A1 rack, the maximum calculated dose rates through the pool walls are less than the currently designated radiation level limit of 20-mrem/hr for these areas. The area adjacent to the A1 rack is normally occupied only briefly during the local and integrated leak rate tests which are conducted every 5 years. Access to the area is controlled.

The dose rates in Table 7.2 are considered an upper limit since they are calculated for freshly discharged fuel. The dose rates will reduce by a factor of six, 60 days after the fuel is discharged into the pool.

The above discussion indicates that the shielding available around the spent fuel pool is adequate for installation of the high density storage racks.

The radiation dose level at the side of the pool and on the spent fuel pit crane bridge due to the transfer of a peak power fuel assembly are 2.5 mrem/hr and 2.0 mrem/hr, respectively. These calculations assume a minimum of 10 feet of water cover over the active fuel. If the transfer of fuel assemblies into the spent fuel cask pit becomes necessary, the water cover will be less than 10 feet over the active fuel, however, the dose rate during this fuel movement will be much lower than for the transfer of the peak power assembly noted above since the radiation level of the fuel assembly will have had time to decay to a level which would more than compensate for the loss of water cover shielding.

Since the fuel transfer operation normally lasts less than 4 days (88 assemblies at 1 assembly per hour), the above radiation field does not create excessive operator exposure.

#### 7.7 RADIOLOGICAL CONSEQUENCES

The design basis fuel handling accident (dropped assembly) in the Fuel Handling Building in Section 15.7 of the FSAR was reviewed for possible effects on radiological dose consequences. The review determined that the conclusions in the FSAR were still valid and that offsite radiological dose consequences were well within 10CFR100 limits.

#### 7.8 RERACKING OPERATION

Installation of the fuel racks will include removal of the existing racks, making minor pool modifications, and cleaning and installing the new racks. The existing racks are bolted to the pool floor.

The new racks will be cleaned prior to installation. The fuel handling building overhead crane will be used to place the racks in the pool. This effort will be performed after the first refueling for Unit 1. The existing

fuel racks will have been exposed to spent fuel and should only be nominally contaminated. Therefore, doses to individuals involved in the reracking should be minimal.

All pool modifications that can be completed prior to filling the pool with water have been done to minimize underwater work. Although divers may be needed for some tasks, all of the work associated with the installation will be sequenced to minimize potential radiation exposure of personnel due to the spent fuel located in the pool. ALARA considerations will be fully incorporated in the installation procedures for this condition. When the fuel handling building overhead crane is used over the pool, physical stops will be installed on the crane to preclude carrying racks over any stored fuel assemblies.

Exact disposition of the existing racks has not been determined. They will be decontaminated and/or cleaned and disposed of in accordance with the applicable Federal and State regulations.

## 7.9 CONCLUSIONS

Based upon the industry experience and evaluations discussed in previous sections, the following conclusions are made:

Minor increases in radiological burden to the pool water, if any, can be adequately handled by the fuel pool cleanup system (filter and demineralizer), thereby maintaining the radionuclide concentration in the water at an acceptably low level.

No appreciable increase in solid radioactive wastes (i.e., filter media and demineralizer resin) is anticipated.

No increase in release of radioactive gases is expected since any long-lived inert radioactive gas potentially available for release (i.e. Kr-85) will have leaked from the fuel either in the reactor core during operation or during the first few months of residence in the pool. Further, Vol. 1, Reference 3 (pp. 4-16) has shown airborne activity to be considerably lower than that allowable by Table 1 of 10CFR Part 20, Appendix B. Therefore, the planned expansion will not significantly increase the release of radioactive gases.

The existing spent fuel pool cooling system will keep the pool water temperature at an acceptable level (see Section 5, Thermal-Hydraulic Considerations).

The existing radiation protection monitoring systems and program are adequate to detect and to warn of any unexpected abnormal increases in radiation level. This provides sufficient assurance that personnel exposures can be maintained as low as is reasonably achievable.

Since the reracking will occur after the first refueling, procedural controls and necessary precautions will be taken to reduce radiation exposure to as low as is reasonably achievable, and hence, radiological impact will be minimized.

Expanding the storage capacity of the spent fuel pool will not significantly increase the onsite or offsite radiological impact above that of the currently authorized storage capacity, nor is any significant increase in environmental radiological or nonradiological impact anticipated.



REFERENCES TO SECTION 7

1. FSAR, Byron Nuclear Power Plant.
2. NUREG-0575, "Handling and Storage of Spent Light Water Power Reactor Fuel," Vol. 1, Executive Summary and text, USNRC, August 1979.
3. NUREG-0800, USNRC Standard Review Plan, Branch Technical Position ASB9-2, Rev. 2, July 1981.
4. J.R. Weeks, "Corrosion of Materials in Spent Fuel Storage Pools," BNL-NUREG-2021, July 1977.
5. A.B. Johnson, Jr. "Behavior of Spent Nuclear Fuel in Water Pool Storage," BNWL-2 56, September 1977.
6. J.M. Wright, "Expected Air and Water Activities in the Fuel Storage Canal," WAPD-PWR-CP 1723 (with Addendum), undated.
7. ANS 5.4 Proposed Standard, "Method for Calculating the Fractional Release of Volatile Fission Products from Oxide Fuel," American Nuclear Society, issued for review, 1981.
8. "Licensing Report on High Density Spent Fuel Racks for Quad Cities, Units 1 and 2," Docket Nos. 50-254 and 50-265, Commonwealth Edison Company, June 1981.
9. "Licensing Report for High Density Spent Fuel Storage Racks," Rancho Seco Nuclear Generating Station, Sacramento Municipal Utilities District, Docket No. 50-312, June 1982.
10. Final Safety Analysis Report, Limerick Generating Station Units 1 and 2, Section 9.1.
11. Safety Evaluation Report Related to the Operation of Limerick Generating Station Units 1 and 2, NUREG-0991, August 1983.
12. Source Term Data for Westinghouse Pressurized Water Reactors, WCAP-8253, July 1975.



Table 7.1

PHOTON ENERGY PRODUCTION RATES OF  
AN AVERAGE SPENT FUEL ASSEMBLY  
(9 DAYS AFTER SHUTDOWN)

Photon Energy (MeV)	Photon Energy Production Rate (MeV/sec)
< .05	4.16E+18
.05-.10	3.36E+17
.10-.30	2.24E+17
.30-.55	1.40E+17
.55-.90	1.27E+17
.90-1.1	4.50E+15
1.1-1.6	1.70E+16
1.6-2.0	1.82E+14
2.0-2.4	3.13E+14
2.4-2.6	3.26E+14
> 2.6	9.42E+12
TOTAL	<u>5.01E+18</u>

Table 7.2

CALCULATED DOSE RATES IN AREAS ADJACENT  
TO THE SPENT FUEL POOL  
(9 DAYS AFTER SHUTDOWN)

Location	High Density Rack Dose Rate (mrem/hr)
Floor el. 401 ft, 0 in., areas adjacent to the north walls	54.0
Floor el. 426 ft, 0 in., areas adjacent to the edge of the pool.	2.3
Floor el. 401 ft, 0 in., spent fuel pool heat exchanger area	4.0
Fuel transfer canal**	20.0

\* A design water gap of 4-7/8 inches between the high density rack and the wall is used.

\*\* A design water gap of 4 inches between the high density rack and the wall is used.

## 8.0 IN-SERVICE SURVEILLANCE PROGRAM FOR BORAFLEX NEUTRON ABSORBING MATERIAL

### 8.1 PROGRAM INTENT

A sampling program to verify the integrity of the neutron absorber material employed in the high density fuel racks in the long-term environment is described in this section.

The program is conducted in a manner which allows access to the representative absorber material samples without disrupting the integrity of the entire fuel storage system. The program is tailored to evaluate the material in normal use mode and to forecast future changes using the data base developed.

### 8.2 DESCRIPTION OF SPECIMENS

The absorber material used in the surveillance program, henceforth referred to as poison, is representative of the material used within the storage system. It is of the same composition, produced by the same method, and certified to the same criteria as the production lot poison. The sample coupon is of similar thickness as the poison used within the storage system and not less than 4 by 2 inches on a side. Figure 8.1 shows a typical coupon. Each poison specimen is encased in a stainless steel jacket of an identical alloy to that used in the storage system, formed so as to encase the poison material and fix it in a position and with tolerances similar to the design used for the storage system. The jacket has to be closed by tack welding in such a manner as to retain its form throughout the test period and still allow rapid and easy opening without causing mechanical damage to the poison specimen contained within. The jacket should permit wetting and venting of the specimen similar to the actual rack environment.

### 8.3 SPECIMEN EVALUATION

After the removal of the jacketed poison specimen from the cell at a designated time, a careful evaluation of that specimen should be made to

determine its actual condition as well as its apparent durability for continued function. Separation of the poison from the stainless steel specimen jacket must be performed carefully to avoid mechanical damage to the poison specimen. Immediately after the removal, the specimen and jacket section should be visually examined for any effects of environmental exposure. Specific attention should be directed to the examination of the stainless steel jacket for any evidence of physical degradation. Functional evaluation of the poison material can be accomplished by the following measurements:

- 0 A neutron radiograph of the poison specimen aids in the determination of the maintenance of uniformity of the boron distribution.
- 0 Neutron attenuation measurements will allow evaluation of the continued nuclear effectiveness of the poison. Consideration must be given in the analysis of the attenuation measurements for the level of accuracy of such measurements, as indicated by the degree of repeatability normally observed by the testing agency.
- 0 A measurement of the hardness of the poison material will establish the continuance of physical and structural durability. The hardness acceptability criterion requires that the specimen hardness will not reduce the hardness listed in the qualifying test document for laboratory test specimen irradiated to  $10^{11}$  rads. The actual hardness measurement should be made after the specimen has been withdrawn from the pool and allowed to air dry for not less than 48 hours to allow for a meaningful correlation with the pre-irradiated sample.
- 0 Measurement of the length, the width, and the average thickness and comparison with the preexposure data will indicate dimensional stability within the variation range reported in the Boraflex laboratory test reports.

A procedure will be prepared for execution of the test procedure and interpretation of the test data.

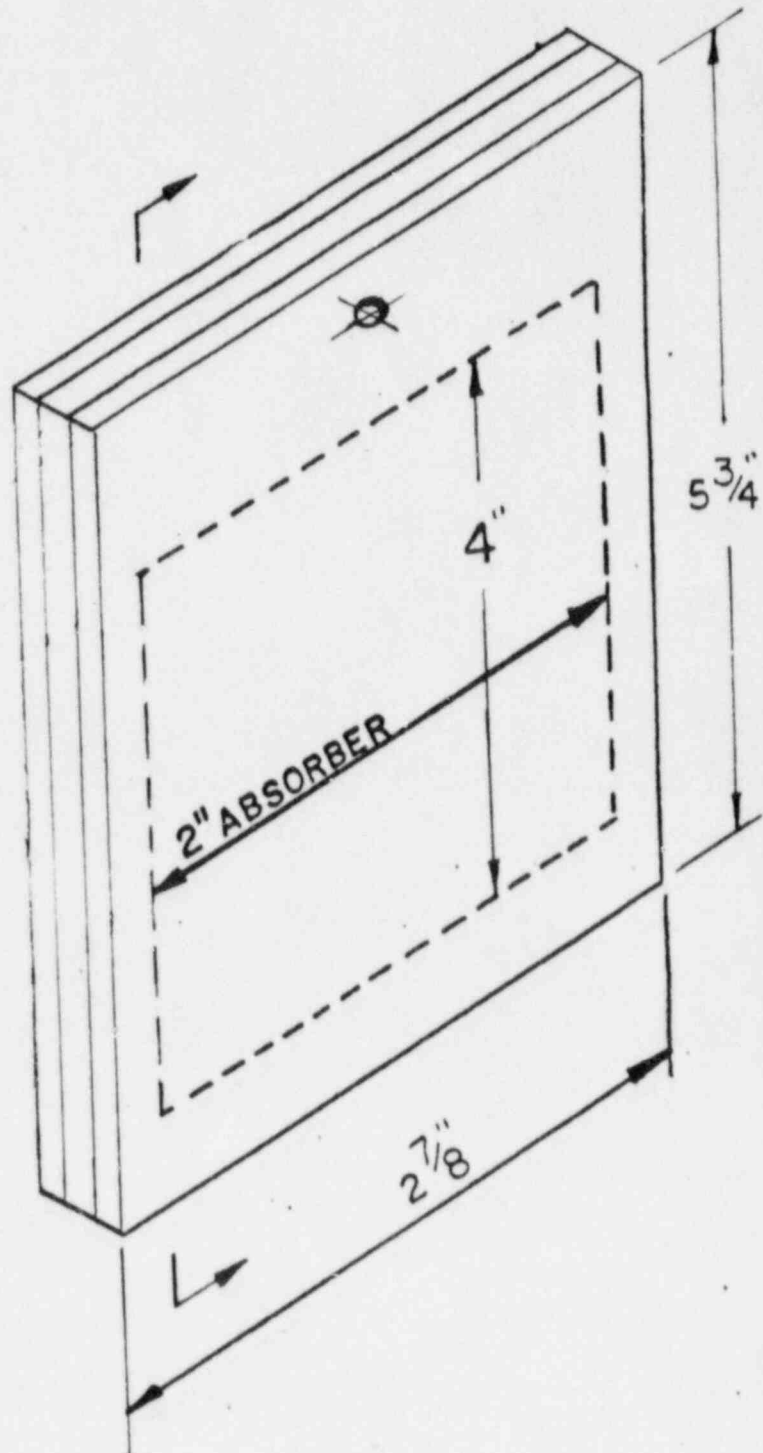
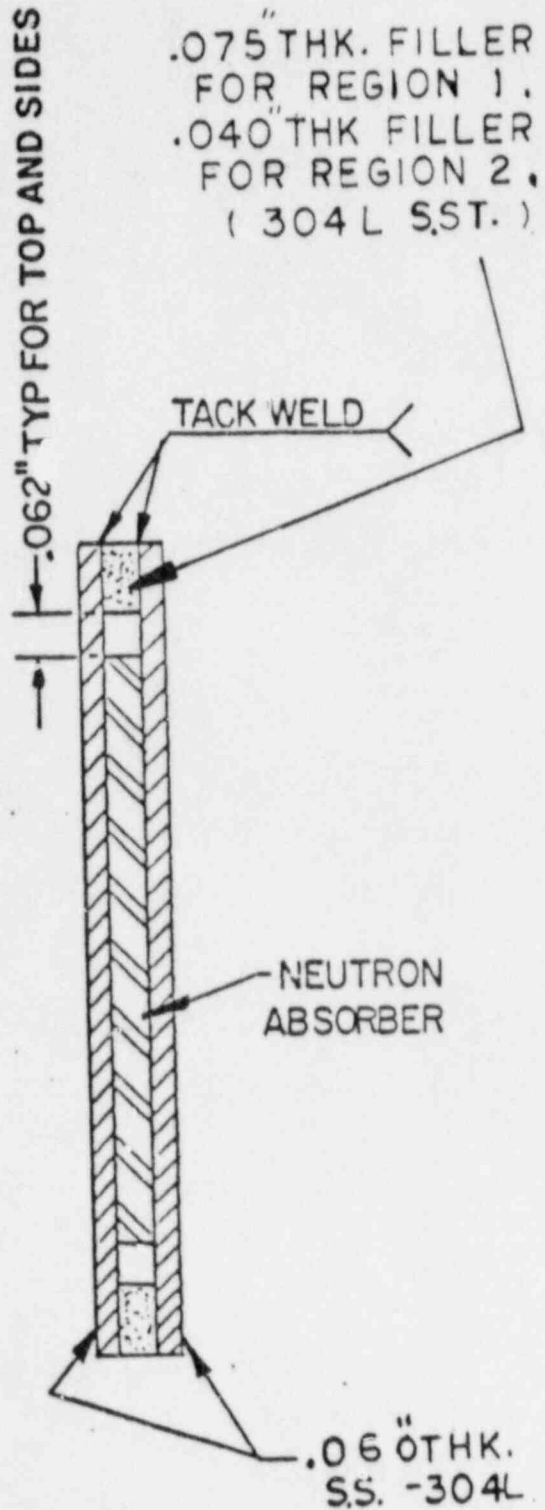


FIG. 8.1 — TEST COUPON

## 9.0 COST/BENEFIT ASSESSMENT

A cost/benefit assessment has been prepared in accordance with the requirements of Reference 1, Section V - Part 1. The assessment demonstrates that the installation of high density spent fuel storage racks is the most advantageous means of handling spent fuel.

The material is presented merely for informational purposes. It is CECO's position that an environmental impact statement need not be prepared because the installation of high density fuel racks provides no significant impact on the environment. NRC precedent establishes that alternatives and economic costs need not be discussed when there is no significant environmental impact. However, for completeness, alternatives to reracking for additional spent fuel storage capacity are discussed in Section 9.3.

### 9.1 SPECIFIC NEEDS FOR SPENT FUEL STORAGE

Disposal of Byron nuclear fuel is scheduled to be carried out by the Department of Energy in or after 1998 in accordance with Public Law 97-425, Nuclear Waste Policy Act of 1982. As Byron spent fuel may not be accorded a high priority under the DOE Program, CECO is seeking to provide a spent fuel storage capacity to support approximately 24 years of nominal operation. No other contractual arrangements exist for the interim storage, or reprocessing of spent fuel from Byron Nuclear Power Station. Therefore, increased storage capacity in the spent fuel pool is the only viable option under consideration. Table 1.1, the Fuel Discharge Schedule, indicates that with the high density spent fuel racks, loss of full core discharge capability (FCDC) will occur in 2009, 15 years beyond the current capability and 11 years beyond the scheduled repository fuel receipt date, per the DOE Mission Plan.

### 9.2 COST OF SPENT FUEL STORAGE

The design and manufacture of the spent fuel storage racks will be undertaken by the organizations described in Section 1. It is expected that the total project cost will be between \$2.6 and \$2.9 million.



CECO has considered the various alternatives to the proposed onsite spent fuel storage. These alternatives are discussed below:

a. Shipment of Fuel to a Reprocessing or Independent Spent Fuel Storage/Disposal Facility

No commercial spent fuel reprocessing facilities are presently operating in the United States. CECO has made contractual arrangements whereby spent nuclear fuel and/or high level nuclear waste will be accepted and disposed of by the U.S. Department of Energy. However, such services are not expected to be available before 1998. The existing Byron spent fuel storage capacity will not provide full core discharge capability beyond 1994. Spent fuel acceptance and disposal by the Department of Energy is not, therefore, an alternative to increased onsite pool storage capacity.

b. Shipment of Fuel to Another Reactor Site

Shipment of Byron fuel to another reactor site could provide short-term relief to the storage capacity problem. However, transshipment of spent fuel merely serves to transfer the problem to another site and does not result in any additional net long-term storage capacity. Accordingly, CECO does not consider the transshipment of spent fuel to be an appropriate alternative to high density spent fuel storage at the site.

c. Not Operating the Plant after the Current Spent Fuel Storage Capacity is Exhausted

As indicated in NUREG-0575, "Final Environmental Impact Statement on Handling and Storage of Spent Light Water Power Reactor Fuel," (Ref. 2) the replacement of nuclear power by coal generating capacity would cause excess mortality to rise from 0.59 - 1.70 to 15 - 120 per year for 0.8 GWY(e). Based on these facts, not operating the plant or shutting down the plant after exhaustion of spent fuel discharge capacity is not a viable alternative to high density storage in the spent fuel pool. The prospective 1986 expenditure of approximately \$2.6 million for the high density racks is small compared to the estimated value of replacement power equivalent to the plant's energy output: approximately \$21 million per month in 1994 and \$32 million per month in 2009.

The subject of the comparative economics associated with various spent fuel options is the subject of Chapter 6 of NUREG-0575 (Ref. 2). Although the material presented is generic, it is of value in comparing the costs of the



various options. Of the options presented in that chapter, high density spent fuel storage at the site is the most economic option at \$ 3.50 per KgU. The price of Independent Fuel Storage Facilities (IFSF), if available, would be \$54.35 per KgU.

#### 9.4 RESOURCE COMMITMENTS

The expansion of the Byron spent fuel storage capacity will require the following primary resources:

- 0 Stainless steel - 284,815 lb/unit
- 0 Boraflex neutron absorber - 22,000 lb/unit of which 10,925 lb is boron carbide ( $B_4C$ ) powder

The requirement for stainless steel represents a small fraction of the total domestic production for 1986 (Ref. 3). Although the fraction of domestic production of  $B_4C$  required for the fabrication is somewhat higher than that for stainless steel, it is unlikely that the commitment of  $B_4C$  to this project will affect other alternatives. Experience has shown that the production of  $B_4C$  is highly variable and depends on need but could easily be expanded to accommodate additional domestic needs.

REFERENCES TO SECTION 9

1. B.K. Grimes, "OT Position for Review and Acceptance of Spent Fuel Storage and Handling Applications," April 14, 1978.
2. NUREG-0575, "Final Environmental Impact Statement on Handling and Storage of Spent Light Water Power Reactor Fuel," Vols. 1-3, USNRC, August 1979.
3. "Mineral Facts and Problems," Bureau of Mines Bulletin 671, 1990.

## 10.0 QUALITY ASSURANCE PROGRAM

### 10.1 INTRODUCTION

This chapter provides a general description of the quality assurance program that is implemented to assure that the quality objectives of the contract specification are met.

### 10.2 GENERAL

The quality assurance program used on this project is based upon the system described in Oat's Nuclear Quality Assurance Manual. This system is designed to provide a flexible but highly controlled system for the design, manufacture, and testing of customized components in accordance with various codes, specifications, and regulatory requirements. The Oat Nuclear Quality Assurance Program has been accepted by ASME and has been approved by the CECO Quality Assurance Department and placed on CECO's Qualified Suppliers List.

The philosophy behind Oat's Quality Assurance System is that it shall provide for all controls necessary to fulfill the contract requirements with sufficient simplicity to make it functional on a day-to-day basis. The system readily adapts to different designs and component configurations, making possible the construction of many varied forms of equipment. The following paragraphs provide an overview of the system and how it has been applied to Commonwealth Edison's specifications.

### 10.3 SYSTEM HIGHLIGHTS

The design control is organized to provide for careful review of all contract requirements to extract each individual design and quality criterion. These criteria are translated into design and quality control documents customized to the contract requirement and completely reviewed and approved by responsible and qualified personnel.

The system for control of purchased material includes generating detailed descriptions of each individual item of material along with specifications for any special requirements such as impact testing, corrosion testing, monitoring or witnessing of chemical analysis, provision of over-check specimens, special treatments or conditioning of material, source inspection, and provision of performance documentation on any of the above.

Material receipt inspection includes a complete check of all material and its documentation. Upon acceptance, each item of material is individually listed on a control sheet issued once a week to assure that only accepted material goes into fabrication.

The fabrication control system provides that a shop traveller is prepared for each subassembly and assembly in each contract. The traveller is generated specifically to provide step-by-step instructions for fabrication, inspection, testing, cleaning, packaging, etc., which address all standard and special requirements of the contract specifications. Special attention is given to deployment of fabrication sequence and inspection steps to preclude the possibility of missing poison sheets or incorrect sheets (incorrect B<sup>10</sup> loading). All nondestructive examination procedures and test procedures are custom written to apply to CECO's requirements.

The system provides for qualification and written certification of personnel performing quality-related activities including nondestructive examination and fabrication inspection, welding, engineering, production supervision, and auditing.

Other CECO requirements are fully covered in the Quality Assurance Program, including document control, control of measuring and test equipment, control of nonconforming material and parts, corrective action auditing, and other areas as specified by CECO.

#### 10.4 SUMMARY

Dat's quality assurance system provides the full measure of quality assurance required by the contract. All special requirements of the specifications are

covered, including source inspection of material and witnessing of material testing by the engineer, furnishing of material certifications and test reports within 5 days of shipment, and obtaining verification of qualification testing of poison materials.

APPENDIX A

BENCHMARK CALCULATIONS

## 1. INTRODUCTION AND SUMMARY

The objective of this benchmarking study is to verify both the AMPX (NITAWL)-KENO (Refs. 1 and 2) methodology with the 27-group SCALE cross-section library (Refs. 3 and 4) and the CASMO-2E code (Refs. 5, 6, 7, and 8) for use in criticality calculations of high density spent fuel storage racks. Both calculational methods are based on transport theory and have been benchmarked against critical experiments that simulate typical spent fuel storage rack designs as realistically as possible. Results of these benchmark calculations with both methodologies are consistent with corresponding calculations reported in the literature and with the requirements of Regulatory Guide 3.41,\* Rev. 1, May 1977.

Results of these benchmark calculations show that the 27-group (SCALE) AMPX-KENO calculations consistently underpredict the critical eigenvalue by  $0.0106 \pm 0.0048 \Delta k$  (with a 95% probability at a 95% confidence level) for critical experiments selected to be representative of realistic spent fuel storage rack configurations and poison worths. Similar calculations by Westinghouse suggest a bias of  $0.012 \pm 0.0023$ , and the results of ORNL analyses of 54 relatively "clean" critical experiments show a bias of  $0.0100 \pm 0.0013$ .

Similar calculations with CASMO-2E for clean critical experiments resulted in a bias of  $0.0013 \pm 0.0018$  (95%/95%). CASMO-2E and AMPX-KENO intercomparison calculations of infinite arrays of poisoned cell configurations show very good agreement and suggest that a bias of  $0.0013 \pm 0.0018$  is the reasonably expected bias and uncertainty for CASMO-2E calculations.

---

\*Validation of Calculational Methods for Nuclear Criticality Safety. (See also ANSI N16.9-1975.)



The benchmark calculations reported here indicate that either the 27-group (SCALE) AMPX-KENO or CASMO-2E calculations are acceptable for criticality analysis of high density spent fuel storage racks. The preferred methodology, however, is to perform independent calculations with both code packages and to utilize the higher, more conservative value for the reference design infinite multiplication factor.

## 2. AMPX (NITAWL)-KENO BENCHMARK CALCULATIONS

Analysis of a series of Babcock & Wilcox (B&W) critical experiments (Ref. 9), which include some with absorber sheets typical of a poisoned spent fuel rack, is summarized in Table 1, as calculated with AMPX-KENO using the 27-group SCALE cross-section library and the Nordheim resonance integral treatment in NITAWL. The mean for these calculations is  $0.9894 \pm 0.0019$ , conservatively assuming the larger standard deviation calculated from the  $k_{\text{eff}}$  values. With a one-sided tolerance factor ( $K = 2.502$ ), corresponding to 95% probability at a 95% confidence level (Ref. 10), the calculational bias is  $+0.0106$  with an uncertainty of  $\pm 0.0048$ .

Similar calculational deviations reported by Westinghouse (Ref. 11) are also shown in Table 1 and suggest a bias of  $0.012 \pm 0.0023$  (95%/95%). In addition, ORNL (Ref. 12) has analyzed some 54 critical experiments using the same methodology, obtaining a mean bias of  $0.0100 \pm 0.0013$  (95%/95%). These published results are in good agreement with the results obtained in the present analysis and lend further credence to the validity of the 27-group AMPX-KENO calculational model for use in criticality analysis of high density spent fuel storage racks. Variance analysis of the data in Table 1 suggests the possibility that an unknown factor may be causing a slightly larger variance than might be expected from the Monte Carlo statistics alone. However, such a

Table 1

RESULTS OF 27-GROUP (SCALE) AMPX-KENO CALCULATIONS  
OF B&W CRITICAL EXPERIMENTS

Experiment Number	Calculated $k_{eff}$	$\sigma$	Westinghouse Calculated-meas. $k_{eff}$
I	0.9889	$\pm 0.0049$	-0.008
II	1.0040	$\pm 0.0037$	-0.012
III	0.9985	$\pm 0.0046$	-0.008
IX <sup>(1)</sup>	0.9924	$\pm 0.0046$	-0.016
X	0.9907	$\pm 0.0039$	-0.008
XI	0.9989	$\pm 0.0044$	+0.002
XII	0.9932	$\pm 0.0046$	-0.013
XIII	0.9890	$\pm 0.0054$	-0.007
XIV	0.9830	$\pm 0.0038$	-0.013
XV	0.9852	$\pm 0.0044$	-0.016
XVI	0.9875	$\pm 0.0042$	-0.015
XVII	0.9811	$\pm 0.0041$	-0.015
XVIII	0.9784	$\pm 0.0050$	-0.015
XIX	0.9888	$\pm 0.0033$	-0.016
XX	0.9922	$\pm 0.0048$	-0.011
XXI	<u>0.9783</u>	<u><math>\pm 0.0039</math></u>	<u>-0.017</u>
Mean	0.9894	$\pm 0.0011$ <sup>(2)</sup>	-0.0120 $\pm$ 0.0010
Bias	0.0106	$\pm 0.0019$ <sup>(3)</sup>	0.0120 $\pm$ 0.0010
Bias (95%/95%)	0.0106	$\pm 0.0048$	0.0120 $\pm$ 0.0023
Maximum Bias	0.0154		0.0143

- (1) Experiments IV through VIII used B<sub>4</sub>C pin absorbers and were not considered representative of poisoned storage racks.  
(2) Calculated from individual standard deviations.  
(3) Calculated from  $k_{eff}$  values and used as reference.

factor, if one truly exists, is too small to be resolved on the basis of critical-experiment data presently available. No trends in  $k_{eff}$  with intra-assembly water gap, with absorber sheet reactivity worth, or with soluble poison concentration were identified.\*

### 3. CASMO-2E BENCHMARK CALCULATIONS

#### 3.1 GENERAL

The CASMO-2E code is a multigroup transport theory code utilizing transmission probabilities to accomplish two-dimensional calculations of reactivity and depletion for BWR and PWR fuel assemblies. As such, CASMO-2E is well-suited to the criticality analysis of spent fuel storage racks, since general practice is to treat the racks as an infinite medium of storage cells, neglecting leakage effects.

CASMO-2E is closely analogous to the EPRI-CPM code (Ref. 13) and has been extensively benchmarked against hot and cold critical experiments by Studsvik Energiteknik (Refs. 5, 6, 7, and 8). Reported analyses of 26 critical experiments indicate a mean  $k_{eff}$  of  $1.000 \pm 0.0037$  ( $1\sigma$ ). Yankee Atomic (Ref. 14) has also reported results of extensive benchmark calculations with CASMO-2E. Their analysis of 54 Strawbridge and Barry critical experiments (Ref. 15) using the reported buckling indicates a mean of  $0.9987 \pm 0.0009$  ( $1\sigma$ ), or a bias of  $0.0013 \pm 0.0018$  (with 95% probability at a 95% confidence level). Calculations were repeated for seven of the Strawbridge and Barry experiments

---

\*Significantly large trends in  $k_{eff}$  with water gap and with absorber sheet reactivity worth have been reported (Ref. 16) for AMPX-KENO calculations with the 123-group GAM-THERMOS library.

selected at random, yielding a mean  $k_{\text{eff}}$  of  $0.9987 \pm 0.0021$  ( $1\sigma$ ), thereby confirming that the cross-section library and analytical methodology being used for the present calculations are the same as those used in the Yankee analyses. Thus, the expected bias for CASMO-2E in the analysis of "clean" critical experiments is  $0.0013 \pm 0.0018$  (95%/95%).

### 3.2 BENCHMARK CALCULATIONS

CASMO-2E benchmark calculations have also been made for the B&W series of critical experiments with absorber sheets, simulating high density spent fuel storage racks. However, CASMO-2E, as an assembly code, cannot directly represent an entire core configuration\* without introducing uncertainty due to reflector constants and the appropriateness of their spectral weighting. For this reason, the poisoned cell configurations of the central assembly, as calculated by CASMO-2E, were benchmarked against corresponding calculations with the 27-group (SCALE) AMPX-KENO code package. Results of this comparison are shown in Table 2. Since the differences are well within the normal KENO statistical variation, these calculations confirm the validity of CASMO-2E calculations for the typical high density poisoned spent fuel rack configurations. The differences shown in Table 2 are also consistent with a bias of  $0.0013 \pm 0.0018$ , determined in Section 3.1 as the expected bias and uncertainty of CASMO-2E calculations.

---

\*Yankee has attempted such calculations (Ref. 14) using CASMO-2E-generated constants in a two-dimensional, four-group PDQ model, obtaining a mean  $k_{\text{eff}}$  of 1.005 for 11 poisoned cases and 1.009 for 5 unpoisoned cases. Thus, Yankee benchmark calculations suggest that CASMO-2E tends to slightly overpredict reactivity.

Table 2

## RESULTS OF CASMO-2E BENCHMARK (INTERCOMPARISON) CALCULATIONS

B&W Experiment No. (1)	$k_{\infty}$ (1)		$\Delta k$
	AMPX-KENO (2)	CASMO-2E	
XIX	1.1203 $\pm$ 0.0032	1.1193	0.0010
XVII	1.1149 $\pm$ 0.0039	1.1129	0.0020
XV	1.1059 $\pm$ 0.0038	1.1052	0.0007
Interpolated (3)	1.1024 $\pm$ 0.0042	1.1011	0.0013
XIV	1.0983 $\pm$ 0.0041	1.0979	0.0004
XIII	1.0992 $\pm$ <u>0.0034</u>	1.0979	<u>0.0013</u>
Mean	$\pm$ 0.0038		0.0011
Uncertainty			$\pm$ 0.0006
BWR fuel rack	0.9212 $\pm$ 0.0027	0.9218	-0.006

(1) Infinite array of central assemblies of 9-assembly B&W critical configuration (Ref. 9).

(2)  $k_{\infty}$  from AMPX-KENO corrected for bias of 0.0106  $\Delta k$ .

(3) Interpolated from Fig. 28 of Ref. 9 for soluble boron concentration at critical condition.

REFERENCES TO APPENDIX A

1. Green, Lucious, Petrie, Ford, White, Wright, "PSR-63/AMPX-1 (code package), AMPX Modular Code System for Generating Coupled Multigroup Neutron-Gamma Libraries from ENDF/B," ORNL-TM-3706, Oak Ridge National Laboratory, March 1976.
2. L. M. Petrie and N. F. Cross, "KENO-IV, An Improved Monte Carlo Criticality Program," ORNL-4938, Oak Ridge National Laboratory, November 1975.
3. R. M. Westfall et al., "SCALE: A Modular Code System for Performing Standardized Computer Analyses for Licensing Evaluation," NUREG/CR-0200, 1979.
4. W. E. Ford, III et al., "A 218-Neutron Group Master Cross-section Library for Criticality Safety Studies," ORNL/TM-4, 1976.
5. A. Ahlin, M. Edenius, H. Haggblom, "CASMO - A Fuel Assembly Burnup Program," AE-RF-76-4158, Studsvik report (proprietary).
6. A. Ahlin and M. Edenius, "CASMO - A Fast Transport Theory Depletion Code for LWR Analysis," ANS Transactions, Vol. 26, p. 604, 1977.
7. M. Edenius et al., "CASMO Benchmark Report," Studsvik/RF-78/6293, Aktiebolaget Atomenergi, March 1978.
8. "CASMO-2E Nuclear Fuel Assembly Analysis, Application Users Manual," Rev. A, Control Data Corporation, 1982.
9. M. N. Baldwin et al., "Critical Experiments Supporting Close Proximity Water Storage of Power Reactor Fuel," BAW-1484-7, The Babcock & Wilcox Company, July 1979.
10. M. G. Natrella, Experimental Statistics, National Bureau of Standards, Handbook 91, August 1963.
11. B. F. Cooney et al., "Comparisons of Experiments and Calculations for LWR Storage Geometries," Westinghouse NES, ANS Transactions, Vol. 39, p. 531, November 1981.
12. R. M. Westfall and J. R. Knight, "Scale System Cross-section Validation with Shipping-cask Critical Experiments," ANS Transactions, Vol. 33, p. 368, November 1979.
13. "The EPRI-CPM Data Library," ARMP Computer Code Manuals, Part II, Chapter 4, CCM3, Electric Power Research Institute, November 1975.

REFERENCES TO APPENDIX A (Continued)

14. E. E. Pilat, "Methods for the Analysis of Boiling Water Reactors (Lattice Physics)," YAEC-1232, Yankee Atomic Electric Co., December 1980.
15. L. E. Strawbridge and R. F. Barry, "Criticality Calculations for Uniform, Water-moderated Lattices," Nuclear Science and Engineering, Vol. 23, p. 58, September 1965.
16. S. E. Turner and M. K. Gurley, "Evaluation of AMPX-KENO Benchmark Calculations for High Density Spent Fuel Storage Racks," Nuclear Science and Engineering, 80(2): 230-237, February 1982.



APPENDIX B  
NRC QUESTIONS FROM DECEMBER 22, 1986 MEETING

NRC Questions from December 22, 1986 Meeting:

QUESTION #1

The information provided to BNL does not address potential damage to fuel resulting from fuel to cell wall and baseplate impacts. Have these effects been evaluated?

ANSWER #1

The fuel assembly has been analyzed by the fuel manufacturer and found to withstand lateral accelerations an order of magnitude greater than those developed due to rattling between the fuel assembly and the cell wall (less than 1.0g). The testimony by a Westinghouse expert during the Turkey Point ASLB hearings gives the details on the fuel assembly load bearing ability.

The fuel assembly has a rugged inlet nozzle assembly which imparts considerable axial load bearing ability to it. Moreover, the forces developed due to bouncing of the assembly on the base plate are quite small compared to the loads associated with fuel drop accidents.

QUESTION #2

Has the pool floor evaluation included a check for potential local perforation of the liner due to rack foot impact? How was this done?

ANSWER #2

Perforation of the stainless steel pool liner plate due to rack foot impact loading has been evaluated. A local bearing stress is calculated based on the maximum foot reaction. The net bearing area assumes a 9" x 9" shim plate distributing load over the leak chase channels. The critical bearing stress is 6275 which is less than the allowable concrete bearing stress of 6545 psi.

The design compressive strength of the spent fuel pool basemat is 5500 psi whereas the walls are 3500 psi. The latter value has previously been given in response to the second set of NRC questions.

QUESTION #3

Since the seismic impact loads may be sensitive to gap sizes, are there QA procedures in place to assure that the proper inter-rack and wall to rack gaps are maintained during initial installing and subsequent loading/unloading of fuel?

ANSWER #3

The rack to wall gaps will be maintained by temporary spacer blocks. The nominal gap between racks is zero inches and will be checked to insure the actual gaps are below the 1/2 inches considered in the seismic analysis.

QA procedures are in the process of preparation and will be available to the NRC once they are approved. The procedures are designed to assure the assumed rack to rack gaps are not exceeded and rack to wall gaps are maintained.

Since the load exerted by the fuel handling bridge crane is limited by the "load cell", the maximum load exerted on the rack during fuel loading and unloading is a small fraction of the weight of the module. Therefore, rack movement during fuel loading and unloading is not a credible phenomenon.

QUESTION #4

How was the conservatism of the single rack model demonstrated? The model appears to limit the amount of sliding and tilting of the rack between small gaps. This would not account for potential pileup of racks against the pool wall. Has this possibility been investigated?

ANSWER #4

The analysis of multi-rack motion has been carried out to determine the response of an array of four racks in the Byron spent fuel pool. The object of this analysis was to determine whether the peripheral rack module hits the wall. Another related purpose of this analysis was to obtain maximum values of rack kinematic displacements. The mathematical characterization of the modules in this analysis is not detailed enough to furnish refined data for predicting stress levels. The imposed seismic loading is the E-W SSE and the VERTICAL SSE. The four racks studied are labelled B1, C2, C4, and D4 in Fig 2.1. This array is the second row from the north wall.

Realistic spring constant values for girdle bars are based on impact at the ends of girdle bars with the full rack height providing flexibility. An effective cross coupling gap was established based on our previous directions from the NRC for Diablo Canyon analyses. All racks were assumed to be full with consolidated fuel (weight - 3000#/cell). This fuel weight is identical to the single rack design basis 3-D analyses.

Runs were made for .2 and .8 interface coefficients of friction. The table below provides results for comparison of key displacement data between the multi-rack and single rack analyses. The displacements increase over the single rack analysis but the units do not impact the wall.

	Friction Coefficient	Multi-Rack Model	3-D Single Rack
Maximum E-W Displacement	0.2	1.1027 inch	.318 inch
At top of rack	0.8	2.74 inch	.346 inch

QUESTION #5

How has the conservatism of the rattling mass representation of the fuel within the rack cells been demonstrated? The model does not appear to account for the flexural rigidity of the fuel and the potential amplified response of its resonant modes. Has this been investigated?

ANSWER #5

The answer to this question is given in Section 6.2.1(a) of this report.

QUESTION #6

Describe how rack and rack to wall fluid coupling was handled by the model (note p.11 2 was missing from BNL copy of seismic report).

ANSWER #6

The missing page was provided at the meeting and the manner of handling fuel coupling was explained to be an extension of Fritz's classical paper.

QUESTION #7

Uplift of fuel from rack baseplate and resulting impact loads were not considered in the model. How was this effect evaluated?

ANSWER #7

There is indeed no degree of freedom associated with uplift of the fuel assembly mass located at the baseplate elevation. However, due to the low seismic accelerations involved, the resulting error is expected to be small. Furthermore, the fuel drop case considers drop of the fuel from 36 inches above the rack and is critical compared to fuel uplift due to seismic effects.

QUESTION #8

How were the rack to rack and rack to wall gap spring constants determined? How are the impact loads evaluated?

ANSWER #8

The required rack to rack impact spring constant is at the girdle bar and baseplate elevations where the inter-module impacts may occur. The actual impact spring constant at the girdle bar location is estimated by treating the problem of a laterally loaded beam on an elastic foundation. The spring constant value used in the dynamic analysis is, however, several times higher in order to maximize the computed impact forces. The impact loads in the spring elements are cracked at every time integration step. The maximum values are saved and printed out. A strength-of-materials type analysis is subsequently performed to establish that the locations subject to impacts will not fail as structural members.

QUESTION #9

Have any studies been performed to test the impact load sensitivity to gap size?

ANSWER #9

Studies to test the impact load sensitivity to fuel assembly/storage cell size were not performed. However, the fuel mass in a rack is lumped together so it moves in phase resulting in an extremely conservative estimate of fuel impact effects.

QUESTION #10

How are the pool wall motions included in the analysis? Do the walls experience the same motion as the floor?

ANSWER #10

Yes the walls experience the same motion as the floor since the walls are thick and rigid.

QUESTION #11

Is the bouyant force of water considered in the calculation of frictional resistance of the rack feet.

ANSWER #11

Yes, the bouyant force of water is included in the evaluation of the net vertical force on a support leg which is used in the friction spring elements to compute the lateral friction force at each time step.

QUESTION #12

How were the floor time histories used as input generated? Provide the corresponding response spectra.

ANSWER #12

Time histories were generated based on the design basis spectra at the spent fuel pool floor level. The reponse spectra generated from the time histories match the design basis spectra closely (Ref. section 6.1). Plots comparing the design basis spectra and spectra generated from synthetic time history are shown in Figures B-1, B-2, and B-3.

QUESTION #13

Clarify equation for  $P_i$  in Table 6.1 on page 6-23 of the licensing report.

ANSWER #13

$P_i$  are the "absolute" generalized coordinates,  $q_i$  are the associated "relative" generalized coordinates (with respect to the coordinate frame attached to the pool floor and walls).

QUESTION #14

Explain the criteria used for the selection of fuel to rack eccentricity values ( $X_{B1}, Y_B$ ) considered in the middle.

ANSWER #14

The center of gravity of the assemblage of fuel assemblies in the horizontal plane defines the coordinates  $X_e$  and  $Y_m$ .

QUESTION #15

Define the parameters given in the DYNALIS computer run input and output.

ANSWER #15

This was explained at the meeting. Some proprietary data was sent to BNL for their review.

QUESTION #16

Rack to rack and rack to wall gaps in the computer runs do not appear consistent with gaps shown on the fuel pool layout drawing. Explain.

ANSWER #16

The rack to rack gaps for impact spring considerations should be looked up in the non-linear spring tables. The marked output mentioned above explains the details.

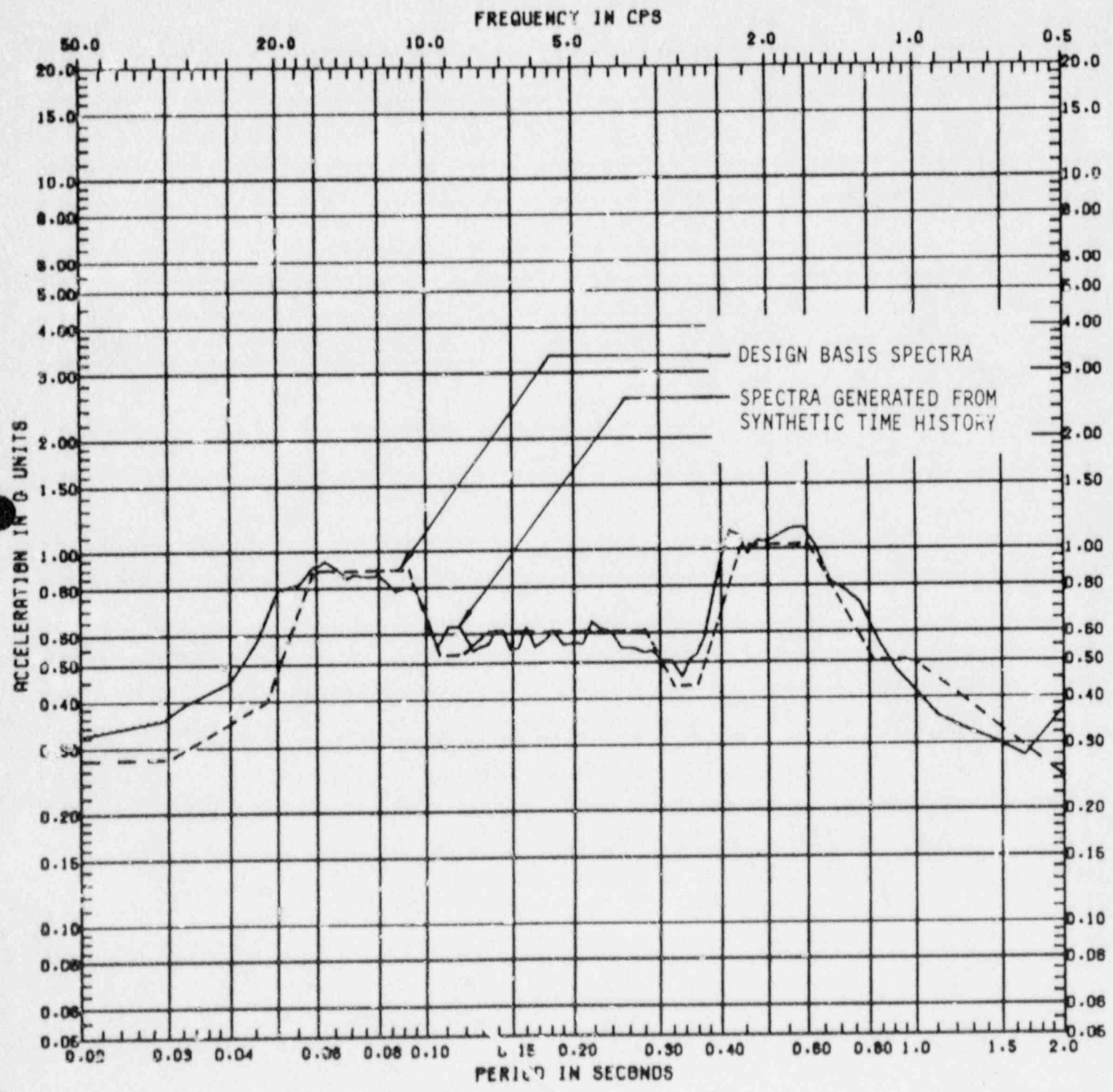


19 JUN 87  
SJH608

CALC NO.  
PROJECT BYRON  
PROJECT NO. 7500-03  
DAMPING 0.040  
PAGE

REV

Fig. B-1 Response Spectra at Spent Fuel Pool Floor



SEISMIC ACCL SPECTRUM-SSE

MODE

DIRECTION K-S

ANGLE

SPECTRA NO.

ELEVATION

LOCATION

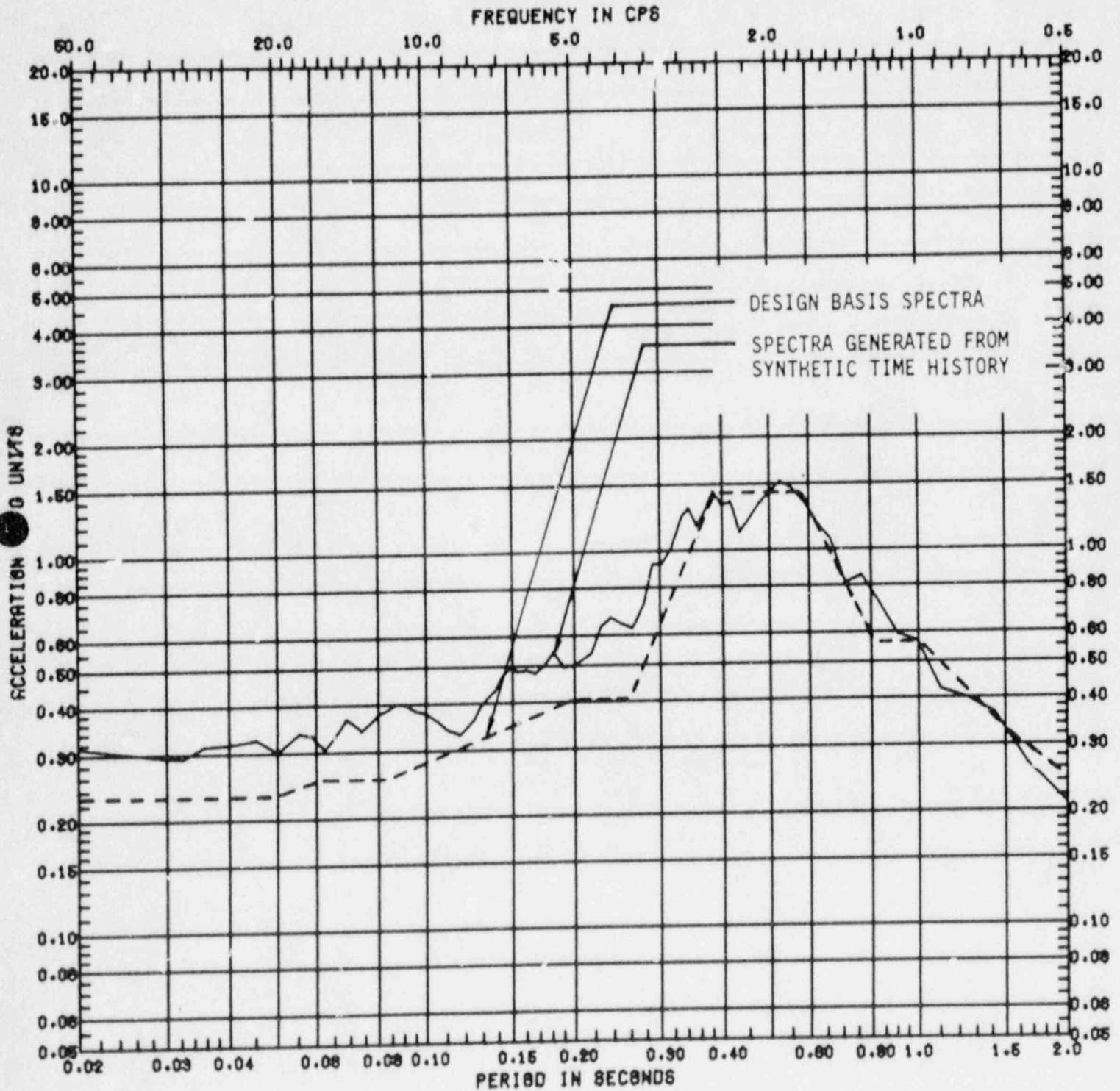
SPENT FUEL POOL





04 FEB 87  
SJH604

Fig. B-2 Response Spectra at Spent Fuel Pool Floor



SEISMIC ACCL SPECTRUM-SSE

MODE

DIRECTION E-W

ANGLE

SPECTRA NO.

ELEVATION

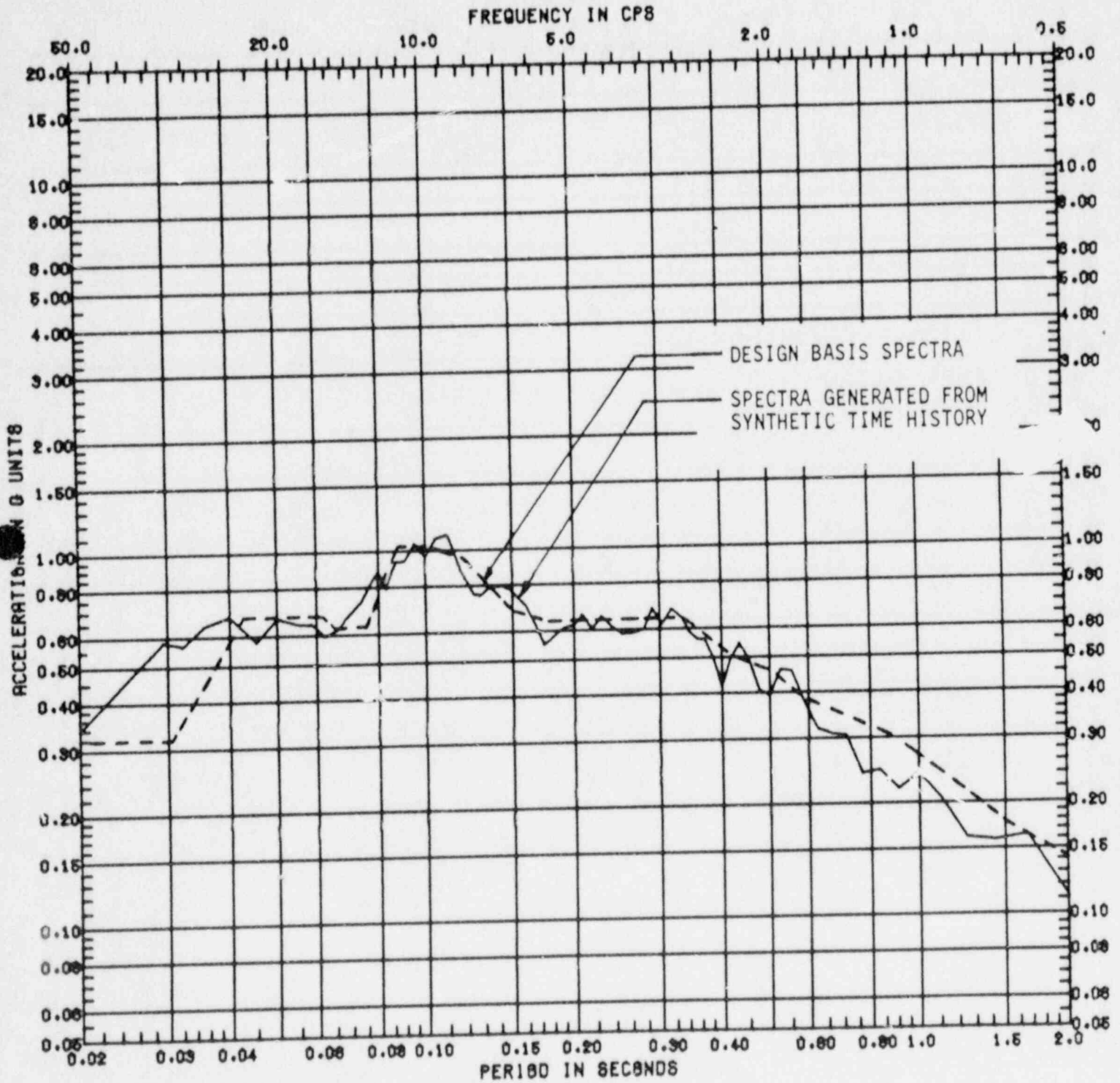
LOCATION

SPENT FUEL POOL



04 FEB 87  
SJH604

Fig. B-3 Response Spectra at Spent Fuel Pool Floor



SEISMIC ACCL SPECTRUM-SSE  
MODE  
DIRECTION VERT ANGLE

SPECTRA NO.  
ELEVATION  
LOCATION SPENT FUEL POOL



1